205,. McPherron, R.L., Physical processes producing magnetospheric substorms and magnetic storms, in Geomagnetism, Vol 4, edited by J. Jacobs, pp. 593-739, Academic Press Ltd., London, England, 1991. (chapter)

7

Physical Processes Producing Magnetospheric Substorms and Magnetic Storms

ROBERT L. McPHERRON

1 INTRODUCTION

1.1 Geomagnetism

The Earth's magnetic field is produced by a self-exciting dynamo in its liquid core. Outside the Earth this field would be approximately dipolar if it were not for a variety of secondary sources which distort its shape. In the crust the main field induces magnetization in susceptible rocks that is observed as anomalies in the main field. In the ionosphere solar heating and tides drive electrical charges across dipole field line, producing a current. This ionospheric dynamo generates a magnetic field which can be observed by stations passing beneath it. At radial distances of 4–6 R_e, charged particles of the Van Allen radiation belts drift because of gradients in the main field. Since charges of opposite sign drift in opposite directions they produce a ring current around the Earth. The growth and decay of this current over a period of several days is called a magnetic storm. At distances of 10 R_e and beyond, the impact of solar wind charges on the outer fringes of the main field creates a boundary current that confines the field inside a region called the magnetosphere. A frictional interaction between the solar wind and this boundary drags field lines away from the Sun producing yet another current system whose effect is the creation of a long comet-like magnetic tail. This drag induces convection of magnetic field lines and their attached particles and causes additional currents to flow in

GEOMAGNETISM VOL. 4
ISBN 0-12-378674-6

the ionosphere. Sudden changes in the strength of the solar-wind interaction and instability of the convective flow temporarily connect the magnetospheric and ionospheric currents along field lines. Intervals, of several hours, when this occurs are called magnetospheric substorms.

The scientific discipline which studies the Earth's magnetic field is called geomagnetism. Geomagnetism has many subdisciplines including dynamo theory, palaeomagnetism, ionospheric physics, and magnetospheric physics. The subject of this article is magnetic substorms and storms, which belongs to the fields of ionospheric and magnetospheric physics. However, ultimately, the Sun is the primary cause of geomagnetic activity and the solar wind is its agent. Thus it is necessary to study solar physics and solar wind physics as well to fully understand the causes of magnetic activity.

1.2 Solar-terrestrial physics

Solar-terrestrial physics is the name given to the study of relations between phenomena in the Earth's upper atmosphere and on the Sun. The field of study began about 1850 when it was first recognized that the periodicity of spots on the Sun was related to a similar periodicity in magnetic disturbances (see review by Chapman, 1967). The early history of this field is characterized by the use of indices of solar and magnetic activity in studies of the causal relations between phenomena on the Sun and on the Earth. One of the outstanding results of this period was the Chapman–Ferraro theory of magnetic storms (Chapman and Ferraro, 1930; 1931a,b; 1932). This theory postulated that a magnetic storm is caused by an electrically neutral stream of charged particles emitted from the Sun in a solar flare. The particles travel to the Earth and become trapped in its magnetic field. Once trapped they drift in a ring about the Earth creating a current whose effects are seen on the ground as a magnetic storm. Although the basic idea was correct, the multitude of processes by which these particles are trapped and energized are not yet fully understood. A comprehensive review of this early phase of solar-terrestrial physics is given in the classic books *Geomagnetism*, Vols I and II (Chapman and Bartels, 1962).

The second era of solar-terrestrial physics began with the launch of the first spacecraft in 1957. One of the first important discoveries made by early spacecraft was the continuous presence of a magnetized solar wind transmitting the Sun's influence to the Earth (Snyder *et al.*, 1963). The solar wind interacts with the Earth's field producing a variety of current systems whose effects can be measured both on the ground and throughout the magnetosphere surrounding the Earth.

It was quickly recognized that it is the solar wind that couples the Sun

to the Earth, transferring to it mass, momentum and energy originating at the Sun. This article reviews the two main candidates for this coupling mechanism: viscous interaction and magnetic reconnection. The topic of solar-wind–magnetosphere coupling has become an important subdiscipline of solar-terrestrial physics. The discipline uses observations of the solar wind and its effects in the magnetosphere to study the complex phenomena involved in the coupling processes. The books entitled *Physics of Geomagnetic Phenomena*, Vols 1 and 2 (Matsushita and Campbell, 1967a,b) were an attempt to summarize initial results of spacecraft measurements.

1.3 Magnetic activity

Magnetic activity is the name given to time variations in the magnetic field observed by magnetometers on the Earth's surface. We generally assume that such variations are a consequence of fluctuations in currents external to the Earth. Although the magnitude of changes in the internal field are comparable to that of substorms and weak storms, their timescale is much longer. Currently the magnitude of the Earth's field is decreasing about 50 nT $year^{-1}$ (out of 50 000 nT). For comparison, this is about the magnitude of changes measured at mid-latitudes from substorms, and about one-third that of a moderate magnetic storm. A sudden change in solar-wind pressure can cause this change in 1 min and an auroral display can cause it in 1 h.

The pattern of magnetic activity over the Earth's surface can be quite complex and its characterization is not an easy task. This has traditionally been done through the use of magnetic indices (Lincoln, 1967; Mayaud, 1980). Originally the indices were defined with little understanding of the processes responsible for the activity. The international character figure *Ci* and the planetary range index *Kp* are examples of such indices. As understanding grew, indices of greater physical significance were developed. For example, the disturbance storm-time index *Dst* is directly proportional to the total energy in the drifting particles which create the storm-time ring current (Dessler and Parker, 1959). Recently, new indices such as the auroral electrojet index *AE* have been defined to characterize the currents that flow in the ionosphere during auroral displays. Reviews of the definitions and procedures for calculation of modern magnetic indices are given by Rostoker (1972) and Baumjohann (1986a).

Time variations are always present in ground observations of the Earth's magnetic field, even when the causes of activity are not present in the solar wind. The rotation of the Earth is a major cause of such changes. Since

various current systems are not symmetric about the rotation axis, ground stations rotate through spatially varying magnetic fields. The ionospheric dynamo current is immediately above ground stations in the sunlit hemisphere and this current is the major cause of magnetic variation on quiet days. A second cause of change is variations in the angle between the solar-wind velocity vector and the dipole axis. The shape of the magnetopause and the pattern of the boundary current depend on this angle (Olson, 1969). So too does the location of the tail current which is effectively hinged to the magnetic equator at about 11 R_e (Russell and Brody, 1967). As the dipole tilt changes due to the Earth's rotation, the location, distribution and strength of these currents are modulated. This modulation is observed as time variations in magnetic records.

Changes in the Earth's main field and the solar quiet-day variation

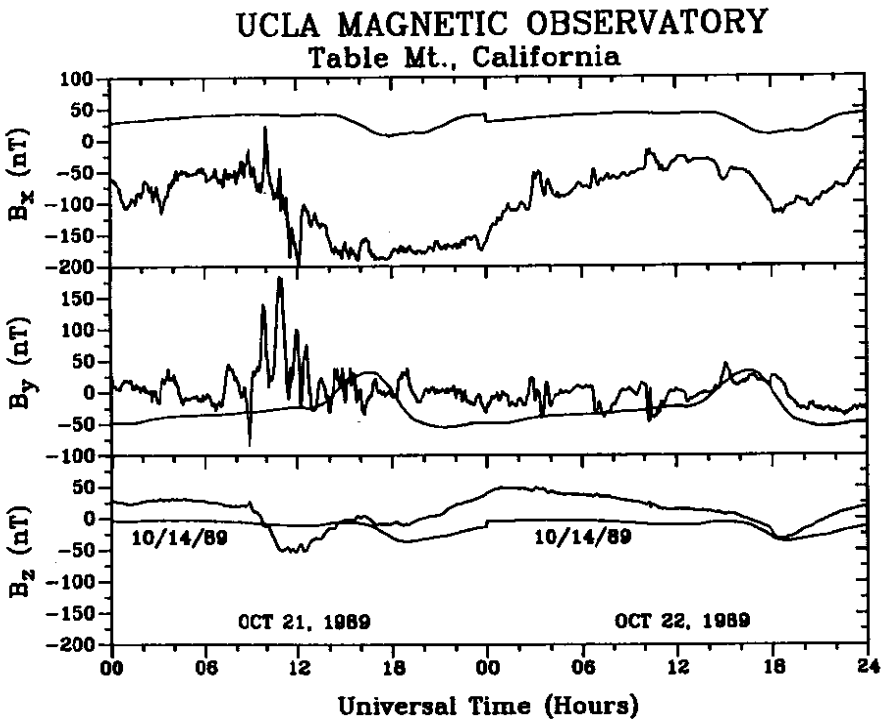

Figure 1. Magnetogram plotted from digital data recorded by the UCLA magnetic observatory at Table Mt., California in October 1989. The X, Y and Z components are respectively geomagnetic north, east and down. The quiet reference day is 14 October 1989 (smooth line), and the disturbed days (solid lines) include 21–22 October 1989.

provide a background upon which all variations of external origin are superposed. These changes must be removed from magnetometer records before they can be used in studies of other phenomena. Because neither can be predicted exactly, there is always some error in the residual variations used to infer physical processes. An example of the difference between quiet and disturbed magnetic variations measured at midlatitudes is presented in Fig. 1. The data were acquired by a fluxgate magnetometer at the UCLA magnetic observatory near Los Angeles in October 1989. The disturbance is a portion of magnetic storm that occurred shortly after the launch of the Magellan and Galileo spacecraft. The three panels display respectively the X (north), Y (east) and Z (down) components of the magnetic-field vector for a quiet day (smooth line), and a disturbed day (solid line). The original data were measured in a field-aligned coordinate system, but for consistency with other observatories they have been rotated to geomagnetic coordinates. Many observatories still use magnets as the sensor of field variations. Such systems routinely record the declination D (angle of horizontal disturbance to true north), the horizontal magnitude H and the downward component Z of the field variation.

1.4 Solar-wind control of magnetic activity

One of the first discoveries of the era of spacecraft was that magnetic activity is caused by the solar wind. Daily averages of solar-wind velocity measured by the first interplanetary probe Mariner 2 were very highly correlated with daily sum Kp index (Snyder *et al.*, 1963). High activity occurred at times of high solar-wind velocity. Furthermore, high velocities occurred periodically with the 27-day solar rotation period suggesting the source of high-speed streams was fixed on the Sun.

Several years later, Wilcox *et al.* (1967) demonstrated that the intervals of high velocity were simply a manifestation of an ordered structure in the solar wind that he named 'sector structure'. Almost all wind parameters are organized by the sector boundaries. For example, they found that the magnitude of the interplanetary magnetic field (IMF) was also well correlated with Kp. The implications of this were not initially clear. However, Fairfield and Cahill (1966) had demonstrated that magnetic activity occurs only when the IMF outside the magnetopause is southward. This work and that of others led Schatten and Wilcox (1967) to conclude that it was the Z component of the IMF that caused magnetic activity.

A reason why the IMF B_z component might be important was suggested by Dungey (1961). A southward IMF is antiparallel to the Earth's magnetic field at the subsolar point on the dayside magnetopause. This configuration

allows diffusion of the IMF into the interface where it can interconnect with the Earth's magnetic field. He called such a process 'magnetic reconnection'. Dungey noted that interconnection would allow the motional electric field of the solar wind to penetrate the magnetosphere where it could drive an internal convection system. He also pointed out that a second reconnection region had to exist on the night side to disconnect the field from the IMF.

An alternative mechanism for solar-wind control of magnetic activity was suggested simultaneously by Axford and Hines (1961). In their mechanism, solar-wind momentum is transferred across the magnetopause by waves and particles creating a viscous boundary layer. Motion of closed field lines in this boundary layer generates an electric field interior to the magnetosphere, identical to that induced by reconnection. Thus ionospheric effects of the two processes might appear to be the same. It seemed likely that the strength of this process would depend on the solar-wind velocity, but not on the IMF.

Subsequent work established beyond doubt the importance of both the IMF and the solar-wind velocity in the control of magnetic activity (e.g. review by Russell and McPherron, 1972). Most investigators have interpreted this as evidence that the important quantity is the rate at which southward IMF is brought to the nose of the magnetosphere, i.e. $d\Phi/dt = v \cdot B_z$. However, recent studies show that other parameters correlate somewhat better with measures of the strength of the westward electrojet (Maezawa and Murayama, 1985).

1.5 Purpose of this chapter

Our understanding of the causes of geomagnetic activity has increased considerably since the work reviewed above. The reconnection model of the magnetosphere suggested by Dungey has become the dominant explanation for the cause of magnetic activity. However, it is now recognized that the process is more complicated than first thought. The current version of this model is referred to as the near-Earth neutral line model (McPherron, 1979; Baker *et al.*, 1984). This model is not universally accepted, and alternatives such as the driven model (Akasofu, 1981a,b), or the boundary layer dynamics model (Rostoker and Eastman, 1987) have been proposed and vigorously advocated.

The purpose of this article is to describe what we believe is the cause of magnetospheric substorms and magnetic storms. To do this we begin with a description of the magnetic variations that constitute a substorm and a storm. Then we describe the basic structure of the magnetosphere and the processes which produce this structure. With this background we present a review of several current models that try to account for the observations. Our primary emphasis is the near-Earth neutral line model which we attempt to develop in greater detail than has been done elsewhere. Finally we conclude with a discussion of what we think are some of the outstanding questions of substorm and storm physics. It will be apparent that many questions remain to be answered.

Throughout the article we have attempted to explain the underlying processes using schematic diagrams and qualitative arguments. Many of the processes have been examined elsewhere in mathematical detail, or have been simulated on computers. However, we do not attempt to present this mathematical development as it would constitute a book in itself. We have tried to reference important articles which justify various points, but we have not been exhaustive in this endeavour.

2 WHAT IS A SUBSTORM?

2.1 Evolution of the concept of a substorm

A 'substorm' is the systematic sequence of physical processes that occurs repeatedly in the polar regions producing auroral and magnetic disturbances. Akasofu and Chapman (1961) first used the term to represent short intervals of intense magnetic disturbance during magnetic storms. This name was a modification of 'elementary polar magnetic storm', a term used by Birkeland (1908, 1913) to describe such intervals. Today these intervals are called 'polar magnetic substorms' (Akasofu *et al.*, 1965). The polar magnetic substorm is a phenomenological description of the temporal and spatial development of magnetic disturbances during a substorm. The 'auroral substorm' is a phenomenological description of the sequence of changes in aurora that accompany the polar magnetic substorm (Akasofu, 1964).

Many other phenomena in the ionosphere and the magnetosphere are systematically ordered by substorms. For example, Jelley and Brice (1967) noted that morningside electron precipitation occurs whenever an auroral substorm is in progress near midnight. Because of the wide spatial separation of the two phenomena, they concluded that the entire magnetosphere is affected by a substorm. They suggested, therefore, that the underlying set of processes be called an 'elementary magnetospheric storm'. McPherron *et al.* (1967) and Coroniti *et al.* (1968) felt that this term was too complex and suggested instead that the phenomenon be called a

'magnetospheric substorm'. Brice (1967a,b) concurred with this suggestion, but retained the modifier 'elementary'. The term magnetospheric substorm was adopted by Akasofu (1968) as part of the title of his book describing the various types of substorms, and it is now the accepted terminology. The magnetospheric substorm is characterized by phenomenological models which describe the space–time development of phenomena throughout the magnetosphere at the time of auroral disturbances.

There have been several recent attempts to refine the definition of a substorm. McPherron (1979) defined it:

> A magnetospheric substorm is a transient process initiated on the night side of the earth in which a significant amount of energy derived from the solar wind–magnetosphere interaction is deposited in the auroral ionosphere and magnetosphere.

Rostoker *et al.* (1980) have given a somewhat longer definition which attempts to account for some of the complexities known to occur during times of extreme disturbances. According to these authors:

> The term magnetospheric substorm describes an interval of increased energy dissipation confined, for the most part, to the region of the auroral oval. The onset of this process is signaled by explosive increases in auroral luminosity in the midnight sector, and the entire process encompasses an interval during which the strength of the current in the auroral electrojets increases from and returns to the background level from which the substorm arose. During this interval there may be a sequence of intensifications of the westward electrojet, each associated with a Pi 2 micropulsation burst and a westward travelling surge. As the substorm develops, the region of discrete auroras in the midnight sector expands poleward and westward (the poleward bulge). Eventually, the region of disturbed aurora reaches a maximum latitude and begins to recover toward its pre-substorm location. The interval of time between the first Pi 2 burst and the time the aurora reaches a maximum latitude has been called the expansion phase. The interval during which the aurora in the midnight sector returns to lower latitudes is called the recovery phase.

2.2 The auroral oval

A fundamental feature of all substorm models is the 'auroral oval'. The auroral oval is defined at any instant of time as the roughly circular region around one of the magnetic poles within which aurora are observed. The auroral oval was discovered through analysis of all sky camera pictures made during the International Geophysical Year (IGY) (Khorosheva, 1962; Feldstein, 1963). Simultaneous pictures from many locations demonstrated

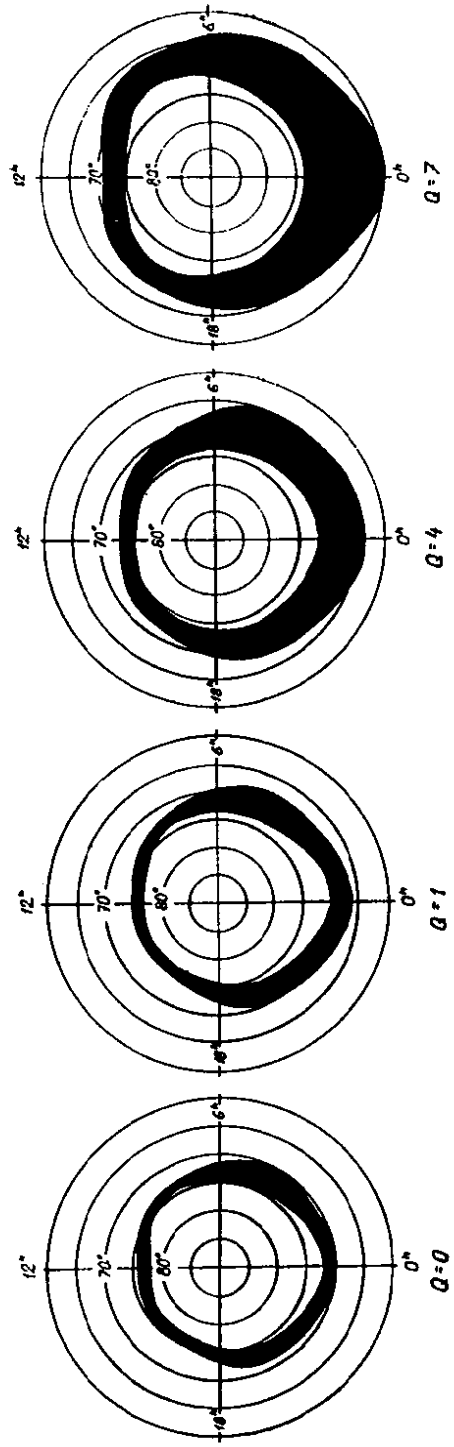

Figure 2. The auroral oval for different levels of magnetic activity plotted in dipole latitude-magnetic local time coordinates (Feldstein and Starkov, 1967).

that auroral arcs tend to occur in two roughly oval belts surrounding the magnetic poles. The belts are at their highest magnetic latitude on the day side of the Earth (~ 75–80°) and lowest on the night side (~ 60–65°). The diameter of the oval is a function of activity, expanding to lower latitudes as activity increases. Figure 2 taken from Feldstein and Starkov (1967) illustrates the shape of the oval at different levels of activity.

The 'auroral zone' is defined as the locus of most frequent occurrence of bright arcs. Since arcs are brightest in the auroral oval near midnight, the auroral zone is a circle of constant dipole magnetic latitude passing through the centre of the midnight oval located at 67°.

The first clear demonstration that the auroral oval is actually a single continuous belt of auroral emission was provided by scanning photometers

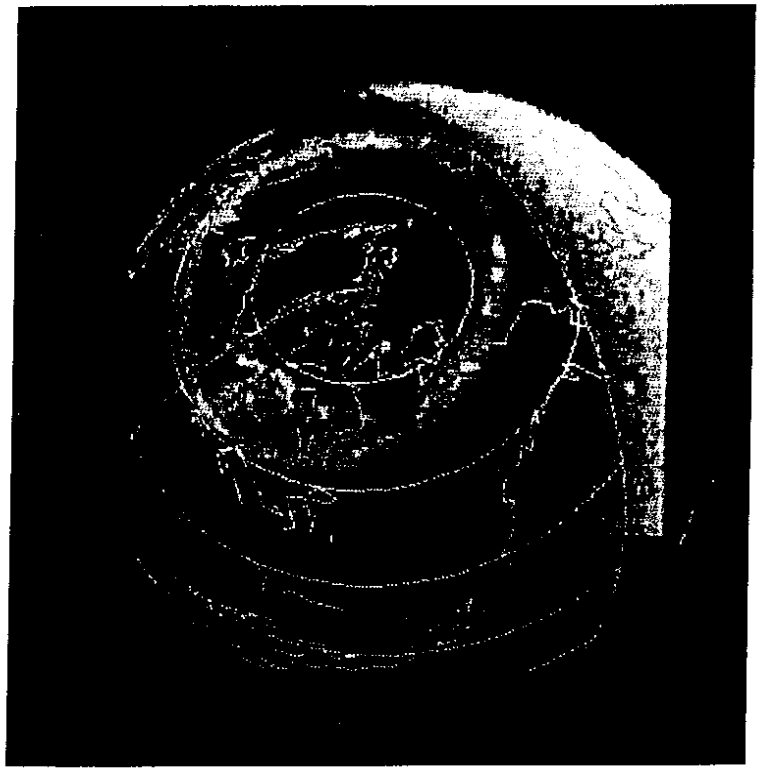

Figure 3. A false colour image of the auroral oval as seen from space in November 1981 by the University of Iowa global auroral imaging instrument on Dynamics Explorer 1 (DE-1) (Frank *et al.*, 1985). An overlay of the North American coastline shows the oval extending nearly to the northern border of the USA on the night side and to the terminator on the day side.

on the spacecraft ISIS-2 (Lui and Anger, 1973; Lui *et al.*, 1975). By combining the motion of an oscillating mirror and the spacecraft the instrument was able to obtain an image of the entire polar cap in the 15 min it took to cross the polar cap. The images showed not only that the oval was continuous, but that it consisted of two parts. The first part is the discrete aurora of the type observed from the ground by all sky cameras. The second part is a band of diffuse aurora that had not been previously observed. The diffuse aurora has a sharp equatorward edge which is located at about 65° near midnight. Its poleward edge is less well defined, but typically occurs around 68°. Discrete auroral arcs are generally located just poleward of the discrete aurora.

The shape of the auroral oval was re-examined by Holzworth and Meng (1975). Using the data published by Feldstein (1963) the authors concluded that the oval is actually a circle about a point displaced 4° towards the night side from the dipole axis. Meng *et al.* (1977) verified this conclusion by examining more than 50 DMSP (Defense Meteorological Satellite Program) satellite images of extended quiet arcs. Additional work by Holzworth and Meng (1984) utilized 150 auroral images showing that the auroral circles are controlled by the IMF. The location of the centre of each circle depends on the strength of the dawn–dusk component (B_y) while its size depends on the vertical component (B_z).

The first high-quality images of the auroral circles were obtained by an imaging photometer on the high-altitude spacecraft DE-1 (Frank *et al.*, 1982). Figure 3 presents one such image in which the entire auroral ring can be seen projected against an outline of North America (Frank *et al.*, 1985).

2.3 Phases of a substorm

The ordered sequence of events which constitute an isolated substorm can be divided into distinct phases. These phases include the growth phase, the expansion phase and the recovery phases. Within each phase some phenomena exhibit distinct stages of development. During very disturbed intervals it is not always possible to identify individual substorms. Operational definitions of the substorm phases are given below.

2.3.1 The expansion and recovery phases

The auroral substorm developed by Akasofu (1964) had two distinct phases, the expansive phase and the recovery phase. The various stages of these two phases are summarized in Fig. 4. Figure 4a shows the quiet state before a substorm begins. Multiple quiet arcs in the midnight sector of the

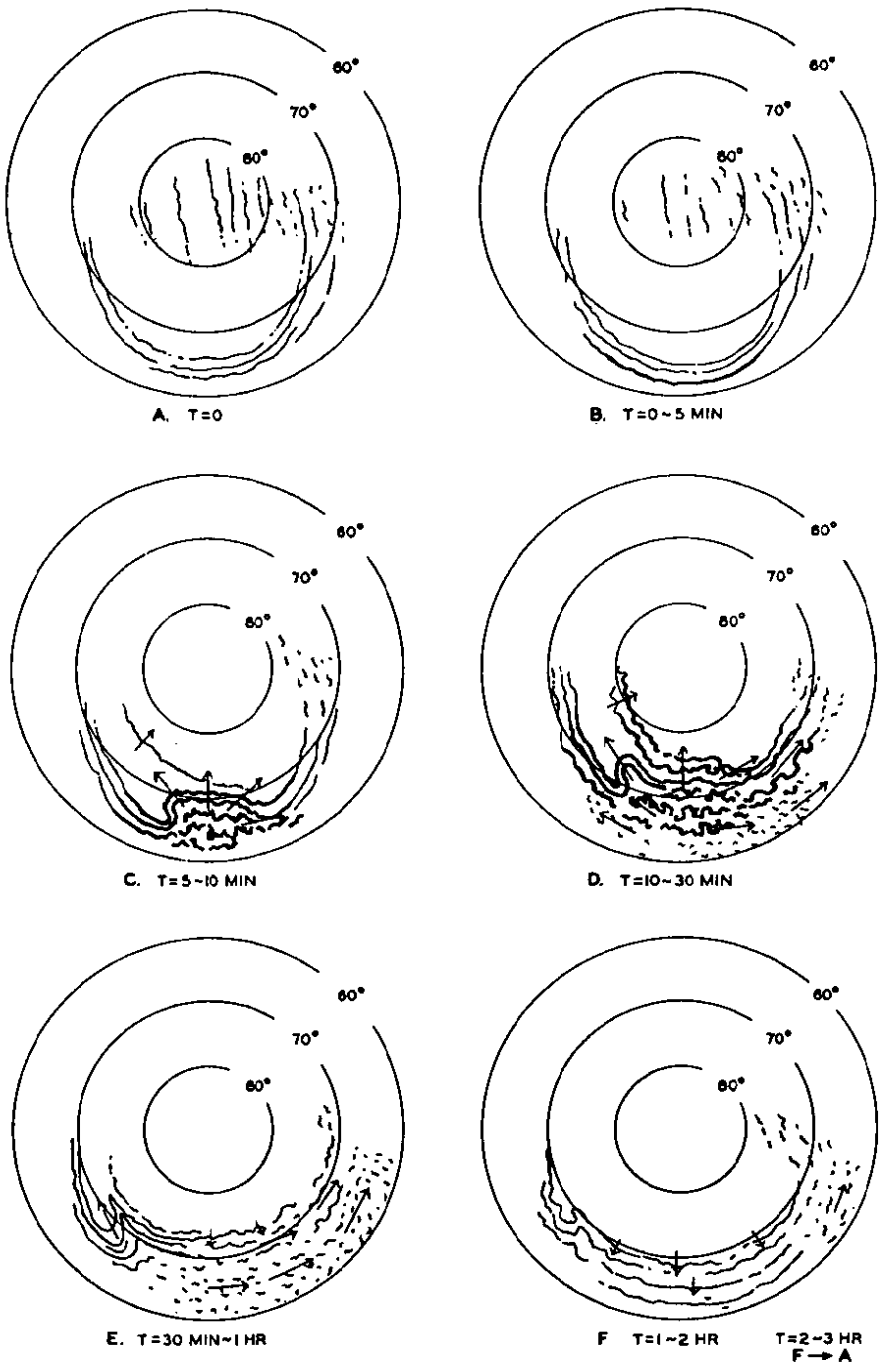

auroral oval drift slowly towards the equator. At the onset of the substorm expansive phase (Fig. 4b), the most equatorward arc in the region of discrete aurora suddenly brightens. This arc expands poleward (Fig. 4c), filling the region behind it with rapidly moving, turbulent auroral forms (the poleward bulge). The duskward edge of this bulge forms a wave-like disturbance called the westward-travelling surge that appears to propagate along the previously brightened arc (Fig. 4d). In the morning sector the poleward edge of auroral activity becomes very wave-like, with omega shaped bands of aurora drifting slowly eastwards. At the equatorward edge of the morningside auroral oval, arcs break up into eastward-drifting, pulsating patches. Eventually the poleward expansion stops and auroral arcs begin to reform and drift equatorward (Fig. 4e). Finally, as shown in Fig. 4f, the westward surge breaks down into a large loop that continues drifting westward as quiet arcs reappear in their former locations. As indicated in the various panels of this diagram the duration of the expansive phase is approximately 30–60 min, and the recovery phase 60–120 min. Similar sequences can often be seen to repeat every few hours during disturbed times.

The model of the auroral substorm was later confirmed and extended through an examination of low-altitude DMSP satellite images (Akasofu, 1974, 1976). These images showed that each of the features deduced from collections of all sky camera photos was present in the more encompassing DMSP images. Figure 5, taken from Akasofu (1976), summarizes these observations. The DMSP images were helpful in defining the relationship between the diffuse and discrete aurora, as well as in revealing the structure of dayside aurora.

The polar magnetic substorm described by Akasofu *et al.* (1965) also had two phases corresponding to those of the auroral substorm. Figure 6 shows two different models of the ionospheric currents (electrojets) once thought to be responsible for the magnetic disturbances. According to Akasofu *et al.* (1965), at the time of the sudden auroral brightening there is also an intensification of the westward electrojet immediately below the brightened arc. With time, the region of enhanced westward electrojet expands westward with its leading edge defined by the westward-travelling surge and its poleward edge defined by the expanding auroral bulge. The eastward electrojet increases in intensity coincident with these developments in the westward electrojet. This coincidence led Akasofu *et al.* (1965) to suggest

Figure 4. A schematic diagram showing the development of the auroral substorm as proposed by Akasofu (1964). (a) Quiet phase. (b) Expansion onset. (c–d) Expansion phase. (e–f) Recovery phase.

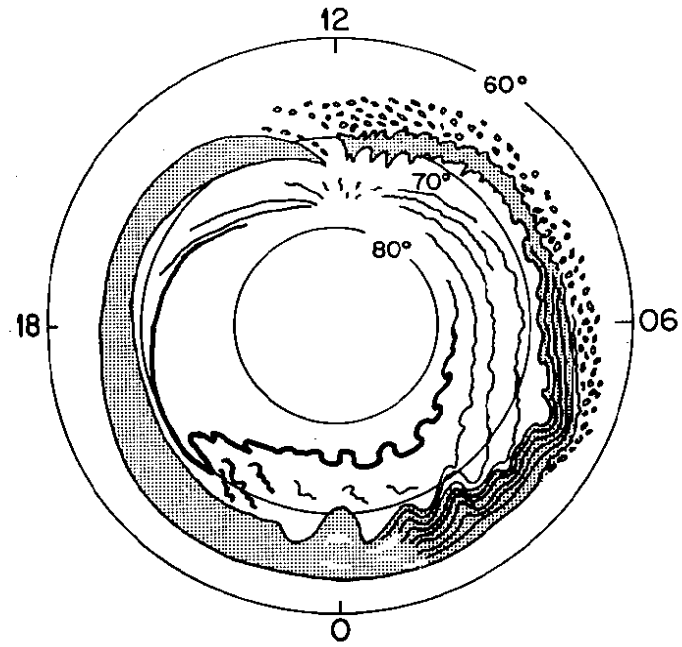

Figure 5. A schematic summary of the various types of auroral displays observed during an auroral substorm. Discrete arcs are indicated by lines and diffuse aurora by shading. Details of the dayside distribution and refinements of the nightside distribution are based on Defense Meteorological Satellite (DMSP) observations (Akasofu, 1976).

that the eastward electrojet was simply the return current from the westward electrojet as shown by Fig. 6b.

2.3.2 *The growth phase*

The substorm model developed by Akasofu was later modified by the addition of a growth phase (McPherron, 1970). The growth phase is defined as an interval of time prior to the onset of the expansion phase during which disturbances in a variety of phenomena become increasingly apparent. The most easily observed effect is a gradual increase in the strength of the eastward and westward electrojets. Figure 7 taken from McPherron (1970) demonstrates a growth phase as recorded by magnetometers at auroral zone stations in the night sector.

Another manifestation of the growth phase noted by McPherron *et al.* (1968) is an increasing probability of localized auroral activations or

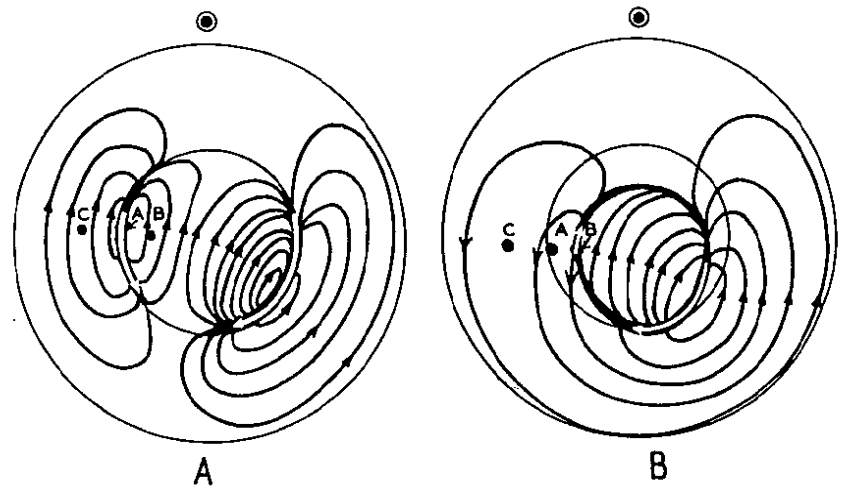

Figure 6. A schematic diagram showing two equivalent current systems proposed as explanations for the magnetic perturbations of the auroral electrojets (Akasofu *et al.*, 1965). Panel (a) is closer to the modern view based on more extensive data. Panel (b) is a single electrojet system proposed by Akasofu *et al.* to explain both positive and negative perturbations in the horizontal component of the magnetic field.

'pseudo break-ups' (Akasofu, 1964). Psuedo break-ups are similar to substorm expansion phases with a typical event including brightening and activation of an auroral arc, a burst of Pi 2 micropulsations, and a weak enhancement of the westward electrojet. The features which distinguish these from substorm expansions include their short lifetime (~ 5 min), their extreme localization (a small portion of the field of view of a ground observer), and the weak magnetic perturbations which accompany them (~ 100 nT).

2.3.3 *The expansion onset*

The substorm onset was originally defined as the beginning of the explosive brightening and expansion of the aurora. With the introduction of the substorm growth phase this time was no longer the first event in a substorm. This had led to some confusion in terminology and considerable controversy concerning the cause of substorm activity (McPherron, 1979). The terminology used in this article is illustrated in Fig. 8 using the auroral electrojet indices of Davis and Sugiura (1966).

Figure 8 contains two curves plotted about a common baseline. The positive curve is the upper envelope of magnetic disturbance in the horizontal

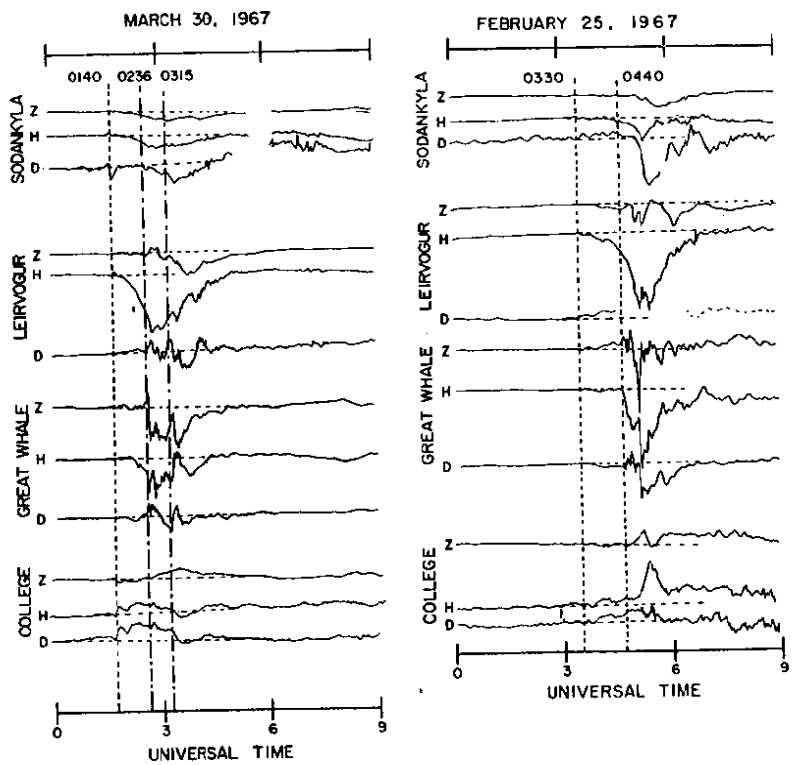

Figure 7. Magnetic perturbations recorded during a substorm by a chain of stations spanning the night sector of the auroral oval. H is the magnitude of the horizontal component, D is the declination of H with respect to geographic north, and Z is the vertical component positive towards the centre of the Earth. The growth phase (McPherron, 1970) is the interval of time between the beginning of disturbance and the onset of a sudden decrease in the H component at a station near midnight (Great Whale).

component of the field recorded by a worldwide chain of auroral zone magnetic observatories. The negative curve is the lower envelope. These curves are called respectively the AU (aurora upper) and AL (aurora lower) indices of magnetic activity. Since the eastward electrojet causes a positive ground disturbance, AU is a measure of its strength. Similarly, AL measures the strength of the westward electrojet. In general the station contributing to AU lies in the late afternoon or early evening sector while the station contributing to AL lies in the early morning hours (3–4 a.m.). However, during the expansion phase the station contributing AL is usually near midnight (Allen and Kroehl, 1975).

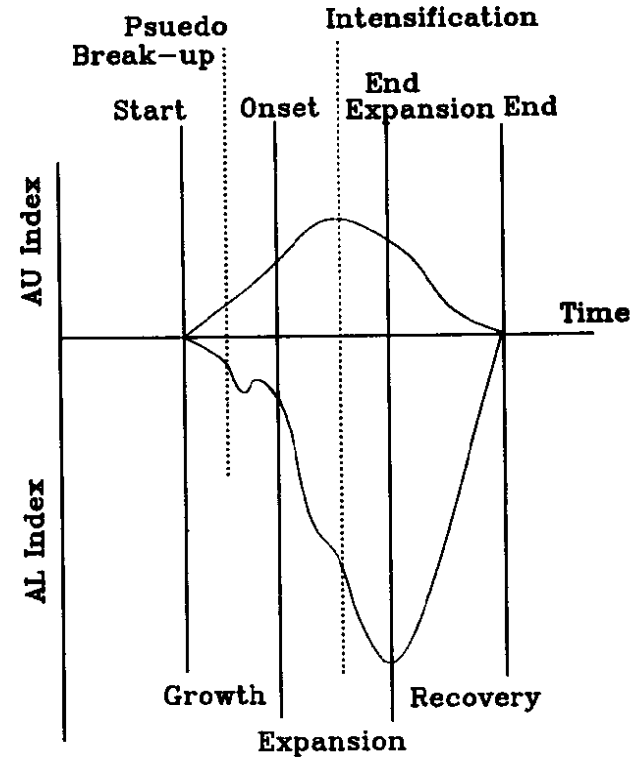

Figure 8. Phases of a substorm as shown schematically by auroral electrojet indices during an idealized substorm. The AU and AL electrojet indices are defined in the text.

The AU and AL indices plotted in Fig. 8 depict an isolated substorm gradually emerging from a quiet background and eventually fading back into this background. The beginning of the substorm is the time of first observable disturbance in the AU and AL indices. Similarly, the end of a substorm is the time of the last observable disturbance. The expansion phase onset (substorm onset) is the time of sudden enhancement of the westward electrojet near midnight. The end of the expansion phase occurs when the AL index reaches a minimum and begins to recover towards its quiet baseline. The duration of the substorm is the time interval between the beginning and end of magnetic disturbance. The growth phase, the expansion phase and the recovery phase are respectively defined as the time intervals between the beginning of the substorm and expansion onset, expansion onset and the beginning of recovery, and the beginning of recovery and the end of the substorm.

Substorms usually exhibit more complex time variations in the auroral electrojet indices than this idealized, isolated event. Two forms of such complexity are indicated schematically in Fig. 8. The first is a pseudo break-up indicated by a small dip in AL during the growth phase. The second is a later intensification of the substorm expansion phase indicated schematically by a change in slope of the AL index.

There can be significant errors in the determination of important fiducial times, even during simple isolated substorms without complexity. Since the indices are defined by only one field component from a very limited collection of magnetic observatories, it is quite likely that the start of a substorm, or the onset of the expansion phase, actually occurred somewhat earlier than observed. Similarly the ends of the expansion phase and of the substorm may actually be later than observed. Ideally one would like to have continuous high time and spatial resolution images of the aurora from above the poles to define these times. Such images have only recently become available, and for some time in the forseeable future will never be available for the majority of events. We are thus forced to make use of those data routinely collected for other purposes (e.g. magnetograms) to define the chronology of substorms.

2.4 Complex substorm activity

2.4.1 Pseudo break-ups

One of the factors which complicates the study of substorms is the rather frequent occurrence of 'pseudo break-ups' (Elvey, 1957). Akasofu (1964) describes these in the following manner 'When the substorm is very weak the brightening and some development of irregular folds are the only consequences. ...the poleward motion lasts only for a few minutes and other arcs may not be seriously affected'. We have observed pseudo break-ups while flying balloons measuring substorm electron precipitation (Parks *et al.*, 1968). An event begins with a gradual increase in energetic electron precipitation and a Pi 2 micropulsation burst. Within a few minutes a small section of an auroral arc becomes visibly brighter and begins to develop rays and folds. These move rapidly along the arc. Often the lower edge of the arc turns red. A ground magnetometer measures a weak negative bay. The entire event lasts 5–10 min before it fades back into a quiet arc.

Pseudo break-ups are often seen during the growth phase of substorms. One of the major causes of controversy concerning the existence of the substorm growth phase is the occurrence of such events. It has been argued that the first of these should be taken as the actual onset of the expansive

phase (Rostoker *et al.*, 1980). As will be shown later in this chapter, however, more global measurements seldom show any evidence of these, while the effects of a major break-up are quite obvious throughout the magnetosphere. Nonetheless, it has not been demonstrated that pseudo break-ups differ in any way except their degree of localization and strength from major substorms.

2.4.2 Multiple onset substorms

Another source of confusion is the occurrence of multiple onsets or intensifications of the expansion phase. The name 'intensification' was introduced by Kisabeth and Rostoker (1971) who used latitude chains of magnetometers to study the temporal development of the westward electrojet. The authors found that the strength of the electrojet usually does not grow smoothly with time. Frequently its strength suddenly increases as a filament of westward ionospheric current appears at the northern edge of the pre-existing electrojet. These intensifications appear quasiperiodically every 10–20 min.

The low-latitude magnetic effects of multiple onset substorms were studied by Clauer and McPherron (1974) and Weins and Rostoker (1975). In simple substorms with a single onset, low-latitude magnetic observatories record a characteristic pattern of magnetic perturbations in the D (East) and H (North) components which is summarized in Fig. 9. The pattern can be modelled by a three-dimensional field-aligned current system which flows out of the magnetosphere on the dawn side of midnight and into the magnetosphere on the dusk side. Within the ionosphere it flows westward as a segment of the westward electrojet. During multiple onset substorms the pattern is more complex as illustrated in Fig. 10. Original magnetic observations plotted at the left side have been converted to contour maps showing the development of the perturbed X (north) component in local time and universal time. In the substorm shown it is apparent that there were at least four onsets, and that there is no obvious pattern to the location of each onset.

Pytte *et al.* (1976) carried out a detailed study of the ground signature of multiple onset events. They demonstrated that a typical onset (or intensification) observed at low latitudes is associated with a number of phenomena, including a Pi 2 burst, brightening of an auroral arc, formation and motion of a westward-travelling surge, low-latitude and subauroral magnetic perturbations characteristic of the substorm current wedge, and sudden increases in energetic electron precipitation. The surge appears to be responsible for carrying these phenomena westward along the auroral oval. Successive surges are not always initiated further west than

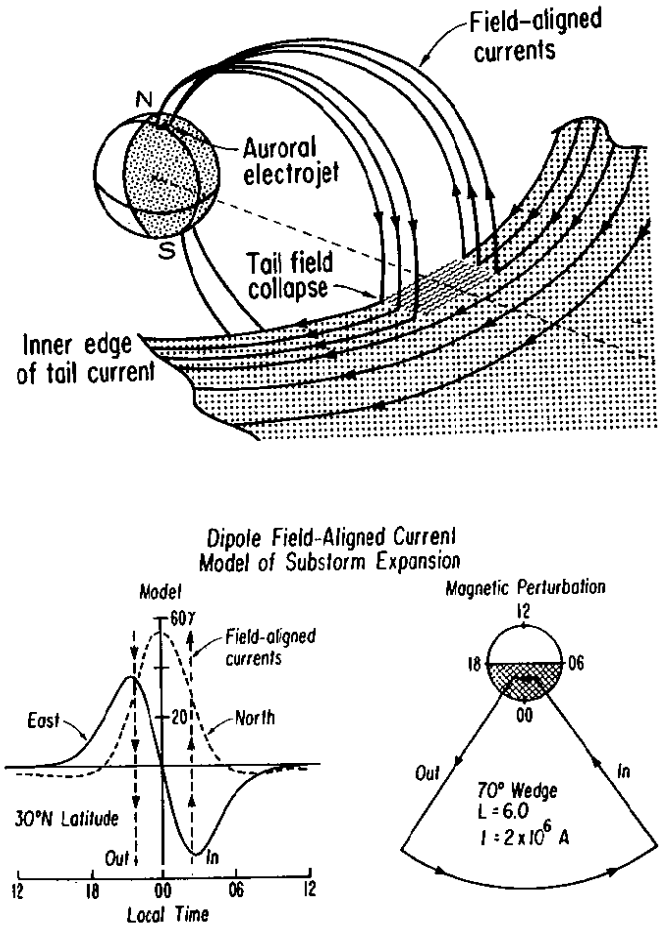

Figure 9. A perspective view of the substorm current wedge which creates the magnetic perturbations at low latitudes during the expansive phase of a substorm. The bottom right panel shows the equivalent current which must be added to the tail current to obtain this current system. The bottom left panel shows the magnetic variations produced by the perturbation current (Clauer and McPherron, 1974).

their predecessors, and in fact signatures of several surges may be simultaneously present in the auroral oval. However, when Pi 2 bursts and auroral brightening occur without low-latitude signatures of the current wedge there is no westward travelling surge observed in the oval.

Weins and Rostoker (1975) disagreed with the conclusion of Pytte *et al.* (1976), claiming that westward surges do not actually move. Instead they proposed that the appearance of motion is caused by the quasiperiodic

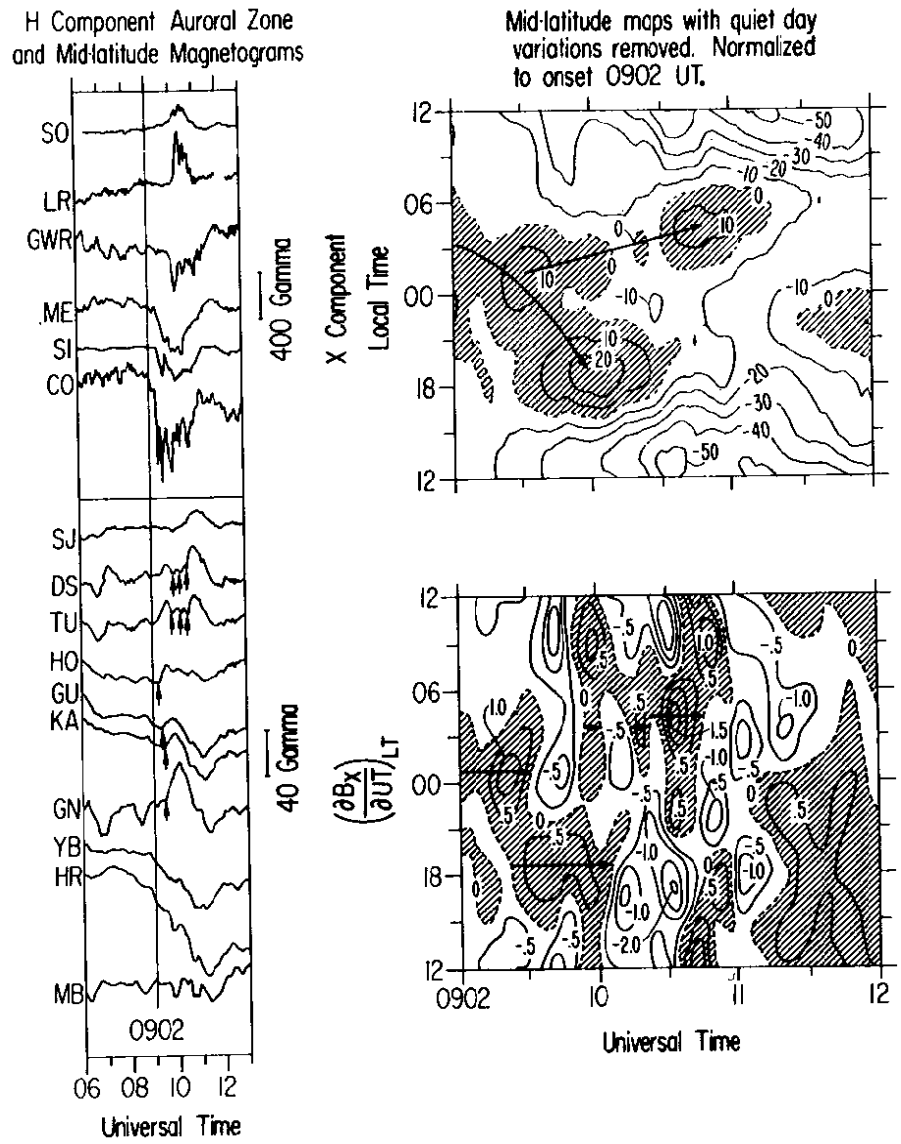

Figure 10. An example of a multiple onset substorm (Clauer and McPherron, 1974). Original magnetograms plotted on the left show the perturbations in H recorded in the auroral oval and at mid-latitudes during a substorm. The upper right panel displays a contour map in the local time–universal time plane of the mid-latitude H perturbations (labelled X). The bottom right panel contains a map of the rate of change of the H component. Horizontal arrows denote the interval of increasing H in each onset.

generation of a sequence of progressively more northward and westward filaments of westward electrojet. Each filament terminates in an auroral spiral (surge) from which emanates an outward tube of field-aligned current. This controversy concerning the motion of westward-travelling surges is only now being resolved. Observations by the VIKING imager (Rostoker *et al.*, 1987) suggest that one or more surges may form anywhere along the premidnight auroral oval. Sometimes they move westward from their point of origin, but at other times they remain stationary with a new one forming later at a different location.

2.4.3 Convection bays

A type of magnetic activity also occurs for which it is impossible to identify individual expansion phases. This activity is called a 'convection bay' (Pytte *et al.*, 1978). A convection bay is the opposite extreme from a pseudo break-up. It is a prolonged interval of intense magnetic disturbance during which the identifying signatures of an expansion phase are absent. Caan *et al.* (1973) noted that such intervals are caused by a relatively steady southward IMF. They suggested that the energy input to the magnetotail by reconnection is continuously dissipated in magnetic activity without the familiar sequence of growth, expansion and recovery. In a study of substorm expansions triggered by storm sudden commencements (SSC), Kokubun *et al.* (1977) found that nearly always the SSC was preceded by southward IMF. One exception was a convection bay. Further study revealed that the current pattern was similar to that of substorms during the growth and recovery phase, but did not have the intensification of the westward electrojet near midnight characteristic of a substorm expansion phase. Pytte *et al.* (1978) examined similar events and concluded that convection bays represent nearly steady magnetospheric convection with reconnection on the day and night side nearly balanced.

2.5 Magnetic storms

Magnetic storms differ from substorms in the duration, strength and cause of the magnetic disturbance. Magnetic storms are best observed at mid-latitudes where their primary effect is a reduction in the strength of the horizontal magnetic field. Very great magnetic storms with $\Delta H < -500$ nT occur two to three times per solar cycle and can have disturbances greater than 1000 nT (Chapman and Bartels, 1962, p. 328). Great storms ($-300 > \Delta H > -500$ nT) are more frequent, typically occurring about eight times per cycle. Smaller storms with $-50 > Dst > -300$ occur about

400 times per cycle or twice per solar rotation (Russell and McPherron, 1973). For comparison the effect of a large substorm at mid-latitudes is about 50 nT.

The pattern of horizontal magnetic disturbance caused by a magnetic storm is roughly that of a uniform, axial field projected onto the Earth's surface. This pattern suggests that the source of the magnetic disturbance is a ring current circling the Earth in the equatorial plane. Drift of the Van Allen radiation-belt particles creates such a ring current. Fundamental questions in the study of magnetic storms include 'Where do the ring-current particles come from?', 'How are they energized?', 'How are they transported?' and 'How are they lost to the atmosphere?' Some authors believe that the magnetospheric substorm is the mechanism that causes the growth of the ring current (Davis and Parthasarathy, 1967).

2.5.1 Phases of a magnetic storm

A typical magnetic storm consists of three phases: the initial phase, the main phase and the recovery phase. The initial phase is an interval during which the disturbance in the horizontal component at mid-latitudes is larger than normal (~ 50 nT). This phase may persist anywhere from 0 to 16 h. Following the initial phase is the main phase during which the H component rapidly decreases. Coincident with the decrease, the auroral ovals expand equatorward with auroral substorms constantly occurring in the expanded ovals. A typical main phase lasts from a few hours to a substantial fraction of a day. When substorms cease to occur the decrease in H ceases and the recovery phase of the storm begins. The recovery phase lasts for several days unless more substorms occur and there is an additional decrease in mid-latitude H.

2.5.2 Magnetic indices of storm disturbance

The development of the storm is usually measured by a magnetic index called disturbance storm time (*Dst*). This index was originally defined by Moos (1910) in a study of Bombay storm records. A procedure for its routine calculation was developed later by Sugiura (1964). *Dst* is defined as the instantaneous, worldwide average of the deviation of the equatorial H component from a quiet day. Since no chain of equatorial observatories exists, mid-latitude stations are used to calculate *Dst*. Equatorial observations are approximated by dividing the observed perturbation at a mid-latitude station by the cosine of the station's magnetic latitude. This approximation implicitly assumes the axial field perturbation of a ring current as mentioned above.

The magnetic perturbations in H recorded by mid-latitude stations during the main phase of a storm are never symmetric in longitude. Typically they are most negative in the dusk sector (Akasofu and Chapman, 1964). This asymmetric development of the main phase is indexed by a quantity called the asymmetry index ($ASYM$). As defined by Kawasaki and Akasofu (1971), $ASYM$ is the instantaneous difference between the maximum and minimum perturbation in H recorded by a worldwide chain of mid-latitude observatories. Since the usual locations of the maximum and minimum perturbations in H are at dawn and dusk, Clauer and McPherron (1974) used the difference between average H perturbation at stations clustered at these two locations.

2.5.3 *Example of typical magnetic storm and substorms*

The bottom panel of Fig. 11 presents an example of the Dst and $ASYM$ indices for a fairly typical magnetic storm. The storm began at 1636 UT on 7 February 1967 and ended early on 11 February. The storm sudden commencement (SSC) cannot be seen because of aliasing due to 2.5 min sampling. The initial phase was very short and cannot be separated from the main phase. The main phase began very soon after the SSC and reached its maximum development within 7 h at about 2200 UT on 7 February. The recovery phase appears to last for more than 3 days. It exhibited two stages, rapid recovery on 8 February, and slow recovery on following days. The recovery was interrupted twice by intervals of decrease in Dst. The $ASYM$ (asymmetry) index is plotted in the same panel as Dst. The ring current was asymmetric throughout the main phase and the first stage of the recovery phase. In the second stage of the recovery $ASYM$ was near zero indicating that the ring current was symmetric during this interval.

The auroral electrojet indices AU and AL are plotted in the third panel. Both indices were highly disturbed during the main phase and first stage of the recovery. Sudden dips and recoveries in the AL index imply that there were a number of distinct substorm expansions in this interval. The first two were the largest and occurred while the main phase was in progress. The AL and $ASYM$ indices have surprisingly similar time variations. Both were disturbed during the same interval of time, and peaks in $ASYM$ generally correspond with dips in AL. The AU index is disturbed during the same period, but as is typical of AU, it does not define individual substorm expansions.

The time variation during this disturbed period of two important solar wind variables is shown at the top of Fig. 11. Dynamic pressure plotted in the top panel was enhanced throughout the disturbed interval. Also, the interplanetary electric field presented in the second panel was strong and

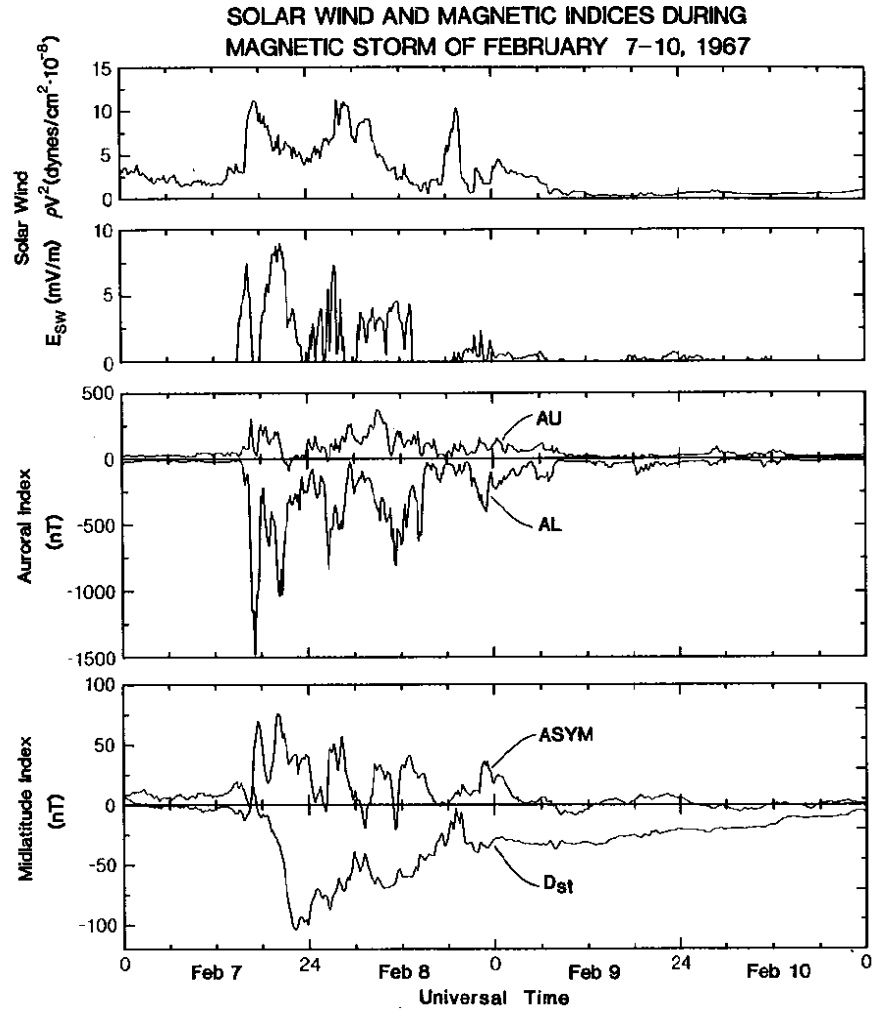

Figure 11. A typical magnetic storm as represented by the Dst and $ASYM$ indices (bottom panel), auroral electrojet indices (centre) and solar-wind parameters (top panel).

had a substantial component directed from dawn to dusk during the disturbed interval. Note that intervals when the interplanetary magnetic field pointed northward in the GSM coordinate system have been set to zero. Burton *et al.* (1975) have demonstrated that this quantity can be used to predict the time history of Dst extremely well.

In anticipation of a more complete interpretation given later we briefly

summarize what is believed to be the cause of the substorms and storm. A solar flare or erupting prominence on the Sun ejects a bubble of plasma. This bubble passes outward toward the Earth through the slower solar wind. The bubble interacts with the slow-speed plasma ahead developing an interaction region containing high density, high pressure and strong magnetic field. Also the plasma is deflected from its radial flow direction and the solar-wind magnetic field is draped around the bubble. This draping forces the field out of the ecliptic creating a component which is parallel (north) or antiparallel (south) to the Earth's dayside magnetic field. If it is southward, magnetic reconnection between the solar wind and earth occurs connecting the normally closed field lines of the Earth with the IMF. Since field lines are generally equipotentials the electric field of the solar wind is transmitted into the magnetosphere and ionosphere by the connected magnetic field lines. This electric field sets up a convection system that moves magnetospheric plasma from the tail behind the Earth to the day side. The ionospheric plasma undergoes the same motion, and in addition conducts electrical currents driven by the electric field. The eastward and westward electrojets are simply concentrations of these currents in two narrow belts of high electrical conductivity created by the same particles that produce the aurora. The growth phase of a substorm is the response of the magnetosphere and ionosphere to dayside reconnection.

Magnetic flux opened on the day side by reconnection is transported to the night side by the solar wind. During the growth phase it accumulates in the tail lobes. The expansion phase begins when rapid reconnection starts on the night side close to the Earth. The electrical current which creates the tail magnetic field is diverted from the region of reconnection. It flows along magnetic field lines to the midnight ionosphere travelling westward for a short distance before returning to the tail along field lines. This diversion of current produces the substorm current wedge, and in the ionosphere it locally enhances the westward electrojet produced by dayside reconnection. The expansion phase continues as long as reconnection is in progress in the near Earth plasma sheet.

The substorm recovery phase begins when the reconnection region moves away from the Earth. Why it begins when it does is not known, but often it occurs within 10–20 min after dayside reconnection is terminated by a northward turning of the IMF. However, as the region moves tailward it continues to reconnect lobe field for some time, leaving in its wake a tail structure similar to that which existed before it was distorted by the growth phase. Eventually, convection and associated ionospheric electrical fields and currents die away and the substorm is over.

The SSC and the initial phase of a magnetic storm are caused by the arrival of enhanced solar-wind dynamic pressure at the Earth. The magnetopause or boundary between the Earth's magnetic field and the solar wind is created by an electrical current flowing in the boundary. Magnetic effects of this current cancel the main field outside the boundary and approximately double it inside. The location of the boundary is determined by a balance of dynamic pressure outside and magnetic pressure inside. An increase in solar-wind dynamic pressure moves the boundary inward, increasing the effect of the magnetopause current at the Earth's surface.

The main and recovery phases of the magnetic storm are produced by the drift of energetic particles in the Van Allen radiation belts 4–6 R_e away from the Earth. This region of space is not normally accessible to particles drifting earthward from the tail. However, when the convection electric field is enhanced by dayside reconnection the boundary of this forbidden region moves closer to the Earth. Particles then drift through the region under the combined effects of the electric field and gradients in the magnetic field. Given sufficient time they would drift out to the magnetopause and be lost. But when the IMF turns northward, the convection electric field vanishes trapping the particles wherever they happen to be. They then drift in circular paths, creating the ring current. In a short time the IMF again turns southward initiating another substorm. Any particles previously trapped in the nightside portion of the ring current will gain additional energy through gradient drift in the enhanced electric field, and will move further earthward. Additional particles are brought earthward from the tail and are energized and trapped when the IMF turns northward. Thus fluctuations in the convection electric field are responsible for the energization and injection of the ring-current particles. Burton *et al.* (1975) have shown that the rate of decrease of *Dst* is directly proportional to the rectified solar-wind electric field.

Whether the ring current grows in intensity or decays depends on a balance between the rate at which particles are injected and the rate at which they are lost. The primary loss mechanism is charge exchange. The Earth is surrounded by a halo of neutral hydrogen atoms whose density increases exponentially towards the Earth's surface. Ring-current particles that approach the Earth due to their motion along field lines may come close enough to a neutral hydrogen to exchange an electron. The result is an energetic neutral atom which is no longer trapped and a cold hydrogen ion that does not drift at a rate sufficient to produce a current. The rate of ring-current decay is proportional to the number of particles which can charge exchange. Thus, stronger currents have a higher decay rate (dN/dt). For any given rate of injection by the convection electric field there is an asymptotic value of *Dst* for which injection and decay are in equilibrium.

The data presented in Fig. 11 can be understood in terms of the foregoing description. The increase in solar-wind dynamic pressure moved the

magnetopause closer to the Earth enhancing the ground effects of its current. This is the initial storm phase of positive *Dst*. For this storm the pressure increase was accompanied by a strong southward IMF (non-zero rectified electric field), which immediately initiated the first substorm growth phase and the beginning of ring-current injection. Changes in this field trapped sufficient particles to create a ring current with $Dst < -100$ nT. Additional fluctuation in electric field injected more particles, but this electric field was weaker and could not balance the rate of decay. Thus the ring current began to decrease in strength initiating the storm recovery phase. Continued southward fluctuations of the IMF partially counterbalanced the ring-current decay and created weaker substorms. Eventually the southward IMF became so weak that the ring current decayed into background.

The close relation between the waveforms of the ring-current *ASYM* index and the westward electrojet index suggests they are causally related. As will be explained later, a fraction of the electrojet currents do not close in the ionosphere. Instead they feed a field-aligned current system which flows outward from the region near midnight where they meet. This current is carried around the dusk side of the Earth by particle drifts in the ring current and eventually flows along field lines to feed the convection electrojets where they begin near noon. Thus asymmetry persists as long as the convection electrojets are present. Clauer *et al.* (1983) have demonstrated that the relation between the IMF and *ASYM* and *AL* is described by virtually the same impulse response function.

There can be a wide variety of developments of magnetic storms. For example, not all storms have an initial phase. Also, most have at least two stages to the recovery phase, an initial one which is rapid and then a later one which is slow. Some storms exhibit two or more main phases. Storms which begin with a positive initial phase usually exhibit SSC. The SSC consists of a few cycles of wave-like disturbance superimposed on the initial increase in *H*. A major reason for the diversity of storm types is differences in the form of the solar-wind dynamic pressure and electric-field variations. A secondary reason not discussed here is that helium and oxygen ions also appear in the ring current with numbers depending on the duration and strength of the convection electric fields. These particles have shorter lifetimes for charge exchange decay and produce the initial rapid recovery.

Subsequent sections of this chapter are devoted to a much more detailed exposition of the physical processes which are important in the creation of substorms and storms. As will become apparent, there are many unanswered questions and considerable controversy about the causes of a variety of processes.

3 THE STRUCTURE OF THE MAGNETOSPHERE

3.1 The closed magnetosphere

3.1.1 The magnetopause

The 'magnetosphere' is the region of space around the Earth within which the magnetic field of the Earth is confined by the solar wind. For years it was a matter of debate whether this region was open to the solar wind or closed. Although we now know it is open (Paulikas, 1974; Fairfield and Scudder, 1985), it is conceptually easier to visualize a closed magnetosphere and we begin our description of magnetospheric structure from this point of view. According to the theory of Chapman and Ferraro (1930, 1931a,b, 1932) the Earth's field is confined by a three-dimensional sheet current that cancels the field outside the sheet and enhances it inside. The current exists whenever ionized particles ejected from the Sun encounter and are deflected by the Earth's magnetic field. Today we know that a 'solar wind' of ionized particles is always present, and that a 'magnetopause' current separates the magnetosphere from the solar wind at all times.

The Chapman–Ferraro theory for the magnetopause is illustrated schematically in Fig. 12. Charged particles from the Sun are carried by the solar wind into the Earth's magnetic field. As they enter they are bent by the

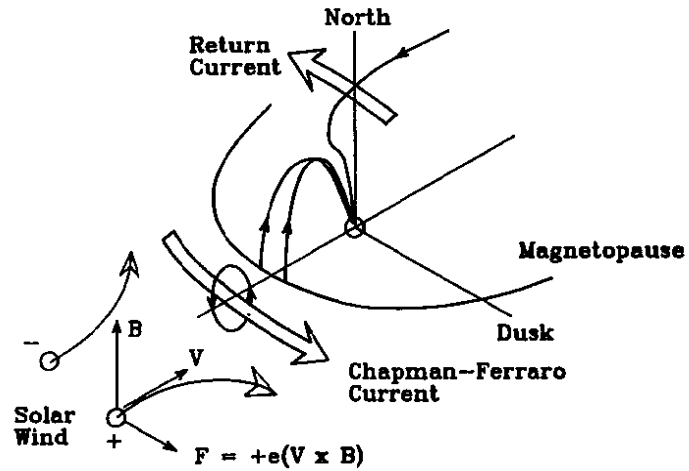

Figure 12. Schematic illustration showing how the Lorentz force separates solar-wind charges in the Earth's magnetic field creating the magnetopause current.

Lorentz force $F = q(v \times B)$, where q is the charge of the particle, v its velocity and B the Earth's dipole field. Charges of opposite sign are turned in opposite directions creating a current. In the equatorial plane in front of the Earth the sense of this current is from dawn to dusk. Upstream, the magnetic field from the current opposes the Earth's field while downstream it enhances it. This weakens the bending upstream and enhances it downstream causing a thinner current sheet to develop. In the limit the current becomes a thin sheet and has just the right configuration and shape to balance everywhere the normal stress exerted by the particles reflected from it. Numerically the boundary is defined as that surface for which the normal pressure exerted by specular reflection of particles exactly equals the magnetic pressure of the perturbed magnetic field immediately inside the current sheet (Mead and Beard, 1964). At the subsolar point this relation is written $k\rho v^2 = (2B_d)^2/2\mu_0$, where k is a factor describing the

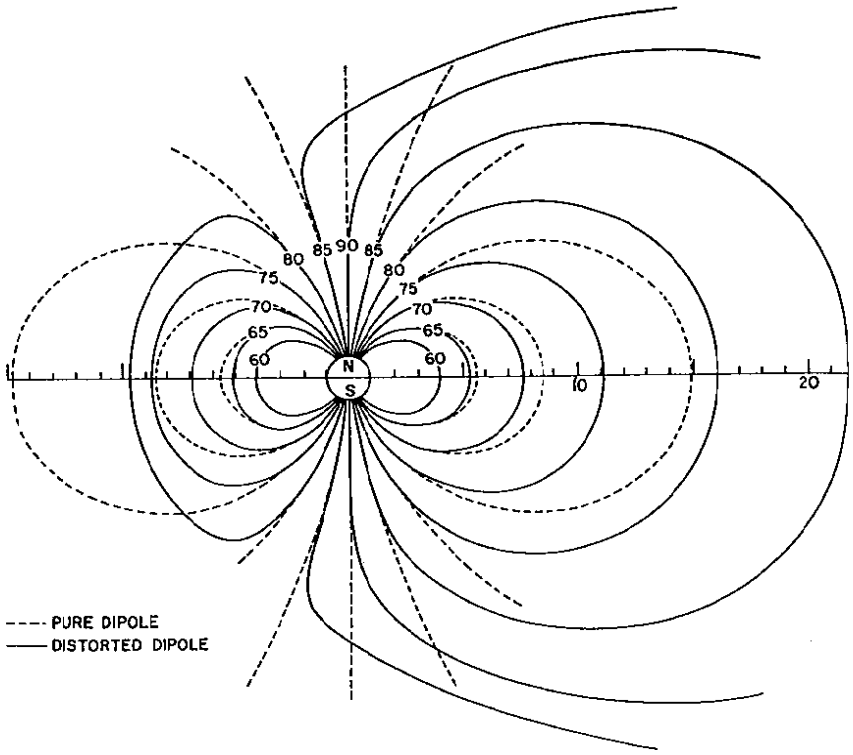

Figure 13. The configuration of magnetic field lines in the noon–midnight meridian plane produced by the superposition of the Earth's magnetic field and the field of the magnetopause current (Mead, 1964).

elasticity of the reflection process, ρ is the mass density of solar wind particles, v is the speed of the solar wind, B_d is the magnetic field strength of the Earth's dipole, and μ_0 is the permeability of free space.

Figure 13 from Mead (1964) illustrates the form of magnetic field lines produced by superposing the field of the magnetopause current on the dipole field. Field lines that would normally close on the sunward side of the Earth appear swept back to the night side. At the subsolar point the magnetopause is perpendicular to the solar wind, but some distance downstream it becomes tangential. Beyond this distance the solar-wind flow no longer exerts a force on the magnetic field and the diameter of the tail should remain constant. However, the thermal and magnetic pressure of the solar wind act perpendicular to the flow and should close the boundary within a short distance forming a 'tear drop' shaped magnetosphere (Johnson, 1960).

The Chapman–Ferraro model predicts that there are two 'neutral points', or points of zero field strength in the superimposed fields of the earth and magnetopause current. These occur in the boundary above the northern and southern polar caps, sunward of the Earth. Magnetic field lines passing through these points are singular. They branch and spread across the entire magnetopause. The regions of funnel-shaped field lines surrounding the neutral points are called the 'polar cusps'. The configuration of the cusp field lines guides particles from the solar wind into the atmosphere generating aurora in the dayside ionosphere. The neutral points are foci for the closure of the magnetopause current. Everywhere between the neutral points the current flows from dawn to dusk, but poleward of these points it flows from dusk to dawn.

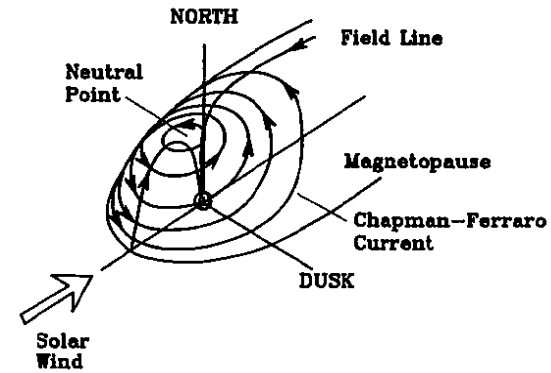

Figure 14. A perspective view of the Chapman–Ferraro current pattern on the magnetopause as it circulates around the northern neutral point.

This reversal is a consequence of the change in direction of dipole field lines between the equator and the pole. Figure 14 presents the geometry of the Chapman–Ferraro (magnetopause current) in perspective.

3.1.2 *The magnetotail*

The magnetosphere does not close on the night side as predicted by either the Chapman–Ferraro or the tear-drop model. Instead, it has a long comet-like 'magnetic tail' (Ness, 1965, 1987; Fairfield, 1987).

The configuration of the magnetic field on the night side of the earth measured by Ness (1965) is shown in Fig. 15. It consists of two long 'lobes' of nearly antiparallel magnetic field connected across the equatorial plane by a sharp bend (not shown). This field configuration requires a sheet of current flowing from dawn to dusk across the centre of the tail. At the mid-plane of this 'tail current' the magnetic field is nearly zero and the region is referred to as the 'neutral sheet'. Pressure balance between this low-field region and the two regions of high magnetic field above and below requires

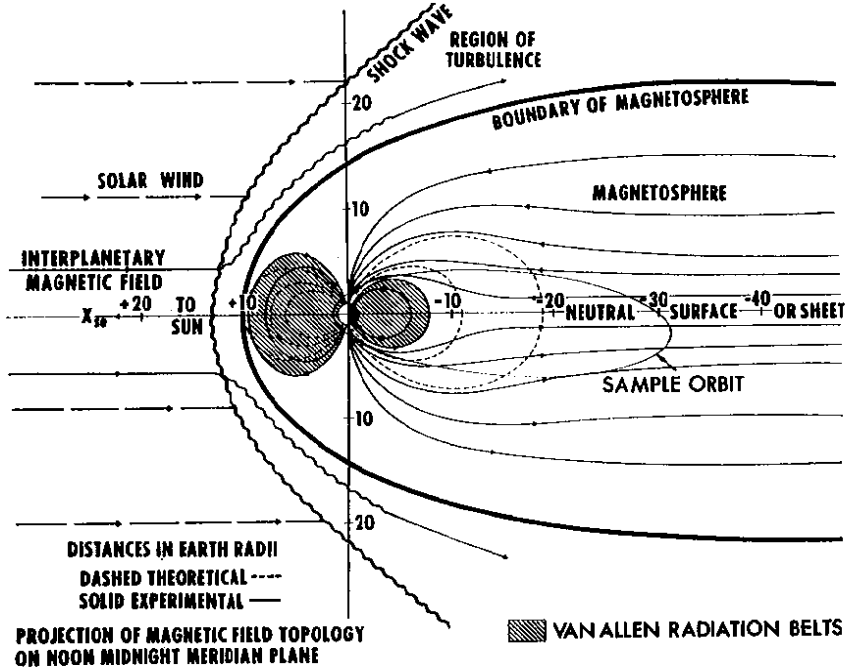

Figure 15. An interpretation of the initial magnetic field observations made on the night side of the Earth, showing how the Earth's magnetic field is drawn out into a long tail (Ness, 1965).

that there be a plasma of finite temperature around the neutral sheet (Bame *et al.*, 1967). Drift of the charges which make up this plasma produces the tail current. This region is called the 'plasma sheet'. The tail current splits at the flanks of the magnetic tail closing on the cylindrical magnetopause above and below the current sheet. Close to the Earth the return currents from the tail current blend into the closure of magnetopause currents.

An extended magnetic tail requires that the solar wind exerts a tangential force on the magnetosphere in addition to the normal forces already discussed. Axford and Hines (1961) proposed a mechanism that could accomplish this in a closed magnetosphere. In their mechanism, solar-wind momentum is transferred to the magnetosphere by one or more processes such as wave or particle scattering across the magnetopause. The momentum carried by the particles or waves is transferred to closed field lines inside the magnetosphere, creating a boundary layer with particles and field moving tailwards at some fraction of the solar-wind flow velocity. Because this process is similar to viscosity in hydrodynamics it is called the 'viscous interaction'. Eventually the tension of the stretched field lines overcomes the tangential drag of the viscous interaction and the field lines are released from the boundary layer into the inner magnetosphere. The field lines flow sunward inside the boundary layers completing closed loops on each flank of the magnetosphere. This two-celled pattern of flux transport is called 'magnetospheric convection'.

Figure 16 illustrates the pattern of magnetospheric convection in the equatorial plane of the magnetosphere as proposed by Axford and Hines (1961). In the diagram each flow line represents the locus of successive mid-points of closed field lines frozen in the moving plasma. As the feet of field lines move through the ionosphere they carry with them the electrons and ions of the ionosphere. In the lower part of the ionosphere (E-region) ions collide more frequently with neutral particles than do electrons. Therefore, on the average they drift slower than the electrons creating an electrical current opposite to the motion of the field line. Axford and Hines interpreted the eastward and westward electrojets, as well as the direction of auroral motions in the oval, as evidence for this pattern of flux convection.

3.1.3 *Convection and associated currents*

In collisionless plasmas such as those of the solar wind or the magnetosphere, plasma motion produces an electric field satisfying the relation $\boldsymbol{E} = -\boldsymbol{V} \times \boldsymbol{B}$. This relation implies that flow lines are orthogonal to $\boldsymbol{E}$ and $\boldsymbol{B}$ so that magnetic field lines lie in equipotential surfaces. Thus the pattern of Fig. 16 indicates that there is a dawn-to-dusk electric field across the interior of the magnetosphere produced by the sunward motion of the

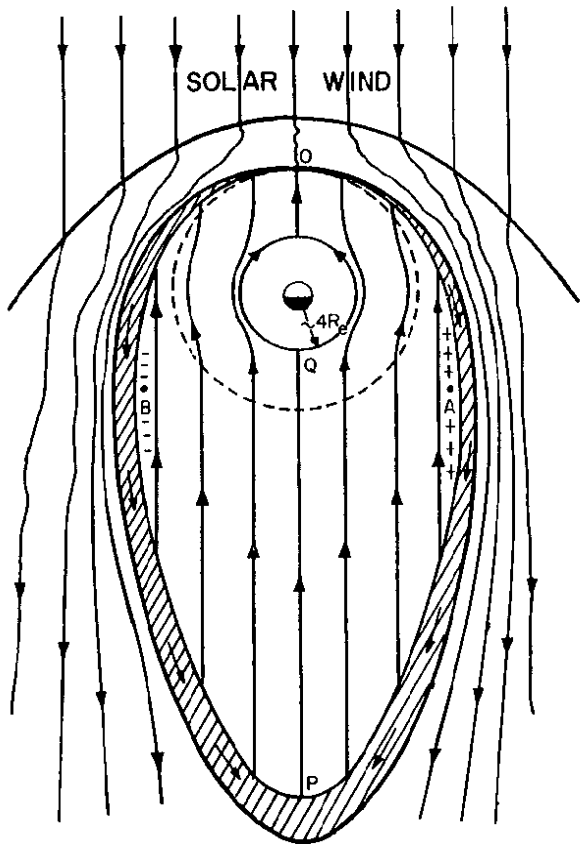

Figure 16. A schematic view of the magnetospheric convection pattern induced in the equatorial plane by the viscous interaction of the solar wind with the closed field lines of the magnetosphere (Axford, 1964).

returning plasma. In the viscous boundary layers the field is oppositely directed from dusk to dawn. The projection of this electric field pattern onto the ionosphere by field lines is illustrated in Fig. 17. On the dawn side of the Earth the boundary layer electric field maps poleward, while on the dusk side it maps equatorward. This mapping produces a polar cap ionospheric electric field that points from dawn to dusk. Field lines that intersect the magnetopause map to a point at the foot of the dayside polar cusp, while field lines inside the boundary layer map to various points in the polar cap. The electric field in the return flow region is also reversed by field-line mapping and points equatorward on the dawn side and

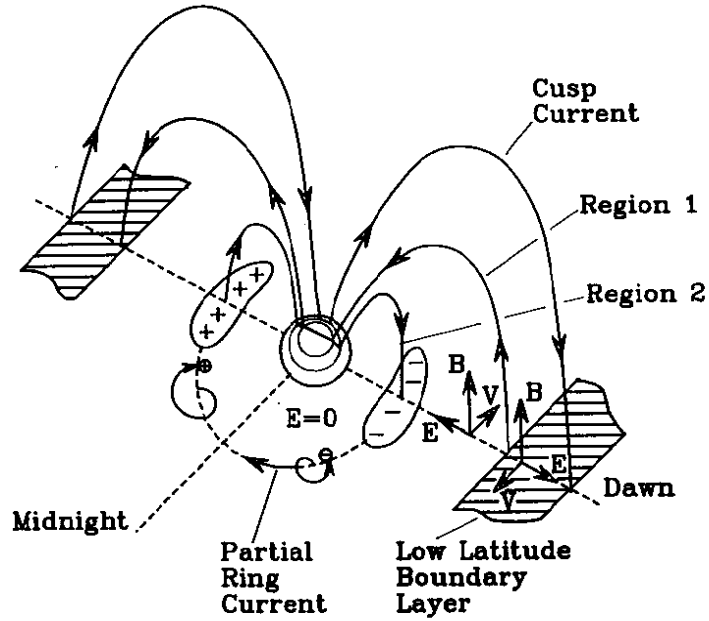

Figure 17. Form of the three-dimensional current system produced by magnetospheric convection. The currents shown include polar cusp, Region 1, Region 2 and partial ring current.

poleward on the dusk side. Field lines embedded in the return flow map to the auroral oval.

The pattern of ionospheric motion produced by mapping magnetospheric convection to the ionosphere is illustrated in Fig. 18. In a closed magnetosphere the electric field and flow reversals at the inner edge of the boundary layer define the boundary of the polar cap. Poleward of these reversals all field lines are convecting antisunward, while equatorward they are moving sunward. These shears are important because the ionospheric electric field has divergence along the shears. On the morning side it points away from the shear, and on the evening side it points towards the shear.

Because the conductivity of the ionosphere is finite and anisotropic an electric field drives a current both parallel (Pedersen current) and perpendicular (Hall current) to itself. Figure 19 illustrates the pattern of these two current systems for the ionospheric electric field produced by magnetospheric convection. The Pedersen current flows away from the morning side shear both to higher and lower latitudes. The portion that crosses the polar cap converges into the dusk shear. The remainder crosses the auroral oval and diverges from its lower boundary as explained later. Since the

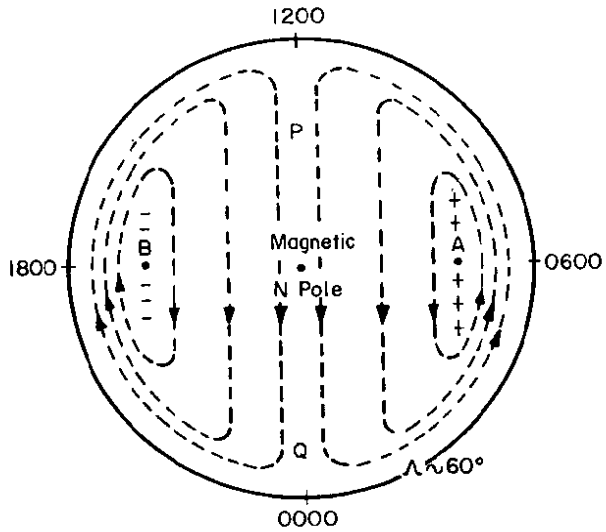

Figure 18. Ionospheric convection produced by viscous interaction (Axford, 1964). In a closed magnetosphere, polar-cap field lines are closed and convect antisunward. The polar-cap boundary is defined by velocity shears centred at dawn and dusk. A dawn-to-dusk electric field connects the centres of the two shear zones.

Pedersen current is divergent, continuity requires that there be field-aligned currents and a magnetospheric closure. In Fig. 17 these field-aligned currents are labelled 'Region 1' and 'Region 2' currents.

The Hall current is produced by a combination of electric field drift and collisions. Both electrons and ions tend to drift with velocity $\boldsymbol{v} = \boldsymbol{E} \times \boldsymbol{B}$ perpendicular to the ionospheric electric and magnetic field (this is the ionospheric flow mentioned above). In a collisionless plasma charges of opposite sign drift with the same velocity and produce no current. But neutral atoms are present in the ionosphere and ions collide with them more frequently than do electrons. This causes positive ions to drift more slowly than electrons creating a current opposite to the general drift, i.e. parallel to $-\boldsymbol{E} \times \boldsymbol{B}$. This Hall current has the same pattern as the ionospheric flow, but is oppositely directed. The pattern is dipolar, flowing sunward in the polar cap and antisunward in the auroral oval. The eastward and westward electrojets are simply the concentration of this current in the high-conductivity channels produced by auroral particle precipitation.

The distribution of ionospheric conductivity has a significant effect on magnetospheric convection. The dayside ionosphere is conductive everywhere as a result of photo-ionization. The nightside ionosphere is

conductive along the auroral ovals because of particle precipitation. The conductivity in the polar cap depends on season. In summer a polar cap is conductive because of photo-ionization. In winter a cap is weakly conductive due to particle precipitation. Generally, the highest conductivity is along the nightside auroral ovals (Spiro *et al.*, 1982).

Conductivity gradients at boundaries between different regions are a source of field-aligned currents as are gradients in electrical field. Conductivity gradients also cause space charge to accumulate within the gradient. The electric field produced by this charge distribution alters the ionospheric electric field and is projected back into the magnetosphere. One important consequence of this polarization electric field is the rotation of the convection pattern away from noon–midnight symmetry. Another consequence is the asymmetric development of magnetic storms.

The mechanism which rotates the convection pattern is illustrated in Fig. 20. The top panel shows a portion of the ionospheric Hall current system described above. The eastward and westward electrojets are created

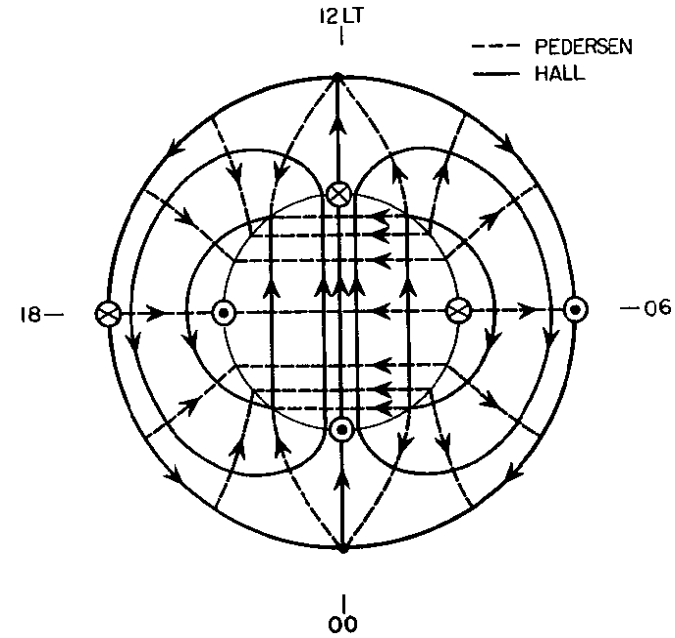

Figure 19. Ionospheric currents driven by the projected electric field of magnetospheric convection. Pedersen current flows parallel to the ionospheric electric field, while Hall current flows perpendicular. Crossed circles and dotted circles respectively denote downward and upward field-aligned currents (Crooker and Siscoe, 1981).

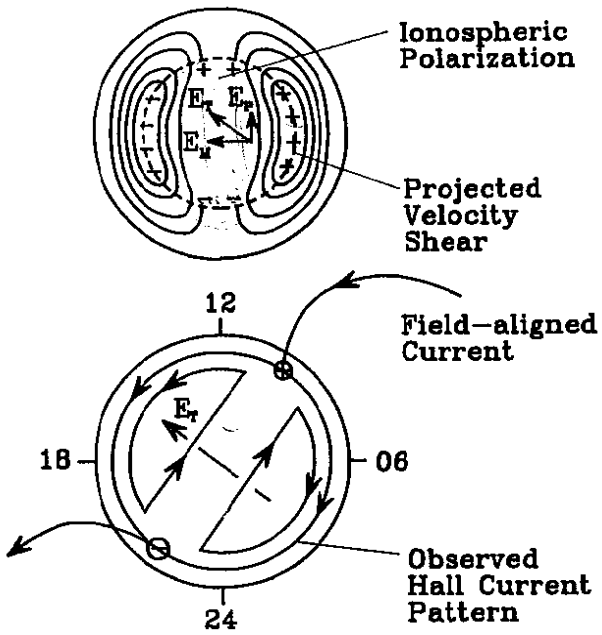

Figure 20. A north polar view of the Earth illustrating the polarization of the ionosphere produced by a discontinuity in Hall conductivity at the poleward edge of the auroral oval. The bottom panel shows the rotation of the convection pattern caused by the polarization.

by concentrating the Hall current in the high-conductivity channel of the auroral oval. If the ionosphere were uniformly conducting this current would close across the polar cap completely in the ionosphere. However, the polar cap has a significantly lower Hall conductivity than does the auroral oval. Charge therefore accumulates at the boundaries where Hall current enters or leaves the polar cap. This polarization produces an electric field directed from midnight to noon. The vector sum of this and the dawn-to-dusk convection electric field points to mid-afternoon. Equipotentials are orthogonal to the electric field and are thus directed from mid-morning to early evening as shown in the bottom panel. Viewed from above the north pole the entire pattern is rotated clockwise (Crooker and Siscoe, 1981).

The current system responsible for the asymmetry of the ring current is shown schematically in Fig. 21. The space charge that rotates the convection pattern can be partially discharged by flowing along field lines into the magnetosphere. In the magnetosphere a possible closure is through particles drifting around the dusk side of the Earth. Near noon the current

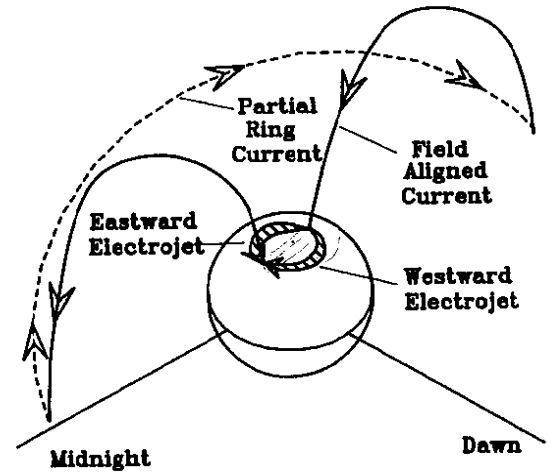

Figure 21. A perspective view of the closure of the electrojets through field-aligned currents connected to a partial ring current.

carried by these particles diverges along field lines, feeding the electrojets in the noon sector. The mid-latitude ground effect of this current system is a decrease in the horizontal field on the dusk side and an increase on the morning side. During magnetic storms particle precipitation into the ovals increases the contrast in conductivity between the oval and polar cap. This increases the angle of rotation of the convection pattern and the strength of the partial ring. The is observed as the asymmetric development of the storm-time ring current.

The idea that some electrojet current closes through a field-aligned current is supported by several studies with ground data. Linear prediction filters relating *AL* and *ASYM* indices to the solar-wind electric field are very similar (Clauer *et al.*, 1983). This suggests that a substantial fraction of the current flowing in the westward electrojet also flows in the partial ring circuit. Latitude profiles of ground magnetic perturbations show a step in the east component at certain local times (Hughes and Rostoker, 1977). This has been interpreted as net field-aligned current out of the auroral oval. Radar observations of ionospheric electric field combined with models of conductivity based on precipitating electrons show net field-aligned currents, in after noon and out before midnight (Foster *et al.*, 1989). Approximately 20% of the total Region 1–2 current closes in this manner.

In Fig. 21 the partial ring current is depicted as closing through particle drifts centred on the dusk side of the earth. It is not known if this closure

is correct. Crooker and Siscoe (1981) point out that simulations of magnetospheric convection by Harel *et al.* (1981) produce a partial ring current centred on midnight as depicted in Fig. 17. Statistical summaries of plasma pressure at synchronous orbit are consistent with a midnight centred ring current (Garret and DeForest, 1979). However, if the closure of the electrojet current is broadly distributed throughout the outer magnetosphere beyond the location of the ring current, it would be difficult to observe with spacecraft instruments. Models of a partial ring current show that most of the ground disturbance is produced by the field-aligned portions of the current system (Crooker and Siscoe, 1974). Thus ground observations provide little insight into the current closure.

As will be explained below, the return flow in the magnetosphere does not penetrate all the way to the Earth's atmosphere. Instead, its velocity goes to zero inside a boundary called the 'plasmapause'. The absence of convective flow inside this boundary implies that the magnetospheric electric field in this region is zero. Mapped to the ionosphere this requires that the ionospheric electric field and Pedersen current vanish equatorward of the projected boundary. To accomplish this the Pedersen current diverges upward along field lines as shown in Figs 17 and 19. On the dawn side this current is outward into the magnetosphere, and on the dusk side it is into the ionosphere. In Fig. 17 this portion of the Pedersen current system is labelled 'Region 2'.

A model for the viscous boundary layer developed by Sonnerup (1980) is summarized in Fig. 22. The diagram presents a view of the dawn meridian as seen from the Sun. Region 1 field-aligned currents flow into the ionosphere throughout the entire boundary layer and outer part of the return flow. Region 2 field-aligned currents flow out of the ionosphere from the inner edge of the return flow (assumed to be the plasmapause), to the maximum of the return flow. These currents are distributed currents rather than sheet currents because of the radial variation in flow velocity pictured in the bottom left inset. A radial variation in flow velocity corresponds to a radial variation in electric field. When this field is projected on the ionosphere it drives a spatially varying Pedersen current which must diverge along field lines to establish current continuity. Neither the field-aligned currents nor the transverse current are entirely balanced in the meridian plane. Some transverse current must flow completely across the regions of flowing plasma to transfer forces to the flow. In both regions the $(\boldsymbol{J} \times \boldsymbol{B})$ force due to this fraction of the transverse current is directed sunward. In the boundary layer the force is opposite to the motion of the flowing plasma slowing it down. In the return flow it is in the same direction accelerating it. Because of the divergence of electric field at the inner edge of the boundary layer the field-aligned current entering the ionosphere

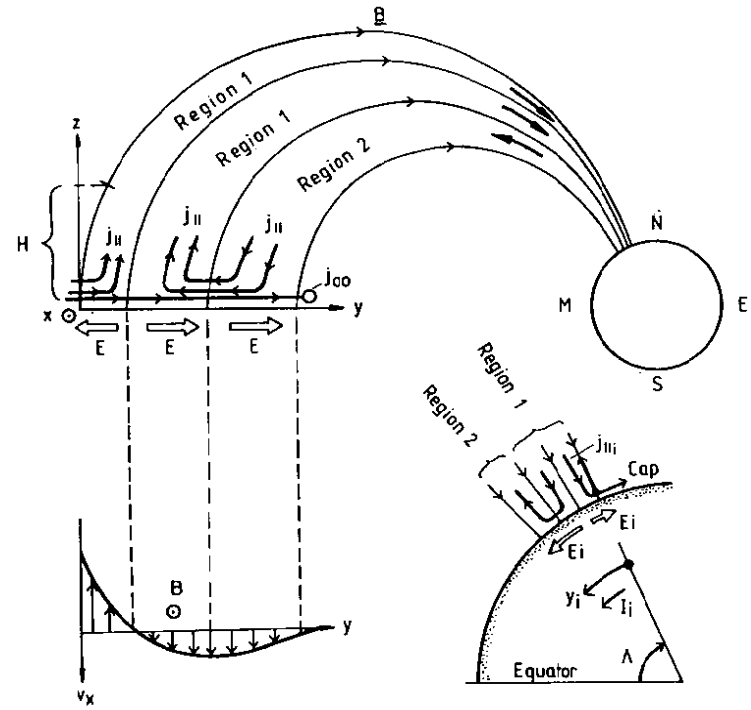

Figure 22. A view of the morningside meridian plane showing the low-latitude boundary layer and return flow. Field-aligned currents generated by gradients in flow velocity are closed by ionospheric Pedersen current (Sonnerup, 1980).

splits at the projected location of the flow reversal. Current that flows equatorward in the ionosphere must eventually return upward along field lines since the ionospheric electric field vanishes equatorward of the projected inner edge of the return flow. The remainder of the inward field-aligned current closes across the polar cap. On the outer edge of the boundary layer the unbalanced transverse currents close either on the magnetopause or through the solar wind, connecting to their counterpart on the opposite side of the magnetosphere. If they close on the magnetopause the closed magnetosphere model suggests they would have to flow along field lines leading to the polar cusp, closing westward through the ionosphere at the foot of the cusp. In a more realistic magnetosphere with an open polar cap their closure is less certain. At the inner boundary of the return flow the unbalanced currents close through particle drifts in the magnetosphere. For example, they probably flow westward around midnight through the inner edge of the tail current, connecting to unbalanced

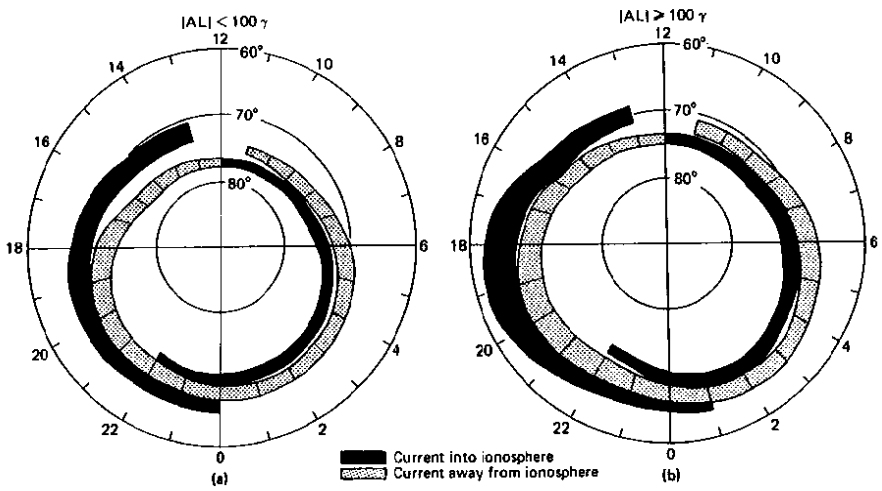

Figure 23. A polar projection showing the average locations in which field-aligned currents are observed entering the ionosphere. The high-latitude ring is named Region 1 and the low-latitude ring, Region 2. Dark shading indicates downward current (Iijima and Potemra, 1978).

currents on the dusk side. These possible closures are shown schematically in Fig. 17.

The field-aligned currents described above are experimentally observed by magnetometers on polar-orbiting spacecraft (Iijma and Potemra, 1976). The two regions of field-aligned current almost completely circle the Earth as shown in ionospheric projection in Fig. 23. The higher latitude current, which presumably originates in the boundary layer and outer portion of the return flow, was named the 'Region 1 current'. The lower latitude current was named 'Region 2'. The currents in each region switch direction near noon and midnight. Statistical results suggest that these two currents are always present in the magnetosphere (Bythrow *et al.*, 1983). Together they create a very large solenoidal current system whose magnetic effects are almost entirely confined to the region between the two cylindrical sheets of current.

3.1.4 Corotation and the plasmasphere

The rotation of the Earth is a second important source of electrical field in the magnetosphere. As illustrated in Fig. 24 this field originates in negative charge forced to the Earth's surface by the Lorentz force $q(v \times B)$ on electrons rotating with the Earth through its own magnetic field (Davis, 1948; Hones and Bergeson, 1965). If only vacuum surrounded the Earth

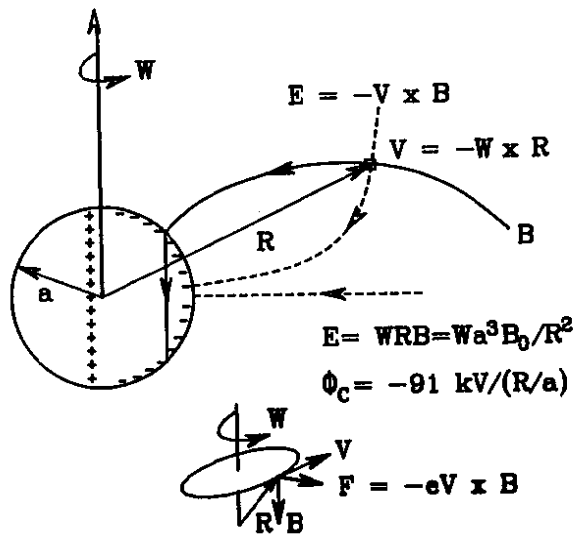

Figure 24. Creation of the corotation electric field through rotation of the Earth. Inset shows Lorentz force on electrons in Earth's surface and atmosphere. Surface charge is modified by field-aligned currents to produce electric field everywhere orthogonal to magnetic field.

this electric field would be that of a quadrapole with components both parallel and perpendicular to the magnetic field (Davis, 1947). Since the magnetosphere is filled with highly conducting plasma, the parallel component of electric field drives currents along field lines. These close through the ionosphere creating a distribution of charge in the magnetosphere for which the total electric field is orthogonal to the magnetic field. This electric field forces all zero-energy charged particles to corotate with the Earth (Birmingham and Jones, 1968).

The electric fields due to corotation and convection are superposed in space around the Earth and cause more complicated plasma drifts than either alone (Brice, 1967a; Kavanagh *et al.*, 1968). Figure 25 displays the particle drift paths (equipotentials) caused by these two sources and their superposition. As a first approximation, drift paths for the return flow are straight lines transporting plasma from the tail to the dayside magnetopause (top left). Drift paths for corotation are circles around the Earth (top right). In the superposed fields, the drift paths are divided by a separatrix into two types. Inside the separatrix particles corotate in closed loops. Outside they drift along paths somewhat like those produced by the solar wind convection alone. However, drift paths close to the separatrix tend to curve around the earth in the direction of corotation. Because cold particles

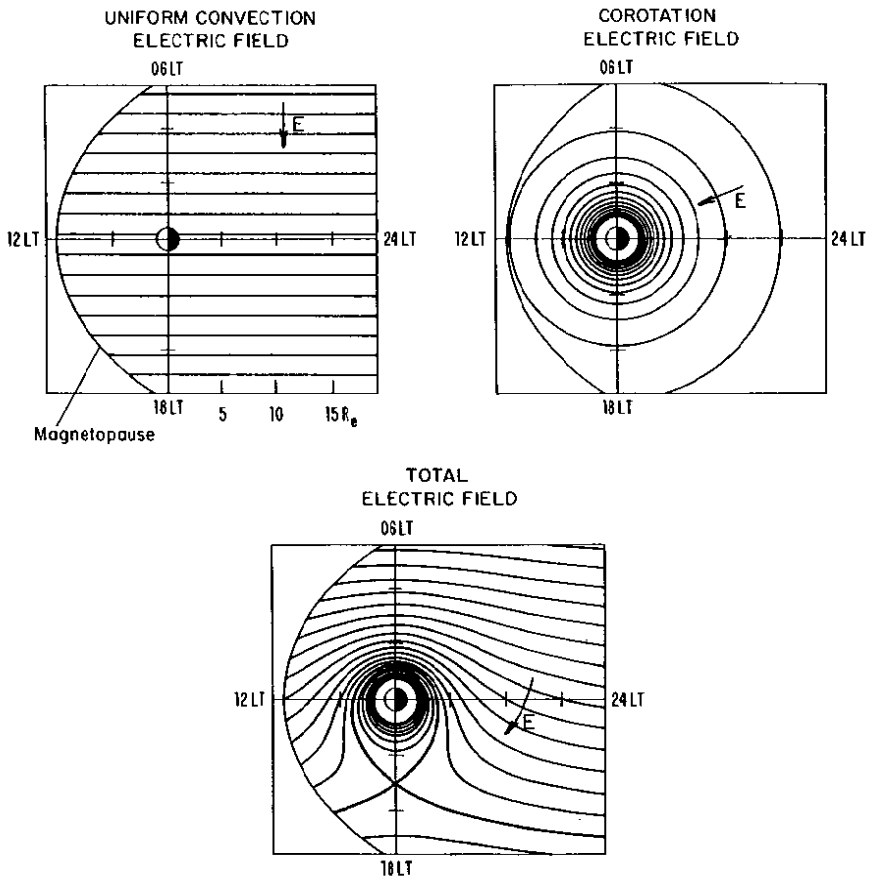

Figure 25. Equipotential patterns produced by convection, corotation and their superposition. In steady state the separatrix between open and closed drift paths creates the plasmapause, a boundary between regions of high and low plasma density (Lyons and Williams, 1984).

drifting sunward from the tail can not penetrate inside the separatrix, this part of the magnetosphere is called a 'forbidden region' for particles originating in the tail.

The ionosphere is a source of cold plasma which, if given sufficient time, can fill a flux tube to high densities (Angerami and Thomas, 1964; Park, 1970). Interior to the separatrix flux tubes circulate the Earth continuously. This provides the time necessary for them to fill. By comparison, flux tubes exterior to the separatrix drift entirely through the magnetosphere in less than a day. This is too fast for the ionosphere to fill them before convection

dumps them into the magnetosheath. As a consequence, the plasma density inside the separatrix becomes significantly larger than it does outside. This boundary between regions of high and low plasma density is called the 'plasmapause'. The high-density interior region is called the 'plasmasphere' (Nishida, 1966; Brice, 1967b). Provided the convection electric field remains stable, the separatrix and the plasmapause are colocated. If there is a sudden increase in convection electric field the separatrix moves quickly inward leaving a region of high-density plasma on drift paths outside the new separatrix. Within about a day, electric field drift dumps this plasma into the magnetosheath. Until this process is complete the separatrix and the plasmapause are located at different distances from the Earth. Conversely, if the convection field decreases, the separatrix moves outward and there is a region inside the new separatrix which takes about a week to fill with ionospheric plasma.

3.1.5 The Van Allen radiation belt and the ring current

The behaviour of energetic particles in the Earth's field is more complex than it is for the cold particles described above (Chen, 1970). Although energetic particles experience the same electric field drift as cold particles, they also drift because of curvature and gradient in the earth's magnetic field. These drifts are charge dependent as illustrated in Fig. 26. Energetic ions drift westward (from midnight towards dusk) while electrons drift eastward. Since charges of opposite sign are moving in opposite directions they create a westward current. The effect of this current at the Earth's surface is a magnetic field directed from north to south parallel to the earth's dipole axis. For low latitudes this effect is observed as a decrease in the horizontal component. Trapped energetic particles constitute the outer Van Allen radiation belt, and the westward current due to their drift is the cause of magnetic storms.

Energetic particles in the outer Van Allen radiation belt are inside the region forbidden to particles drifting earthward from the tail. Those particles become trapped in this region through fluctuations in the convection electric field (Roederer and Hones, 1974). Whenever this is enhanced the boundaries of the forbidden regions shrink earthward (Kivelson *et al.*, 1980). Particles from the tail drift into the newly accessible region. Given a steady electric field they would eventually drift out to the magnetopause. But the electric field is not steady. When it decreases, the forbidden region expands, trapping the drifting particles on closed drift paths. At a later time the electric field is again enhanced. Any particle drifting through the night side will be moving in the direction of the enhanced field and will gain energy and move closer to the Earth. A particle on the day side loses energy

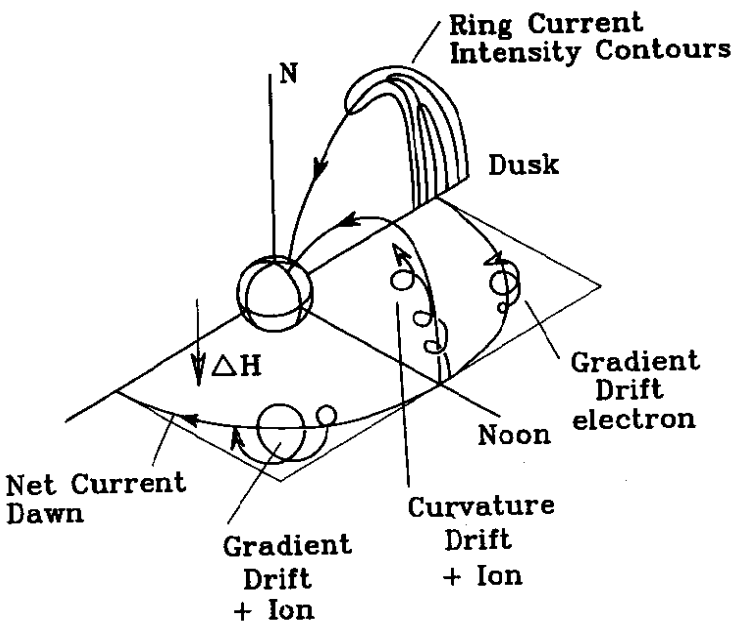

Figure 26. A perspective view of the dayside radiation belt showing creation of the westward ring current by gradient and curvature drift of energetic particles. Contours of constant current form nested toroids around the Earth.

and moves away from the Earth. However, when the electric field decreases suddenly the particle location and energy remain unchanged. A sequence of fluctuations of this type allows some particles to diffuse to high energies (Lyons and Schulz, 1989). The rapid drift and close proximity to the Earth of these more energetic particles are the primary causes of the storm ring current.

3.1.6 Shielding of the plasmasphere

Another important consequence of gradient and curvature drift is electrical shielding of the plasmasphere from the magnetospheric electric field (Schield *et al.*, 1969). As finite-energy particles approach the Earth under the influence of the superimposed electric fields they begin to gradient and curvature drift across the equipotentials of the total electric field. On the night side, the drift is such that both electrons and ions gain energy from the electric field. Also, the curvature and gradient drifts keep the higher energy electrons from approaching the Earth as closely as lower energy electrons. This makes the size of the region forbidden to electrons drifting

from the tail larger for higher energies. For protons the drifts are opposite to corotation and finite-energy ions come closer to the Earth than cold particles. However, the proton drift paths have several separatrices that change with energy. At sufficiently high energies the shape of the forbidden region becomes a somewhat smaller, mirror image of that for electrons. Figure 27 illustrates the differences in the shapes of the forbidden regions for particles of opposite sign. The figure shows that there are regions centred on the dawn and dusk meridians that are inaccessible to particles of one or the other sign. Particles of other energies including cold ionospheric particles may enter this region. Even so there remains a slight accumulation of charge which produces a polarization electric field. The

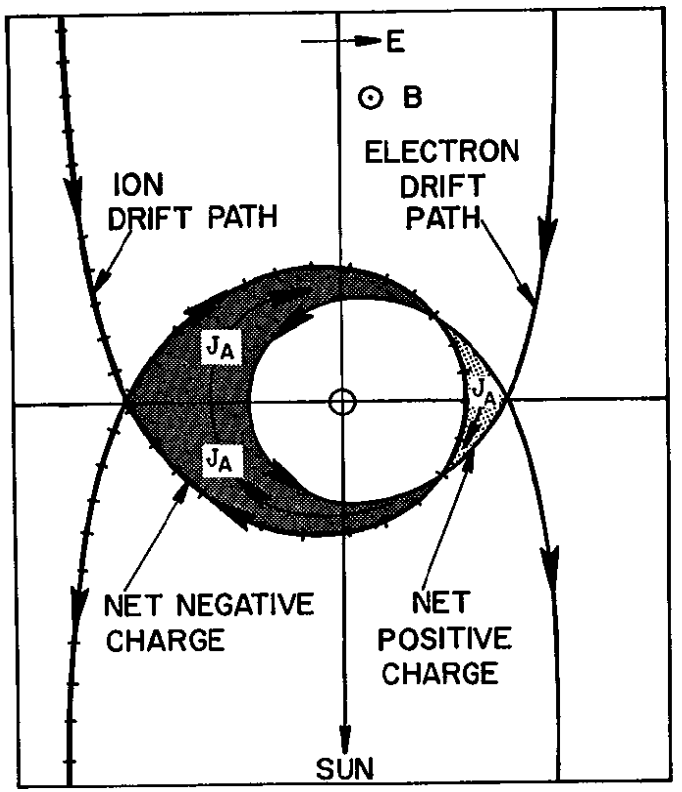

Figure 27. Gradient and curvature drift of energetic particles in the magnetosphere produce forbidden regions in the inner magnetosphere that particles convecting from the tail cannot enter. A difference in the shapes of the electron and ion regions allows space charge to develop, producing an electric field which shields the plasmasphere from the external electric field (Schield *et al.*, 1969).

direction of this field is from dusk to dawn opposite to the convection electric field. Within the plasmasphere this polarization electric field cancels the external field, shielding the plasma from its effects. This process is self-limiting, since when there is no electric field the drift paths are not asymmetric.

A third consequence of the asymmetric drift is the Region 2 field-aligned currents described earlier. Because the magnetospheric electric field vanishes inside the plasmapause, the ionospheric electric field at the feet of the plasmapause magnetic field lines also vanishes. Ionospheric currents driven by this electric field must therefore diverge into the magnetosphere at this boundary. This current is partially carried by ionospheric particles flowing outward to cancel the space charge distributions.

3.1.7 Summary of features of closed model

In summary, many features of the observed magnetosphere may be explained on a basis of the closed model of the magnetosphere. The shape and location of the magnetopause are accounted for by balancing normal stress of solar wind particles against the Earth's magnetic field. The tail magnetic tail and magnetospheric convection could be a consequence of tangential drag created by a viscous interaction in low-latitude boundary layers. Ionospheric electric fields, ionospheric Pedersen currents and field-aligned currents are understood by assuming that closed field lines are equipotentials which map the magnetospheric electric field onto an ionosphere having a spatially varying conductivity. The auroral electrojets are produced by concentration of the ionospheric Hall current in high-conductivity channels produced by particle precipitation. The plasmasphere and the sharp inner boundary for convection earthward from the tail are a consequence of superposition of the electric field of the rotating Earth and convection. Shielding of the plasmasphere and the Region 2 field-aligned current results from difference in the drifts of positive and negative particles of finite energy. The ring current is produced by drift energization and trapping of particles during fluctuations of the convection electric field.

There are several observed features of the magnetosphere which are not explained by this model. They include easy access of solar particles to the polar caps, the existence of a sharp outer boundary to the tail plasma sheet, and the strong dependence of all convection related phenomena on the orientation of the solar-wind magnetic field. To explain these we must discuss an alternative hypothesis for the cause of magnetospheric convection—magnetic reconnection.

3.2 The open magnetosphere

3.2.1 Neutral lines and reconnection

Dungey (1961) was the first to suggest that the magnetosphere is open to the solar wind. He recognized that when the solar-wind magnetic field is antiparallel to the Earth's dipole field at the front of the magnetopause, neutral lines can form in the superposed magnetic fields. The top panel of Fig. 28 illustrates his idea. The solar wind magnetic field is pressed against the Earth's field and merges with it along an 'x-type neutral line'. Subsequently, the solar wind carries the pieces of interconnected field lines over the poles and downstream where they eventually drift together in the equatorial plane reconnecting at a second x-type neutral line.

The two x-type neutral lines in the Dungey model are actually segments of a single, closed neutral line that separates the magnetic fields of the solar wind and Earth. The locus of this neutral line in the equatorial plane is illustrated in Fig. 29. As can be seen by examining Fig. 28, field lines crossing the equatorial plane inside the neutral line, but outside the Earth's surface are closed with both feet attached to the Earth. Field lines crossing

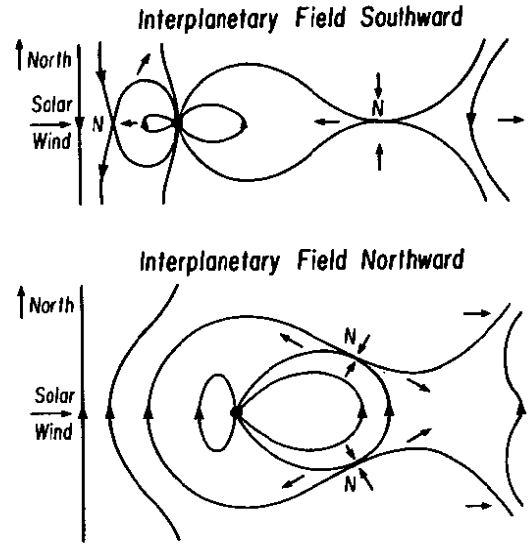

Figure 28. Magnetic reconnection between the solar-wind magnetic field and the Earth's magnetic field at x-type neutral lines. Top panel shows situation for antiparallel fields. Bottom panel shows case of parallel fields (from Russell, 1972, adapted from Dungey, 1963).

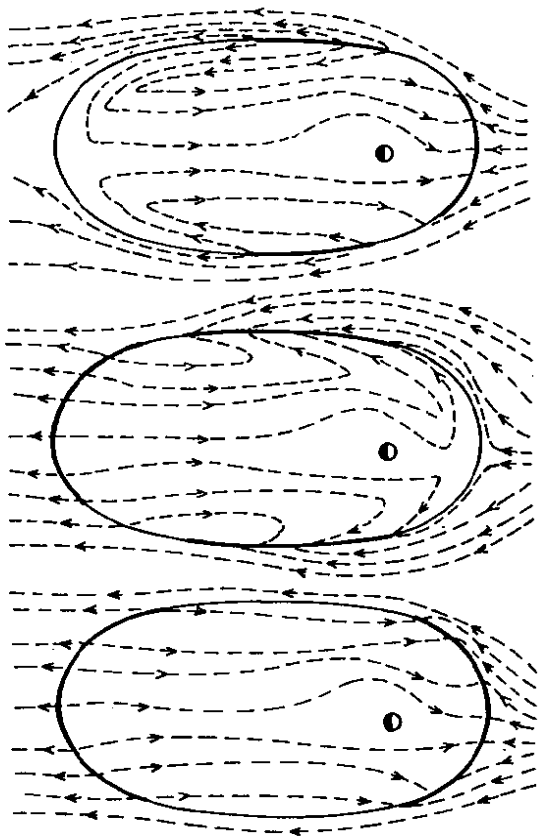

Figure 29. A closed neutral line separates the magnetic fields of the Earth and solar wind when they are antiparallel. Three panels indicate magnetospheric convection expected for different locations of reconnection along the neutral line (Vasyliunas, 1984).

the equator inside the Earth are open with one foot on the Earth and the other in the solar wind. Those crossing outside the neutral line are solar-wind field lines. The 'last closed field lines' are those which connect to the neutral line. These field lines map to closed circles around the magnetic poles and form the boundary of the polar cap. By definition the polar cap is the region poleward of this boundary within which all field lines are open to the solar wind.

Merging and reconnection need not occur everywhere along the neutral line connecting the day- and nightside neutral points of the Dungey model. According to Vasyliunas (1984) it is likely to occur on the front side only

where the solar wind magnetic field is compressed against the Earth's field by the flow of the solar wind (see heavy line in bottom panel of Fig. 29). For similar reasons it is expected to occur on the night side only where field lines drifting across the lobes first come together. Along the sides the solar-wind magnetic field is more likely to slip along the magnetopause without reconnecting, contrary to the suggestion made in the top two panels.

If the magnetosphere is to be in steady state, merging behind the Earth must balance merging on the day side. Otherwise, the amount of magnetic flux in the polar caps would increase while that in the closed regions would decrease. Furthermore, there must be a return flow that transports magnetic flux reconnected on the night side back to the day side. Figure 30 illustrates this entire process showing how rates of dayside merging, transport over the polar cap, nightside reconnection and return must balance to create a steady state.

According to the Dungey model, field lines open to the solar wind allow the solar-wind electric field ($\boldsymbol{E}_{sw} = \boldsymbol{v}_{sw} \times \boldsymbol{B}_{sw}$) to map directly onto the polar ionosphere. For example, above the northern magnetic pole the antisunward solar-wind velocity and southward magnetic field create a dawn-to-dusk electric field across the polar cap. Inside the magnetosphere the return flow from the distant neutral line generates an electric field which is also from dawn to dusk. By comparison with our previous discussion it will be seen that this pattern is identical to that produced by the viscous interaction. Thus magnetic reconnection can also explain phenomena within the magnetosphere which depend on a dawn-to-dusk electric field. Since it is

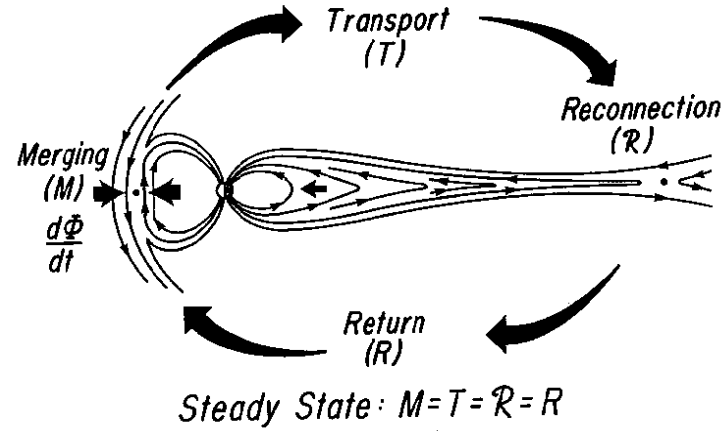

Figure 30. Magnetospheric convection induced by reconnection transports magnetic flux in closed paths through the magnetosphere. Four rates must be equal to produce a steady state.

experimentally observed that convection and magnetic activity become nearly unobservable when the interplanetary magnetic field is northward, it has been concluded that reconnection is more important than the viscous interaction in the Earth's magnetosphere (Cowley, 1982a).

3.2.2 *Boundaries of plasma sheet and ring current*

A major problem with the closed magnetosphere model is that it does not provide an explanation for the sharp outer boundaries of the plasma sheet. The open model explains these very simply in terms of the field topology produced by reconnection. In Fig. 31, field lines in the tail lobes are open and connected to the solar wind. Field lines interior to the plasma sheet are closed and connected to the Earth. Any charged particle gyrating about a field line within the plasma sheet is trapped by the geometry of the field. As particles spiral towards the atmosphere they are reflected by the converging magnetic field. They then travel back along the field line crossing the neutral sheet to be reflected again in the converging field of the opposite

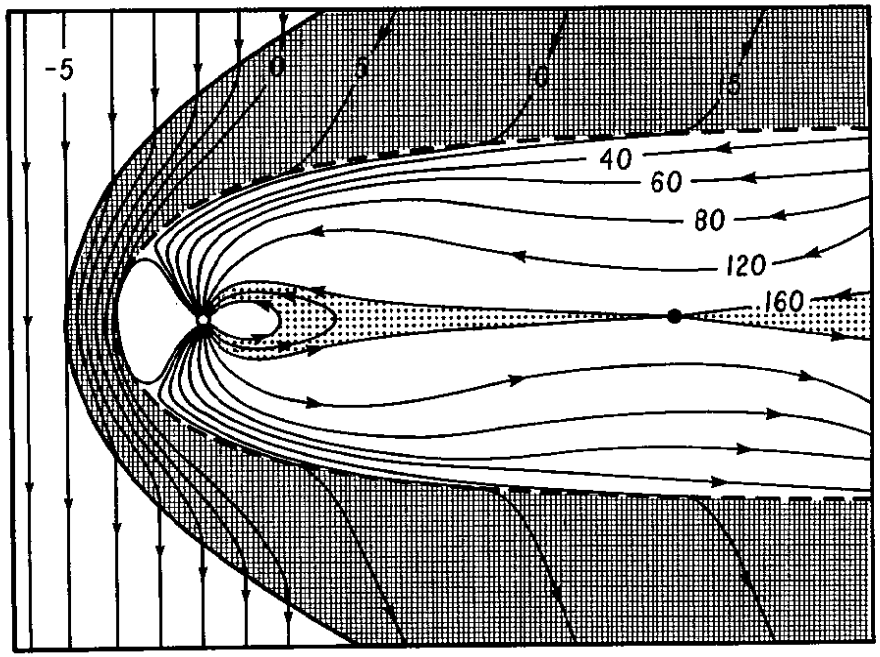

Figure 31. Magnetic field topology in the open magnetosphere. The outer boundaries of the plasma sheet are defined by the last closed field lines (McPherron *et al.*, 1973a).

pole. In contrast, any particle travelling away from the Earth on a lobe magnetic field line is usually lost to the solar wind. Thus, a sharp gradient in particle density develops much as it does at the plasmapause.

The plasma sheet also has an inner edge defined by particle drifts. In steady state, cold particles (zero magnetic moment) flowing earthward cannot penetrate deeper than the plasmapause. Electrons with finite initial energy penetrate less deeply than this because their gradient and curvature drift add to the electric drift turning them at greater radial distances. The greater the initial electron energy the further from the Earth the electron is turned. This produces a relatively sharp inner edge for the electrons in the plasma sheet, and a characteristic increase in electron temperature as radial distance increases (Vasyliunas, 1968).

For ions the situation is much more complex (Chen, 1970; Grebowsky and Chen, 1975). Cold ions drifting sunward from the tail are forbidden entry to regions interior to the plasmapause as are cold electrons. However, ions of slightly higher initial energy (magnetic moment) penetrate closer than the plasmapause. The reason for this is that gradient and curvature drift oppose corotation drift allowing the convection drift to bring ions closer to the Earth. However, ion drifts are very sensitive to the initial magnetic moment of the particle as illustrated in Fig. 32. As the magnetic moment increases, the forbidden regions become singular and change shape. For high moments the shape of the forbidden region is nearly the mirror reflection of the plasmapause, bulging outward at dawn rather than dusk.

Ion and electron drift are generally considered to be adiabatic conserving the first two invariants of particle motion (μ and J). Conservation of $\mu = W_\perp/B$ requires that the perpendicular energy of a particle increase as it drifts into regions of increasing magnetic field. The shapes of forbidden regions are generally shown for particles of fixed μ. Forbidden regions can also be calculated for particles of fixed energy. Grebowsky and Chen (1975) have studied the way in which these change in response to a sudden enhancement of magnetospheric convection. Figure 33 displays results of these calculations. The top left panel shows the initial situation with weak convection. The shaded region is the plasmasphere. Dotted, dashed and solid lines show forbidden regions for progressively higher energy ions. It is apparent that 10 keV ions can penetrate well inside the plasmapause, but still higher energy 40 keV ions cannot. Successive panels show the temporal evolution of these forbidden regions after a sudden enhancement of convection. The regions initially develop long tails which rotate around the Earth. Eventually the shape of the regions stabilize with ions drifting much closer to the Earth. Ions of 40 keV that were initially excluded from the plasmasphere then have total access to the dusk side of the magnetosphere.

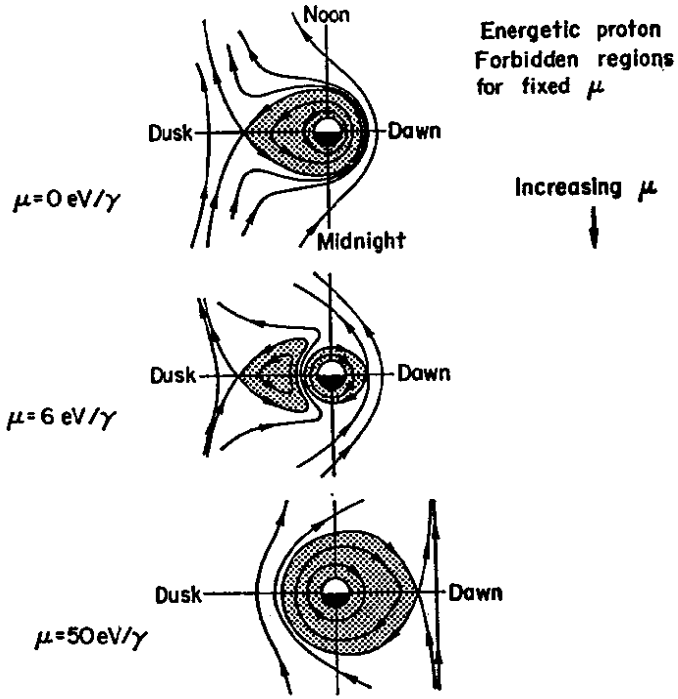

Figure 32. Drift paths followed by ions convecting sunward in the plasma sheet depend critically on magnetic moment of the ion (Grebowsky and Chen, 1975).

A typical magnetic storm consists of many fluctuations in the external convection electric field. Changes in magnetic field accompany each fluctuation. Clearly, the forbidden regions for ions in the real magnetosphere are more complex than those calculated for a step function change in electric field with drift in a dipole field. However, it is apparent that once the convection electric field decreases the forbidden regions will again expand, trapping ions and electrons inside the new boundaries. This process is a major factor in the creation of the storm time ring current.

As soon as the boundaries expand outward the ionosphere begins to fill the region interior to the expanded plasmapause. The density of cold particles increases and the ions and electrons in the ring current become unstable to the generation of cyclotron waves. As the particles give up energy to the waves their pitch angle decreases (Brice, 1964). This allows them to mirror nearer the atmosphere. Eventually the particles may be scattered into the loss cone, collide with atmospheric particles and be lost to the ring current. Ions can be lost by charge exchange as well (Smith *et al.*,

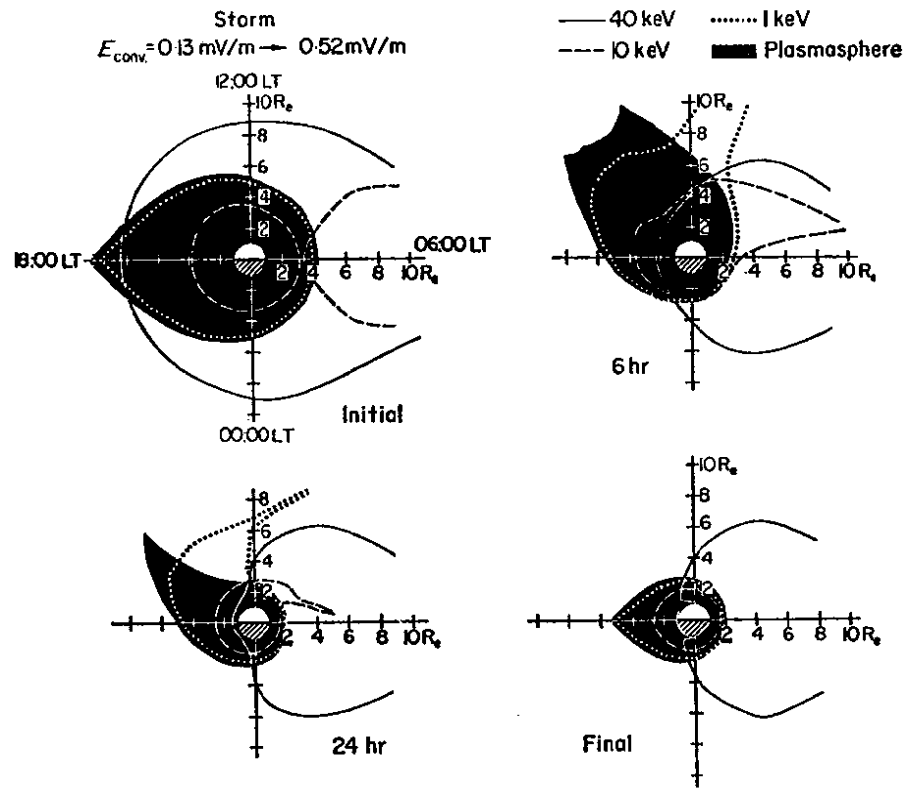

Figure 33. Forbidden regions for ions of specific energy and how they change in response to a step function change in convection electric field (Grebowsky and Chen, 1975).

1981). In this process a cold hydrogen atom located close to the Earth exchanges an electron with the energetic ion. The ring-current is converted to an energetic neutral atom which is lost from the ring current. A cold ion that creates no significant current replaces it. These loss processes are the primary cause of decay of the ring current.

3.2.3 The plasma sheet boundary layer

The upper and lower boundaries of the plasma sheet are considerably more complex than a simple discontinuity between open and closed magnetic field lines (Eastman and Frank, 1984; Eastman *et al.*, 1985). Numerous studies (e.g. review by Takahashi and Hones, 1988) have shown that the transition from central plasma sheet to magnetic lobes is through boundary

layers of thickness 0.5–1 R_e. The characteristic feature identifying these layers is counterstreaming ion beams. Typical plasma parameters for these layers include densities of 0.1–0.3 cm^{-3}, bulk flow speeds 100–700 $km\,s^{-1}$, and mean energies of 0.5–5 keV. Figure 34 shows the structure of one of these layers. In the lobe a plasma instrument normally detects only cold electrons. As a spacecraft enters the plasma sheet the instrument begins to observe hot electrons. Somewhat deeper it detects energetic ion beams streaming earthward along the magnetic field. Deeper still the average energy of the earthward beams begins to decrease, while at the same time the more energetic ion beams are observed streaming tailward. Close to the neutral sheet the plasma distribution becomes isotropic with no detectable streaming. The regions next to the north and south lobes within which the hot electrons and streaming ions are observed are called the 'plasma sheet boundary layers'. The region of isotropic plasma is called the 'central plasma sheet'.

The structure of the plasma sheet boundary layer can be explained as a consequence of the cross-tail electric field and the weak magnetic field near the distant neutral line (Speiser, 1965; Lyons and Speiser, 1982; Cowley,

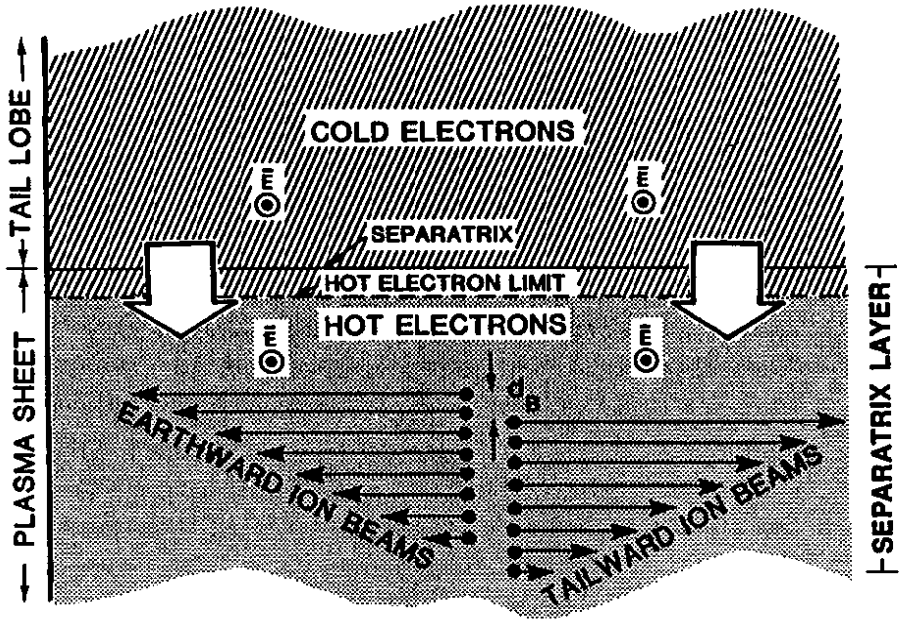

Figure 34. A schematic illustration of the structure of ion beams in the plasma sheet boundary layer (from Takahashi and Hones, 1988, adapted from Forbes *et al.*, 1981).

1985). For reasons to be explained below, assume that energetic electrons and protons are accelerated earthward along closed field lines somewhere near this neutral line. As these charges travel earthward they also drift towards the neutral sheet with a velocity $V_d = (E \times B)/B2$. Electrons travel so fast along a field line that they do not drift a significant distance perpendicular to the field before they are reflected at the foot of the field lines and reappear in the plasma sheet travelling tailward. They are thus observed just below the last closed field line connected to the neutral line. For the same energy, protons with their larger mass travel along field lines 40 times slower than electrons. For them, the E-field drift is significant, and by the time they are reflected near the Earth they have drifted to lower latitude field lines. They are thus seen travelling tailward somewhat lower in the plasma sheet.

After reflection at the ionosphere the electrons and ions try to follow field lines as they curve across the neutral sheet and enter the opposite hemisphere. For low-energy electrons this transition is relatively easy, but higher energy electrons and protons have larger gyroradii, and find it more difficult. As they try to follow the sharp bends in the field they are scattered in pitch angle emerging on the other side of the neutral sheet with nearly isotropic distributions (Lyons, 1984). As they continue to bounce they drift earthward. The region of isotropic ions earthward of where the first reflected ion beam tries to cross the neutral sheet constitutes the central plasma sheet. The region tailward of this is the source of the boundary layer.

To understand the gradual decrease in energy of the ion beams in the boundary layer we must consider a process first suggested by Dungey (1953). Figure 35 illustrates the basic idea which was later developed in detail by Speiser (1965, 1967). Ions drifting adiabatically in the crossed electric and magnetic fields of the tail lobe enter the plasma sheet. If the ion gyroradius is large compared with the thickness of the current sheet they begin to execute serpentine motion (now called 'Speiser orbits') as they are turned in opposite directions by the magnetic field above and below the current sheet. This motion allows the ions to drift in the direction of the cross-tail electric field, gaining energy from it. When there is a weak vertical component of magnetic field across the current sheet it causes the ions to gyrate about a vertical axis, curving earthward as they do so. At some point the velocity of the ions becomes nearly field-aligned and they leave the current sheet, travelling earthward nearly parallel to a field line.

The amount of energy gained by an ion depends on how far it drifts in the cross-tail electric field. The weaker the vertical component, the larger the radius of gyration, and the greater is the energy gained. Since the vertical field is weakest at the neutral line, particles which enter the plasma

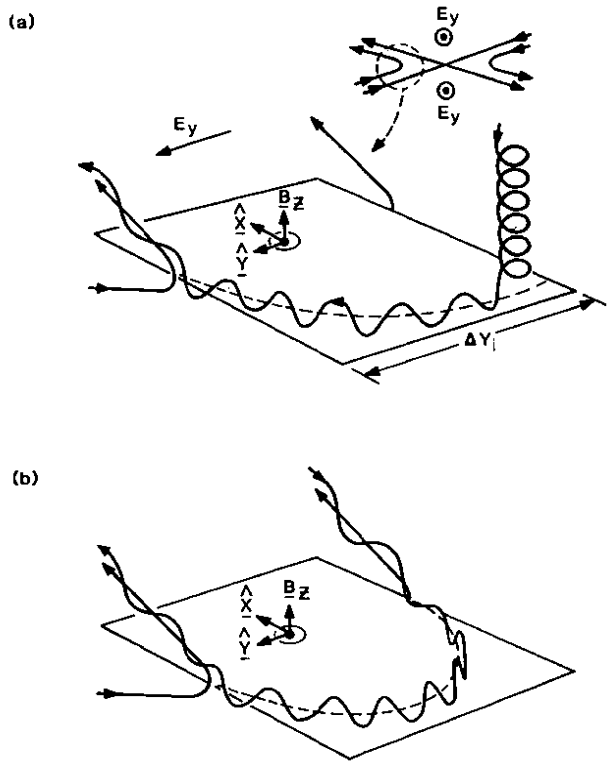

Figure 35. Acceleration of charged particles by non-adiabatic drift across plasma sheet electric field. Top panel shows stationary frame while bottom panel shows frame drifting with convecting flux (Cowley, 1985).

sheet from the lobe near the neutral line gain the most energy. Thus the ions leaving the current sheet along the outer boundary of the plasma sheet are the most energetic. Earthward of the neutral line ions exhibit the same behaviour, but the vertical magnetic field is stronger. They consequently turn faster and gain less energy from the electric field. These ions travel along field lines which map to Earth deeper inside the plasma sheet (below the last closed field line). Some ions emerge from the plasma sheet at locations where higher energy ion beams reflected at the Earth are returning to the plasma sheet. Thus, as a spacecraft enters the plasma sheet it encounters ions of less and less energy which have originated in the current sheet closer and closer to the location of the spacecraft. Eventually it passes through a layer of counterstreaming ion beams and finally enters a region of isotropic ions.

3.2.4 The polar mantle

There are also boundary layers at the interface between the magnetotail lobes and the solar wind. Because these layers cover the entire region of the tail above a polar cap, they are referred to as the 'polar mantle' (Rosenbauer *et al.*, 1975; Sckopke and Paschmann, 1978). Along the Earth's polar axis the average thickness of those layers is about 2 R_e, but downstream they gradually expand to fill both tail lobes. For a spacecraft inbound from the magnetosheath through the upper boundary of the tail, the layer is first observed as a sudden rotation of the magnetic field from an arbitrary and turbulent field in the magnetosheath to a steady field oriented along the Earth–Sun line. The plasma just inside the boundary streams tailward with velocity of order 200 km s^{-1} and with density and temperature comparable to that of the magnetosheath. Deeper in the magnetotail, the plasma density, streaming velocity and temperature decrease until no plasma is detectable with ordinary plasma instruments. From here to the plasma sheet boundary is the region referred to as the lobe magnetic field. The most sensitive plasma instruments observe cold plasma in this region, but with densities and temperatures too low to affect the total pressure significantly (Eastman and Frank, 1984).

The polar mantle is produced by electric field drift as is the plasma sheet boundary layer. Figure 36 illustrates the basic features of this mechanism. Ions accelerated by reconnection at the subsolar x-line form a layer of particles just inside the magnetopause. These ions follow newly reconnected field lines from the merging region down into the polar cusp where most are reflected by the converging magnetic field. At the same time as the ions are guided by the field they simultaneously drift in the dawn-to-dusk electric field present on the newly interconnected field lines. At first this drift is poleward away from the Sun. Later, as the field lines and ions leave the cusp the drift is towards the plasma sheet. For the most energetic ions the drift velocity is small relative to the particle's velocity parallel to the field line. These ions drift only a short distance before they emerge from the cusp (see solid circles in figure). Consequently, they emerge streaming tailwards on field lines close to the magnetopause. Less energetic ions with the same pitch angle (open circles) penetrate the cusp just as deeply, but travel more slowly. They thus have a longer time to drift poleward while near the bottom of the cusp. These ions emerge on field lines much deeper in the tail lobe. Note that the diagram projects the trajectories onto an instantaneous view of the field. In actuality the particles are frozen to the drifting field lines.

The precise distribution of plasma properties in the polar mantle depends on the initial velocity distribution of the particles, where the particles enter

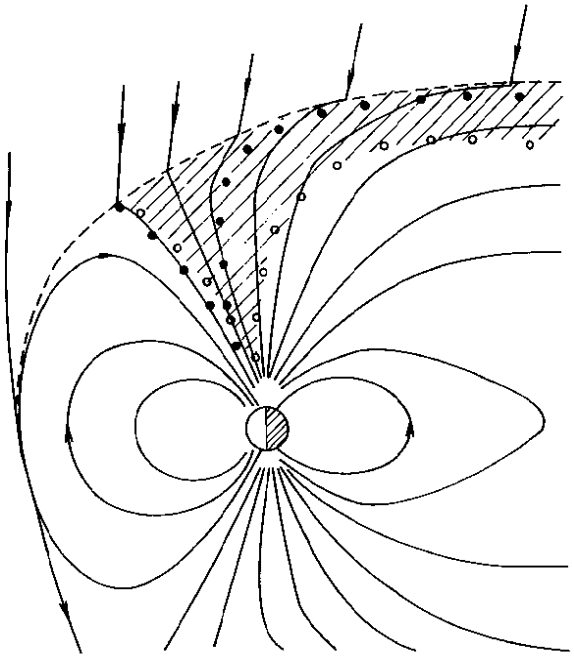

Figure 36. Creation of the polar mantle by electric field drift in the polar cusp. Solid and open circles show the respective trajectories of high and low energy charges (Rosenbauer *et al.*, 1975).

the tail, on the cusp magnetic field configuration, and the cross-tail electric field. Even so it is apparent that the ions that initially have the least energy and smallest pitch angle define the inner boundary of the polar mantle. The mantle thickens with distance down the tail as the ions drift towards the plasma sheet. Low-energy ions reach the plasma sheet closest to the Earth since their total velocity makes the largest angle to the lobe field. Increasingly more energetic ions reach the sheet with greater distance, until the distant neutral line is encountered. Particles with sufficient parallel velocity pass this neutral line before the field line on which they are streaming reconnects and are lost to the solar wind when their field line is cut.

Pilipp and Morfill (1978) have developed a quantitative model for the development of the polar mantle with distance down the tail. Their model considers two different particle sources. The first is entry via the polar cusp as illustrated in Fig. 36. The second source is a 'leaky magnetotail' in which particles enter uniformly everywhere along the top of the tail. The model with the distributed source predicts lower bulk velocities and higher densities at the distant neutral line than does the cusp entry model. Observations in the deep tail by the ISEE-3 spacecraft apparently support the distributed source (Slavin *et al.*, 1985). The implications of this are unclear since it is not apparent how particles can enter the top boundary of the tail flowing tailward parallel to field lines as assumed in the model. The topology of open field lines suggests solar wind particles must enter the magnetotail flowing towards the Earth rather than away. Perhaps reflection of such particles near the atmosphere is the actual source.

3.2.5 The day- and nightside neutral lines

The structure of an *x*-type neutral line is illustrated in Fig. 37. Two regions above and below a plasma interface are threaded by magnetic flux originating in different locations. When the fields are antiparallel a slab current flows in the interface. It is assumed that at some point the electrical conductivity of the plasma becomes finite decreasing the total current along a portion of the interface. The magnetic fields on either side can then diffuse into the interface producing an *x*-type configuration where the fields touch at only one point (Petschek, 1964). Once formed, the $\boldsymbol{J} \times \boldsymbol{B}$ forces in this configuration cause the fields to drift together. When they meet at the centre of the diffusion region they appear to be cut by mutual annihilation. The magnetic energy present in the inflowing plasmas is converted to

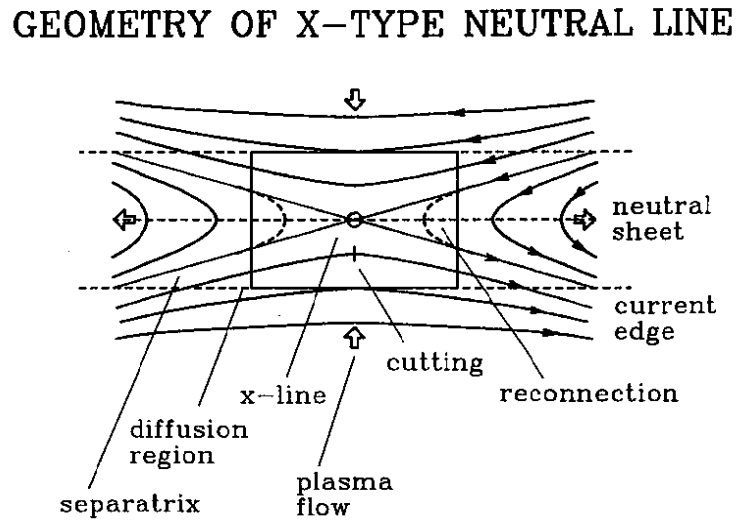

Figure 37. Reconnection at a steady-state neutral line. Two magnetized plasmas flow together and interconnect field lines in a diffusion region created by finite conductivity. Energized plasma flows out along the interface between plasmas.

kinetic and thermal energy of particles, which is forced to flow out of the diffusion region along the interface. When the flow emerges the fields appear to have reconnected in a new configuration with a weak magnetic field threading the interface. The field lines that just touch at the diffusion regions form separatrices between the topologically distinct regions of inflow and outflow.

In general, the conductivity of space plasmas is too high for diffusion to occur in a reasonable length of time. However, when the plasmas are driven together, as for example at the subsolar point on the magnetosphere, gradients in the magnetic field become extremely steep. When the scale of this gradient is shorter than an ion gyroradius inertial terms normally neglected in calculations of conductivity become important and the conductivity becomes finite. Alternatively, some source of wave turbulence may be established by an instability that grows on the gradient. The unstable waves scatter particles producing an anomalous resistivity. In either case the magnetic field can then diffuse into the interface as discussed above.

How finite conductivity develops in magnetospheric plasma is not yet known. However, the existence of an open magnetosphere and IMF control of magnetic activity provides evidence that it does develop. Although a complete theory remains to be worked out there have been numerous experimental attempts to identify the occurrence of x-type neutral lines. Initial work focused on a search for a steady-state neutral line on the dayside magnetopause of the type illustrated in Fig. 37. Both Paschmann *et al.* (1979) and Sonnerup *et al.* (1981) have reported evidence of its occurrence. However, as discussed by Sonnerup (1984) and Elphic (1990) there is considerable evidence that reconnection is more often localized and transient in the form of a flux transfer event or FTE (Russell and Elphic, 1978). A schematic drawing of half of an FTE is shown in Fig. 38. The drawing shows a single flux tube that has been reconnected and pulled out of the magnetopause boundary. It is now thought that during southward IMF a large number of FTEs are generated per unit time. The average effect of these is a relatively steady flow of newly opened flux that is transported over the polar caps as in steady state reconnection.

Until very recently the location of the nightside neutral line was not know. Almost all spacecraft in Earth orbit have had apogees near or inside the orbit of the moon. Data from these spacecraft indicated that most of the time the magnetic field is northward in the plasma sheet out to this distance (Mihalov *et al.*, 1968; Behannon, 1970). Observed gradients in lobe field magnitude suggested, futhermore, that the diameter of the magnetotail was still expanding at this distance. Occasional observations of southward magnetic field in the plasma sheet in association with magnetic

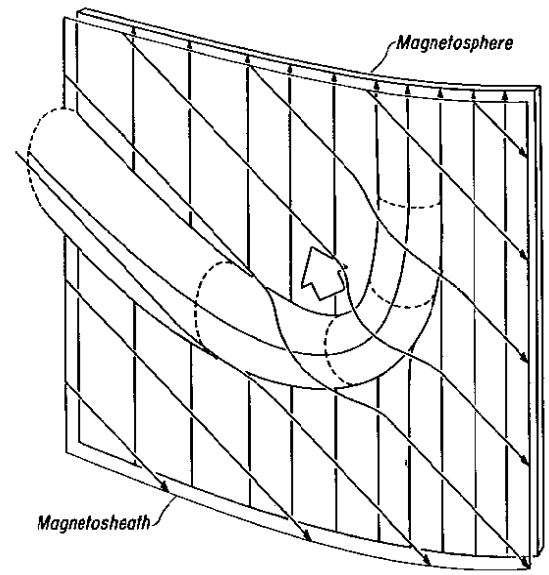

Figure 38. Schematic illustration of the magnetic field configuration north of the equator during a flux transfer event (FTE) (Russell and Elphic, 1978).

activity were interpreted as evidence that transient neutral lines were formed earthward of the Moon. However, there was no evidence of a permanent neutral line as there must be if polar-cap field lines are permanently open.

In 1982 the solar-wind monitor ISEE-3 was moved from the solar wind at the Sun–Earth Lagrange point 250 R_e upstream of the Earth into the tail. A series of complex manoeuvres were performed using the Moon for gravitational assistance. These altered the spacecraft trajectory so that it explored the tail from just inside the Moon's orbit at 60 R_e to beyond 220 R_e. The measurements show that at about 100 R_e the tail lobe field becomes constant, B_z in the plasma sheet becomes nearly zero, and the plasma sheet flow becomes continuously tailward and super-Alfvénic (Slavin and Kamide, 1986). These results suggest strongly that a neutral line is typically located at this distance. However, the absence of negative B_z in the tailward flowing plasma was perplexing. Slavin and Kamide (1986) examined this problem and found that the radial variation in average B_z in the plasma sheet depends on distance across the tail. Figure 39 summarizes their results. At 70 R_e average, B_z is positive at all values of Y across the tail. At 140 R_e, B_z becomes negative in a small region near the centre of the tail. At 200 R_e it is negative in a broader region. They concluded that the

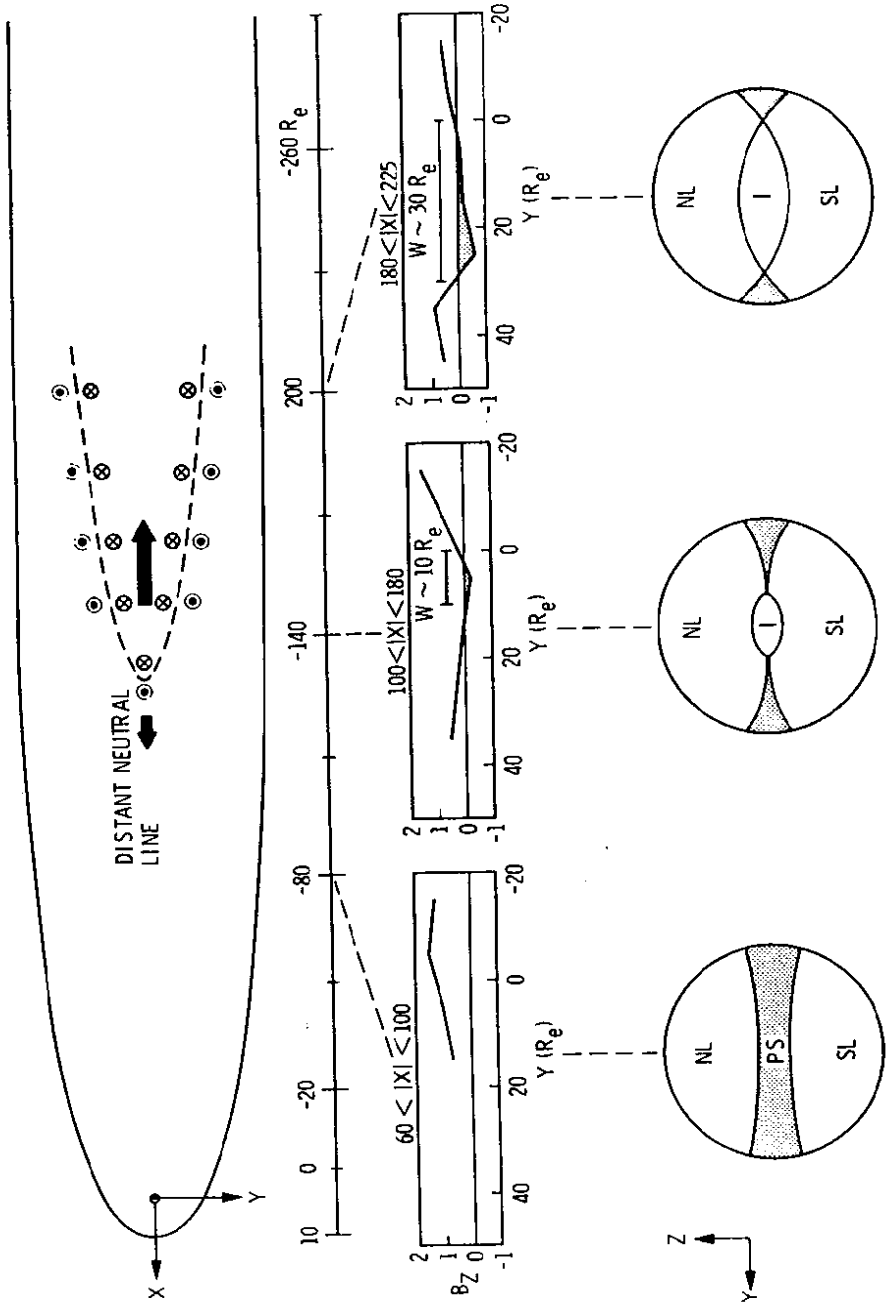

neutral line is parabolic in shape and opens tailward from the point where it is closest to the Earth at 120 R_e.

3.2.6 *Summary of features of the open model*

The most important feature of the open model of the magnetosphere is interconnection between the magnetic fields of the Earth and the solar wind. This interconnection is brought about by magnetic reconnection along a dayside segment of the neutral line separating the magnetic fields of the two plasma regimes. Once interconnected, the motional electric field of the solar wind is transferred directly to the polar-cap ionosphere where it induces drift of ionospheric plasma. This drift carries magnetic flux from the day to the night side where it accumulates in the tail lobes. To avoid a flux catastrophe where all flux is removed from the day side, reconnection must also occur along a nightside segment of the neutral line. Reconnection at this second location allows the possibility of a steady state in which magnetic flux convects in closed loops through the magnetosphere. The ionospheric electric field from this convection is the same as that for the viscous interaction and can be used to explain the same phenomena.

The open model provides explanations for some phenomena for which the closed model does not. One is easy access of solar particles to either polar cap dependent on the sense of the radial component of the solar-wind magnetic field. Another is the existence of the polar mantle. A third is the sharp outer boundary layer to the plasma sheet and the earthward streaming ion beams which are observed within it. Most important of all is that it explains the dependence of magnetic activity on a southward interplanetary magnetic field.

3.3 The composite magnetosphere

The real magnetosphere is a composite of the open and closed models. The viscous interaction is apparently always present at a low level. It transports closed magnetic flux from the day side to the night side and back regardless of the orientation of the IMF. Also, it appears that the polar caps are always open to the solar wind, even when the IMF is northward (McDiarmid *et al.*, 1980). This situation leads to the magnetic topology illustrated in Fig. 40. Open field lines provide a mantle above and below the

Figure 39. Observations of magnetic field and plasma within the plasma sheet beyond the moon suggest a permanent neutral line is located beyond 120 R_e (Slavin and Kamide, 1986).

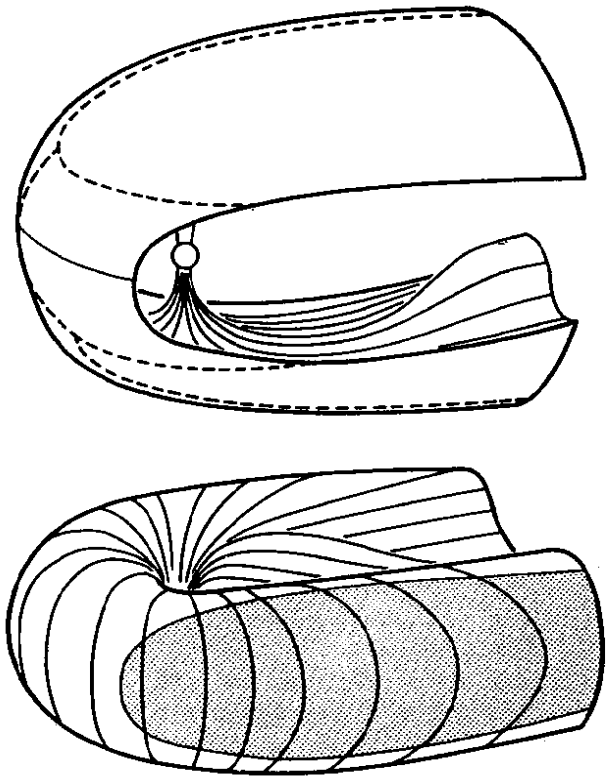

Figure 40. Topologically distinct regions of the composite magnetosphere consisting of open (top) and closed (bottom) field lines are created by reconnection. The solar wind transports open field lines over the poles, while viscous interaction moves closed field lines along the flanks (Crooker and Siscoe, 1986).

equatorial plane which insulates the tail lobes from the viscous interaction (top panel). Only around the equatorial plane do closed field lines make contact with the solar wind (bottom panel). In this region momentum transfer across the magnetopause drags closed field lines tailward creating the low-latitude boundary layers.

The existence of open field lines significantly changes the mapping onto the ionosphere of the convection induced by the viscous boundary layers. In Fig. 18 closed field lines were shown moving tailward across the entire polar cap. The situation in the composite magnetosphere is illustrated in the two middle panels of Fig. 41. Because of the open field lines the viscous cells map equatorward of the polar cap boundary (defined as the locus of last closed field lines). There are now only two thin layers of tailward

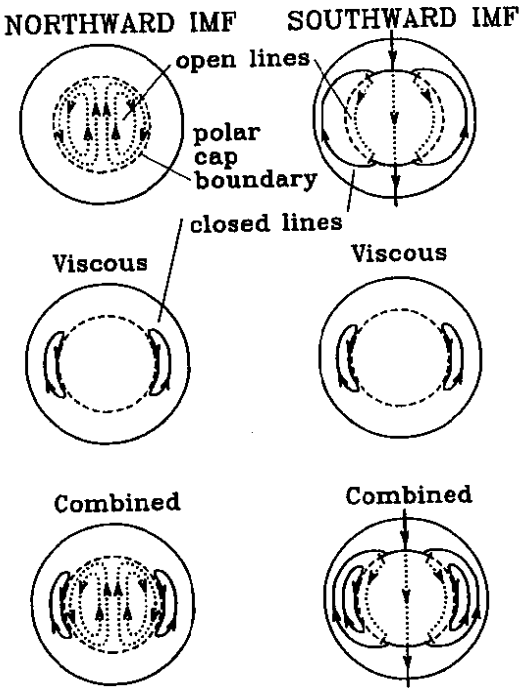

Figure 41. Combined effect of reconnection and viscous interaction as seen in ionospheric convection. Left and right columns show the situation for northward and southward IMF. Top and middle panels show convection due to reconnection and viscous interaction separately. Bottom panel shows the expected combination of the two.

convecting closed field lines located on the poleward edges of the dawn and dusk velocity shears.

The right-hand column of Fig. 41 portrays the effect of superposing convection due to both reconnection with southward IMF and the viscous interaction. The top panel shows two convection cells induced by reconnection alone. The dotted line is the polar-cap boundary and corresponds to the projection onto the ionosphere of the neutral line shown earlier in Fig. 29. The heavy lines are the portion of the neutral line across which reconnection occurs. Field lines are closed equatorward of the polar-cap boundary and become open as they flow across the dayside polar-cap boundary. They are closed again as they cross the nightside boundary. The middle panel shows convection cells due to the viscous interaction. The bottom panel depicts the situation when both types of convection are present. Since flow lines cannot cross one another, the reconnection flow lines

wrap around the viscous cells. The left column of Fig. 41 represents the situation for reconnection during northward IMF as discussed next.

The existence of convection in an open polar cap during northward IMF was unknown until recently. Dungey (1961) speculated that when the IMF is northward reconnection should occur poleward of the polar cusps as illustrated in a rather distorted fashion in the bottom part of Fig. 28. He assumed that magnetotail field lines would be closed under these conditions. If one IMF field line were to reconnect simultaneously to one tail field line as illustrated, the net result would be to remove a field line from the night side and add it to the day side. The portion of the field line originally in the tail lobes would be removed downstream by the solar wind. Russell (1972) and Maezawa (1976) modified the Dungey picture for northward IMF. They assumed that it is more likely that tail field lines are open when the northward IMF condition begins, and that reconnection probably occurs only in one hemisphere. Tilt of the dipole and the B_y component of the IMF should favour such an asymmetry. When they considered the implications of such asymmetric reconnection they concluded that the open flux within each tail lobe would circulate without change in the total flux. Figure 42 illustrates the pattern of field line motion they envisaged. Open field lines flow up through the centre of the tail lobes to a merging line poleward of the polar cusp. After reconnection one segment of the lobe line is disconnected from the Earth and is stripped off the top of the magneto-

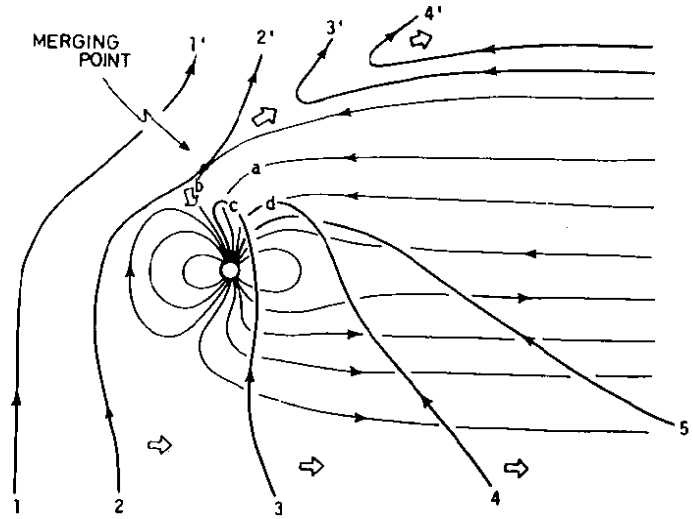

Figure 42. Field and flow pattern induced in the magnetosphere by reconnection of northward IMF at a single point above the northern neutral point (Maezawa, 1976).

tail by the solar wind. The other segment is pulled to either side of the magnetosphere by the solar wind. With time such field lines are transported tailward along the flanks of the magnetosphere slowly moving inward above the boundary of the plasma sheet. When parallel field lines from either side meet in the centre of a lobe they are diverted upward to reconnect again at the top of the lobe. Each field line thus passes through the same neutral line twice, maintaining constant magnetic flux in the lobe.

There is abundant evidence that sunward convection occurs in the polar cap at times of northward IMF (e.g. discussion by Rasmussen and Schunk, 1988). Measured field-aligned current patterns are consistent with such convection (Iijima and Shibaji, 1987). Furthermore, simultaneous observations of field-aligned currents and solar electrons indicate that some, if not all, polar-cap field lines are open at this time (McDiarmid *et al.*, 1980; Heelis *et al.*, 1986). However, there is as yet little agreement on how many convection cells exist during northward conditions, and how they evolve from the two-celled system for southward IMF.

In the ionosphere the feet of lobe field lines reconnecting above the polar cusp are expected to trace a path like that illustrated in the top left panel of Fig. 41. This pattern is the inverse of that produced by reconnection at the subsolar point shown at the top right. Open flux tubes flow sunward along the noon–midnight meridian in the centre of the polar cap, and then antisunward along the dawn and dusk boundaries. If convection is simultaneously present due to viscous interaction the resulting pattern should consist of four cells as illustrated in the bottom left panel (Burke *et al.*, 1979). It should be noted that in this situation activity in the auroral oval would be produced only by the viscous process. Effects produced by the reconnection northward of the cusp are confined to the centre of the polar cap where they are difficult or impossible to observe. However, recent studies show that currents proportional to the strength of the northward IMF are flowing in the polar cap during northward IMF (Friis-Christensen *et al.*, 1985; Iijima and Shibaji, 1987; Knipp, 1989).

A three-dimensional perspective view of the motion of flux tubes produced by the combined processes is shown in Fig. 43. Closed flux tubes dragged tailward along the flanks return sunward just inside of the tailward moving tubes. Flux tubes opened at a subsolar x-line are dragged over the polar caps and drift together at a distant x-line far downstream. They reconnect and flow earthward in the centre of the plasma sheet passing around the Earth outside of the plasmapause, but inside of the flux tubes returning from the boundary layers. Cowley (1982a) has estimated that typically the viscous interaction produces only 5–10% of the maximum potential drop across the magnetosphere. This suggests that during disturbed times the regions of return flow from the viscous boundary layers are quite thin compared with the return flow from the distant neutral line.

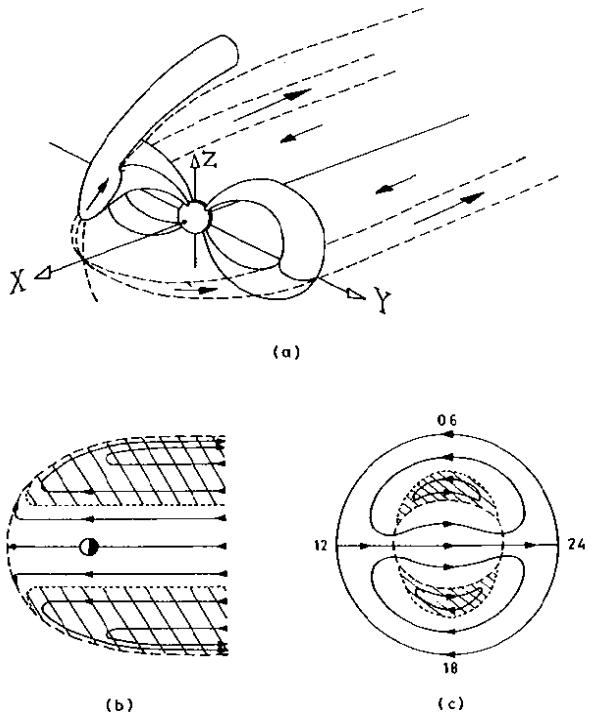

Figure 43. Motion of flux tubes induced by the two basic processes which result from solar wind coupling (Cowley, 1982).

A diagram showing structural features of the magnetosphere projected into the noon–midnight meridian plane at equinox is presented in Fig. 44. For convenience the distant neutral line is placed at 70 R_e, somewhat closer to the Earth than its average location at 110 R_e. Also, the polar mantle is shown as if it consisted of particles with a sharp lower energy cutoff. In actuality, low-energy particles will drift into the plasma sheet well earthward of the distant neutral line. Similarly, the plasma sheet boundary layer is shown as if it were produced by particles of a single energy originating at the distant neutral line.

The main regions of the magnetosphere projected into the equatorial plane are illustrated in Fig. 45. The equatorial view, although not drawn to scale, emphasizes the fact that the distant neutral line is parabolic in shape being closest to the Earth at midnight. Similarly, the inner edge of the plasma sheet (not shown) is curved around the night side, probably extending to local noon on both sides of the Earth. Also, it is clear that the plasmasphere is asymmetric extending furthest from the Earth at dusk. The

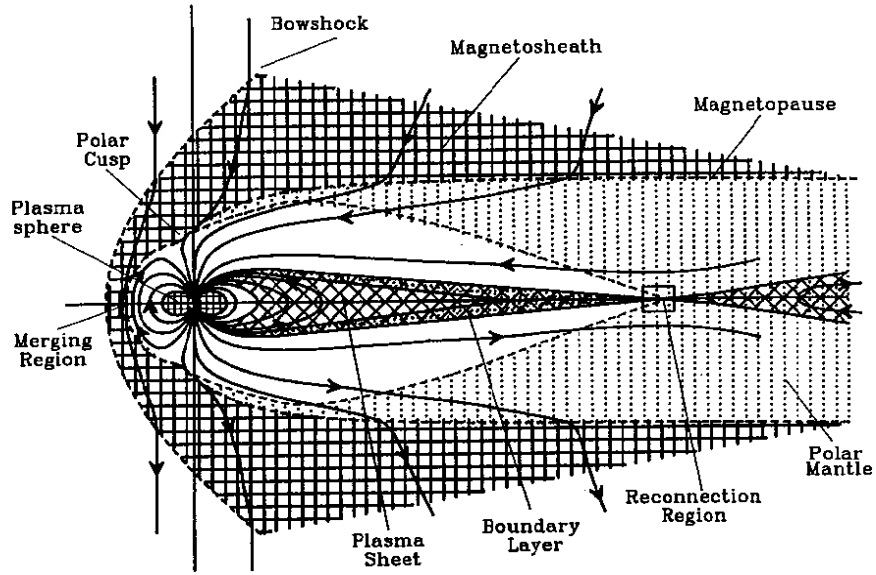

Figure 44. An approximate scale drawing of a noon–midnight cross-section of the Earth's magnetosphere (McPherron, 1987).

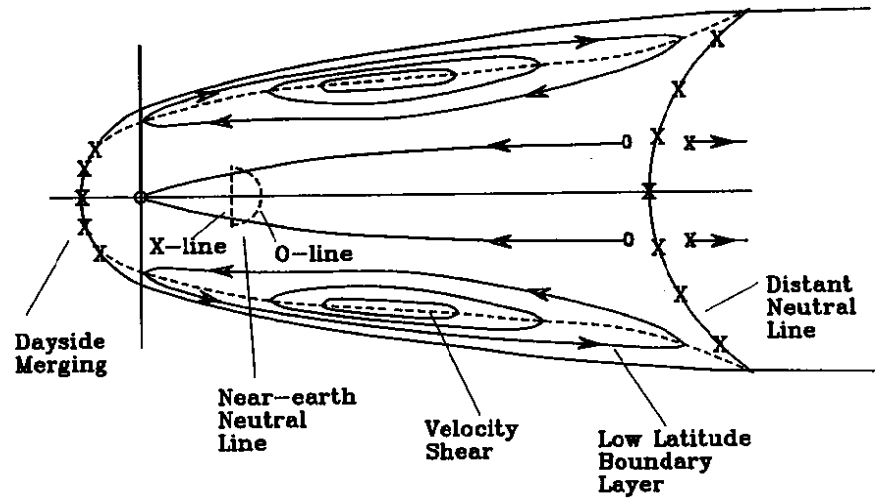

Figure 45. An approximate scale drawing of the equatorial plane of the Earth's magnetosphere.

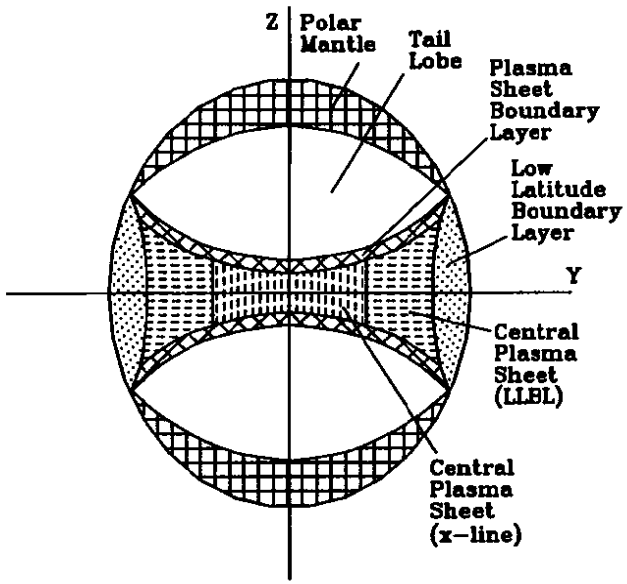

Figure 46. A cross-section of the Earth's magnetotail at about $x = -20\ R_e$. Distinct regions including polar mantle, lobe, plasma sheet boundary layers, central plasma sheet and low-latitude boundary layers are shown by shading patterns.

low-latitude boundary layers on the flanks of the magnetosphere are shown with somewhat exaggerated thickness. Flow lines for the viscous interaction are drawn to emphasize the point that they return sunward just inside the boundary layer, while return flow from the distant neutral line occupies the centre of the tail.

Figure 46 shows a dawn–dusk cross-section of the tail at a distance about $20\ R_e$ downstream of the Earth. The various boundary layers illustrated include the polar mantles, the plasma sheet boundary layers, and the low-latitude boundary layers. Other regions include the lobes of the tail and the central plasma sheet. Several regions within the central plasma sheet are distinguished according to the supposed origin of the return flow.

3.4 The Harang discontinuity

The auroral substorm usually begins in a region located just before midnight at the boundary between diffuse and discrete aurora. Normally the most equatorward discrete arc in this region intensifies and then expands both azimuthally and poleward. As we discuss now, this region of the ionosphere is characterized by complex electrodynamics. Understanding this region and its relation to substorm expansion onset is an outstanding research problem.

Near midnight the eastward and westward electrojets merge along a line trending a little north of magnetic west. This feature of the ionospheric Hall-current system was first studied by Harang (1946) who defined it as a region in the auroral oval across which the direction of magnetic disturbances switches from north to south. Heppner (1972) named this region the 'Harang discontinuity' to recognize Harang's work. According to Harang (1946) this region begins near midnight and is slightly tilted with respect to circles of magnetic latitude so that it is located at higher latitudes at earlier local times. Since north–south magnetic disturbances in the auroral oval are produced by the eastward and westward electrojets, the Harang discontinuity is the boundary that separates them. The tilt of the discontinuity slightly north of west implies that the westward electrojet terminates on the poleward side of the eastward electrojet. As discussed in §3.1.3, and shown schematically in Fig. 21, a fraction of the ionospheric current carried by the two electrojets flows outward along field lines originating in this discontinuity.

Many phenomena are associated with the Harang discontinuity as reviewed by Maynard (1974). For example, Heppner (1954) noted that auroral luminosity is brightest on the morning side of the boundary. Also, auroral forms change across the boundary from homogeneous quiet arcs to active rayed structures. Davis (1962) found that the motion of auroral forms is westward to the west of the Harang discontinuity, and eastward to the east. Westcott *et al.* (1969) used barium clouds released from rockets to show that the ionospheric electric field rotates counterclockwise from northward on the west, through westward in the discontinuity, to southward on the east. Subsequently, spacecraft and ionospheric radar observations confirmed the rocket data showing that the Harang discontinuity is also an electric field discontinuity (Cauffman and Gurnett, 1972; Banks *et al.*, 1973).

Recent work indicates that the magnetic and electric discontinuity are not colocated. Kamide and Vickerey (1983) found that the electric discontinuity is located about 2° north of the magnetic discontinuity. Because the location of the magnetic discontinuity measured on the ground is influenced by field-aligned currents, and by the relative strength of the eastward and electrojets, Kamide and Vickerey argued that the electric discontinuity measured in the ionosphere is more fundamental. Kunkel *et al.* (1986) have confirmed the existence of the offset between the two discontinuities in a study using simultaneous data from the two-dimensional STARE radar and SMA ground magnetometer array. They find that the separation is about

200–300 km. Moreover they show that the electric discontinuity is the location of intense upward field-aligned currents.

The Harang discontinuity is important to substorm models for several reasons. First, it is in this region that auroral substorms begin. For example, Nielsen and Greenwald (1979) demonstrate this with all sky camera records and ground radar measurements of ionospheric electric field. Auroral breakup occurs in the same region as the reversal in the north–south electric field. The Harang discontinuity is also important because the westward travelling surge and the westward edge of the substorm current wedge form in this region coincident with the brightening of the arc (Baumjohann, 1983). After the arc brightens it subsequently becomes folded creating the westward surge. An intense field-aligned current flows outward from the centre of the surge. According to Nielsen and Greenwald (1979), the Harang discontinuity moves equatorward as the auroral expansion develops. However, Kunkel *et al.* (1986) believe this is an artefact of displaying the data in geographic coordinates, and that the motion is westward.

Figure 47 is a schematic summary illustrating the relation of the Harang discontinuity to ionospheric convection. The left panel presents the approximate drift paths of ionospheric plasma, or when reversed, the direction of ionospheric Hall currents. The right panel shows the corresponding ionospheric electric field. The Harang discontinuity is indicated by a heavy

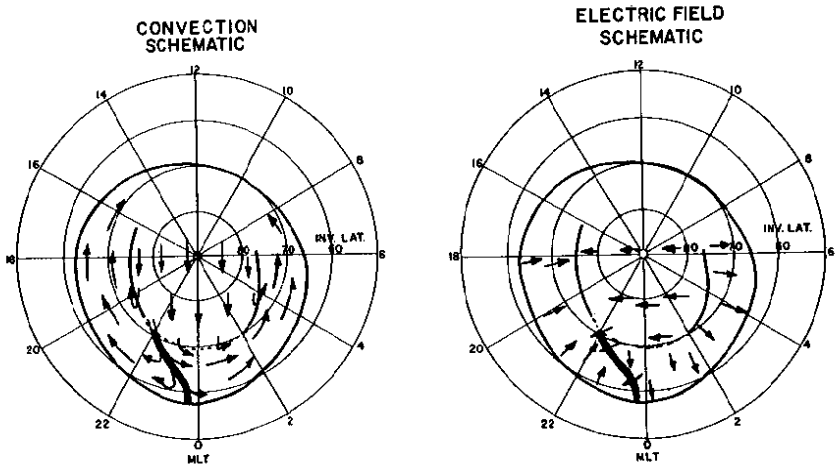

Figure 47. A schematic representation of ionospheric convection and electric fields in the night-time sector. Heavy line near midnight depicts the Harang discontinuity. Dashed line suggests continuation of the discontinuity as the dusk side velocity shear (Maynard, 1974).

line starting at low latitudes near midnight, and moving to higher latitudes at earlier local times. How the Harang discontinuity terminates at high latitudes is unclear from the diagram. Maynard (1974) suggests by a dashed line that it continues as the dusk sector velocity shear associated with the low-latitude boundary layer. It is significant that the ionospheric electric field is westward across the Harang discontinuity since this implies that ionospheric plasma convects across the discontinuity. Heppner (1977) used spacecraft data to construct empirical models of the ionospheric electric field which exhibit this behaviour. Figure 48 presents one of the models corresponding to times of southward interplanetary magnetic field when its east–west component is negative (towards dawn). Drift paths for ionospheric plasma (equipotentials) suddenly change direction at the Harang discontinuity. This diagram also suggests the Harang discontinuity connects continuously to the duskside velocity shear.

Advocates of the boundary layer dynamics model appear to have taken connectivity between the Harang discontinuity and the dusk velocity shear to its logical extreme. Figure 55 (§4.4.1) illustrates the consequences of this assumption. Without doubt the location of the high-latitude ionospheric velocity shear on the dusk meridian is a projection of the velocity shear between the low-latitude boundary layer and the central plasma sheet at some point on the dusk side downstream of the Earth. Rostoker and Eastman (1987) conceptually follow this velocity shear outward in the equatorial plane until it contacts the distant neutral line. They assume this neutral line is parabolic toward the Earth, and that the boundary layers become detached so that tailward flowing plasma reaches the centre of the tail. With these assumptions the duskside velocity shear connects to the distant neutral line at the centre of the tail. Since they assume that the Harang discontinuity is a continuation of the duskside velocity shear, they conclude that the low-latitude edge of the Harang discontinuity at midnight maps to the centre of the tail at or near the location of the distant neutral line.

Several authors have mapped the measured Harang discontinuity into the magnetosphere using simple magnetic field models (Maynard, 1974; Fairfield and Mead, 1975). Figure 49 presents Maynard's results for two levels of magnetic activity. For both a quiet and disturbed main field the midnight termination of the Harang discontinuity maps to the inner convection boundary. For quiet times this is located at 7 R_e and for disturbed times at 3 R_e. It seems highly unlikely that the Harang discontinuity can be mapped via closed field lines to the distant neutral line. Virtually no magnetic flux would cross the neutral sheet outside of synchronous orbit if such a mapping were correct.

We favour an alternative interpretation of the Harang discontinuity

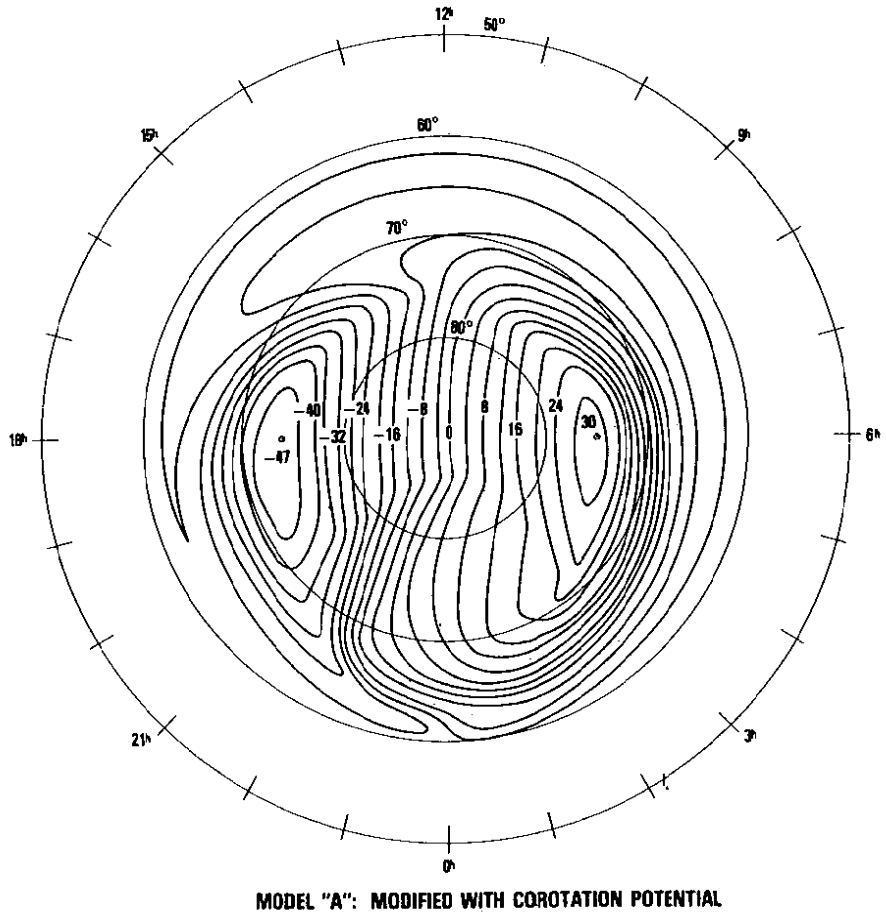

Figure 48. An empirical model of the ionospheric potential field derived from low-altitude satellite data (Heppner, 1977). The Harang discontinuity is shown by a sharp kink in equipotentials beginning at midnight and moving to higher latitudes at earlier local times.

which is topologically more realistic. First we point out that the Harang discontinuity is primarily east–west and therefore represents a shear in azimuthal drift velocity. With this in mind we take the Maynard mapping of the Harang discontinuity to the equatorial plane and consider how the Heppner models of ionospheric flow are projected. The top panel of Fig. 50 is a tracing of the model presented in Fig. 48. Two lines have been added to the original diagram. The line of dots signifies the stagnation line separating polar-cap flow lines closing on the dawn side from flow lines

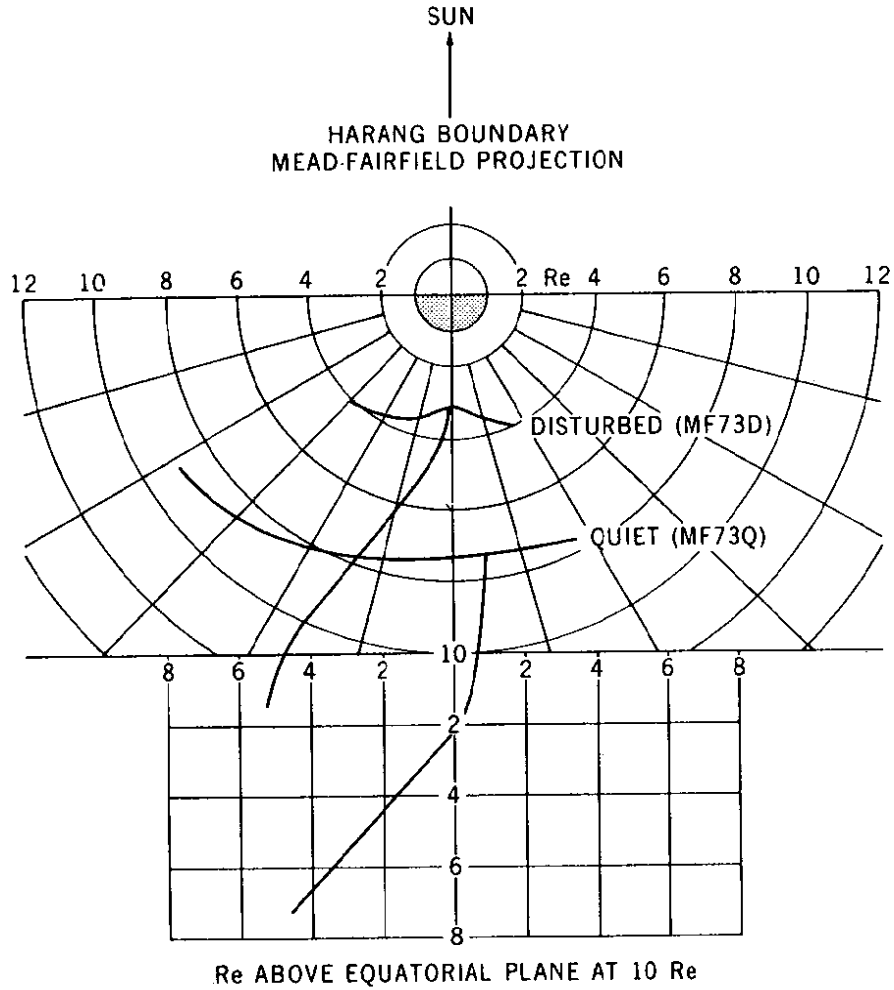

Figure 49. The equatorial trace within the magnetosphere of the Harang discontinuity and inner boundary of convection as projected from ionospheric electric field observations to the magnetosphere using the Mead–Fairfield magnetic field model (Maynard, 1974).

closing on the dusk side. A dashed line connects the Harang discontinuity to the dusk velocity shear. The bottom panel of the figure is a reproduction of the Maynard mapping of the Harang discontinuity to the equatorial plane during disturbed conditions. We have added our assumed projection of the stagnation line which meets the Harang discontinuity at the inner convection boundary. Superposed on this diagram are magnetospheric flow

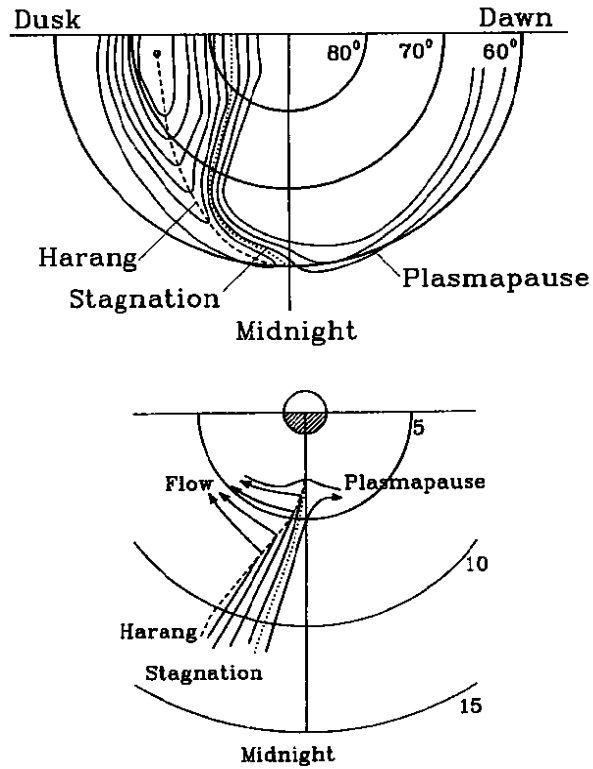

Figure 50. Top panel shows details of Heppner (1977) ionospheric potential map from Fig. 49. Bottom panel shows near-Earth projection of these features using Maynard (1974) mapping.

lines corresponding to some of those shown in Fig. 48. It is apparent that near the inner edge of convection the Harang discontinuity represents a reversal in the dawn–dusk component of magnetospheric flow. Tailward of the projected discontinuity plasma drifts towards the dawn side of the tail. Earthward of the discontinuity it drifts westward towards dusk.

Our extrapolation of the Harang discontinuity further into the equatorial plane of the tail is illustrated in Fig. 51, which shows flow within the magnetotail out to the distant neutral line. Here the neutral line is represented as a parabola facing tailward in agreement with the observations of Slavin and Kamide (1986). The velocity shear at the inner edge of the low-latitude boundary layer is shown on the dusk side by a thin dashed line connected to the end of the neutral line near the magnetopause. Although probably exaggerated in absolute width, the low-latitude boundary layer is

depicted as increasing in width tailward to the midpoint of the boundary layer, and then decreasing in width as plasma reverses direction across the velocity shear. The midpoint is projected as the centre of the ionospheric convection cell near the dusk meridian. The diagram is drawn as if some reconnection were in progress at the distant neutral line with a few flow lines originating at the neutral line, although we doubt that this occurs during northward IMF or the growth phase of substorms. The Harang discontinuity is represented by a heavy dashed line starting close to the Earth at midnight and connecting to the centre of the dusk convection cell. By analogy with the ionospheric observations, all plasma flow has a dawnward component tailward of this line, and a duskward component earthward of it. It can be seen that this definition logically requires that the Harang discontinuity connect to the centre of the convection cell. Atkinson (1985) portrays much the same mapping in his discussion of time dependent magnetospheric flows.

A projection of this mapping back to the ionosphere is shown schematically in Fig. 52. The duskside velocity shear connects continuously with the high-latitude projection of the distant neutral line. However, the Harang discontinuity starts at the centre of this convection shell and drops equatorward toward midnight, terminating at the inner convection boundary. In the magnetosphere there is very little change in the plasma flow velocity

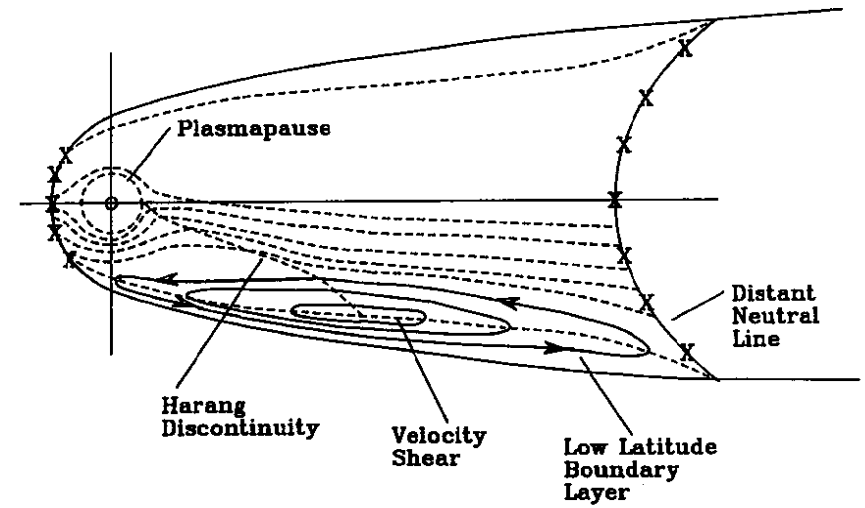

Figure 51. An equatorial view of our proposed geometry of the Harang discontinuity and its relation to the distant neutral line. Figure 52 illustrates the ionospheric projection of this mapping.

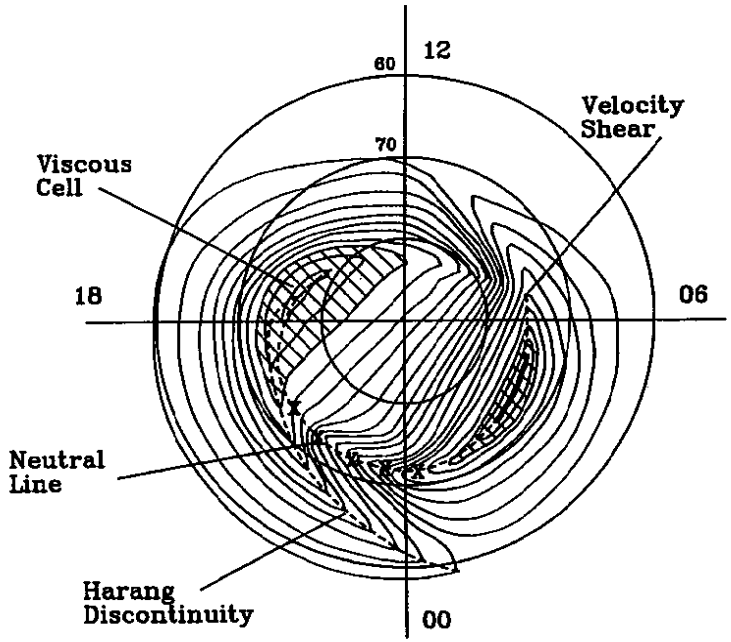

Figure 52. An alternative mapping of the Harang discontinuity into the high-latitude dusk meridian velocity shear which seems more consistent with the definition of the Harang discontinuity.

across the Harang discontinuity where it meets the centre of the velocity shear. Thus we expect there would be little evidence of this change when projected to the ionosphere. However, closer to the Earth the change in velocity becomes larger and larger, exceeding 90° at the inner edge of the discontinuity. Projected effects should be very large here as is observed. An examination of Heppner's diagrams suggests that few changes would be needed to correspond to our suggestion. We note that it is unlikely that the highly variable ionospheric electric field has been measured with sufficient precision to detect the difference between the two mappings.

4 MODELS OF MAGNETOSPHERIC SUBSTORMS

4.1 Overview

Since the existence of magnetospheric substorms was first recognized there have been numerous attempts to explain what causes them. Most explanations have invoked magnetic reconnection in some way to explain the dependence of geomagnetic activity on the orientation of the IMF. Recently four different models have been proposed to explain at least some of the observations. These include the 'driven model', the 'near-Earth neutral line (NENL) model', the 'plasma sheet boundary layer (PSBL) dynamics model', and the 'thermal catastrophe model'. The model which has received the most attention is the NENL model. As an advocate of this model we will devote most of the remainder of this chapter to its description. We are aware of its controversial nature, and the fact that it does not yet explain all of the observations. Many of the questions which it does not yet answer are summarized in a final section. We are confident that extensions of the model will eventually answer these questions. Immediately below we present a brief overview of each of the models highlighting the major assumptions of each model.

4.2 The driven model

The driven model of substorms was introduced by Akasofu (1979a,b) to explain the apparent close relationship between the AE index and the interplanetary energy input parameter 'epsilon'. The epsilon parameter is defined (Perreault and Akasofu, 1978) as $\varepsilon = l_0^2 B^2 \sin^4(\theta/2)$. Here V is the speed of the solar wind, B is the magnitude of its magnetic field, θ is the clock angle of the IMF around the Earth–Sun line, and l_0^2 is a constant proportional to the area on the dayside magnetopause through which magnetic energy is input to the magnetosphere. The logic which led to this definition is the following. Geomagnetic activity is controlled by the strength and orientation of the solar-wind magnetic field. The activity must somehow be proportional to the flux of magnetic energy incident on the magnetopause. It is also controlled (gated) by a strong angular dependence such that there is little activity for northward IMF. However, some activity does occur during northward IMF, so therefore the gating function must never be exactly zero. The function $\sin^4(\theta/2)$ has this property, and yet is a fairly strong function of clock angle. The constant l_0^2 was originally set by equating the estimated rate of energy dissipation in the ring current and auroral ovals to the quantity ε.

Implicit in the definition of the energy parameter ε was the idea that a solar-wind dynamo drives electrical currents in the magnetosphere and ionosphere. The driven model assumes that reconnection occurs, or at least once occurred on the day side, opening the magnetic field lines of the polar cap to the solar wind. Once this happened, motion of the solar wind across the open field lines of the Earth acts as a generator producing a voltage that

is transmitted by the field lines to the polar-cap ionospheres. This voltage drives magnetospheric convection and corresponding electrical currents. The general form of the disturbance during substorms is attributed to changes in the solar-wind ϵ parameter. However, the expansion phase is a result of an instability in the field-aligned currents flowing out of the midnight sector of the auroral oval. As discussed in §3.4, both the Pedersen current and the Hall current diverge along field lines in the Harang discontinuity. This discontinuity is located just before local midnight and is the boundary separating the poleward edge of the eastward electrojet and the equatorward edge of the westward electrojet. When the upward current from this region exceeds a threshold value, the ionosphere becomes unstable and generates a large field-aligned potential drop. This potential structure called an inverted V (Frank and Ackerson, 1971), accelerates electrons downward creating a bright auroral arc. Atmospheric ions are accelerated upward into the plasma sheet. The increased electron bombardment of the ionosphere enhances conductivity which allows more current to flow in the ionosphere for the same applied electric field. But this drives additional portions of the field-aligned current unstable further enhancing ionization in an unstable feedback loop.

Additional details of the substorm mechanism were never clearly specified in the driven model. Substorms subside when the ϵ parameter decreases due to a change in solar-wind parameters. The model did not discuss the fate of the open field lines which generate the polar-cap potential. Presumably they remained open to drive magnetospheric currents again when solar wind conditions were correct.

4.3 The thermal catastrophe model

The thermal catastrophe model, like the PSBL dynamics model, emphasizes the role of the plasma sheet boundary (Smith *et al.*, 1986; Goertz and Smith, 1989). The essential idea in this model is that absorption of waves in the boundary layer causes the temperature to increase until the layer passes through a 'thermal catastrophe' to a new, higher temperature state. The model assumes that some process like reconnection causes convection of plasma through the lobe and PSBL into the central plasma sheet (CPS). The magnetopause, lobes, PSBL and CPS are treated as slabs with the PSBL being an inhomogeneous region of rapidly decreasing Alfvén velocity. It is assumed that Kelvin–Helmholtz waves are always generated on the tail magnetopause by the solar wind. These waves propagate slowly across the lobes as compressional waves and enter the PSBL. Within the PSBL all wave modes are coupled by the inhomogeneity. At some point within the

layer the phase velocity of the incident compressional waves matches the velocity of Alfvén waves along field lines allowing coupling to occur. Because of finite Larmor radius effects involving ions, the transverse Alfvén wave develops a finite electric field parallel to the magnetic field. This interacts with the ions and electrons through Landau resonance transferring energy from the waves to the plasma. The energy added to the boundary layer by this process is transported into the CPS by convection. The temperature within the PSBL is then determined by a balance between heat input from waves and other processes, and heat transported into the CPS by convection.

A substorm growth phase begins when there is an increase in wave energy across the lobes. With time the total energy and temperature in the PSBL increase above their background values. As the temperature increases the properties of the boundary layer change increasing the amount of energy absorbed from the incident waves. At a critical temperature the PSBL becomes totally opaque to the incident waves. Then heat accumulates so rapidly it cannot be convected away. The boundary layer consequently undergoes a rapid phase transition to a higher temperature. However, at the higher temperature the PSBL is a less efficient absorber of waves. Once again heat deposited by the waves causes a gradual increase in temperature, as most of the energy deposited is convected away. The expansion phase of the substorm is attributed to the transition from a low- to high-temperature state at a fixed value of system energy.

At the present time this model has not been developed sufficiently to explain many of the observed features of a substorm. For example, it is known that the substorm growth phase begins with a southward turning of the IMF. However, the thermal catastrophe model does not explain why the Kelvin–Helmholtz instability should increase the wave energy into the PSBL as a result of this change. Similarly, it is known that the tail current is diverted into the ionosphere at expansion onset. Since this model does not explain the details of the transition from one state to another, it does not account for this observation either.

4.4 The plasma sheet boundary layer (PSBL) dynamics model

The PSBL dynamics model is an explicit attempt to include the PSBL in a model of the substorm expansion phase (Rostoker and Eastman, 1987; Eastman *et al.*, 1988). According to its advocates, this model accounts for two essential substorm features that are missing in the near-Earth neutral line (NENL) model as well as providing an alternative explanation for observations attributed to NENLs. An essential difference between the two

models is that the PSBL dynamics model claims that the flows and field perturbations attributed to plasmoids are always present in the boundary layer and are not produced by a transient change in the magnetic topology of the plasma sheet.

4.4.1 Geometry of the PSBL dynamics model

The PSBL dynamics model is based on certain geometric assumptions concerning the mapping of magnetic field lines from the auroral ionosphere to the distant tail as illustrated in Fig. 53. The left panel shows a schematic map of the premidnight auroral ionosphere divided into three regions based on the properties of electron precipitation observed by polar orbiting spacecraft (Winningham *et al.*, 1975). From pole to equator these regions include the polar cap, the boundary plasma sheet (BPS) and the CPS. According to Lyons and Evans (1984), discrete auroras occur in the BPS while diffuse aurora fills the CPS. The BPS is split by an electric field reversal corresponding to a change in the direction of ionospheric flow. Away from midnight, this reversal defines the poleward boundaries of the electrojets. Their equatorward boundaries are the same as the equatorward boundaries of the CPS. In the premidnight sector the electrojets overlap with the westward electrojet flowing westward, poleward of the eastward electrojet. The region of electric field reversal separating the two electrojets

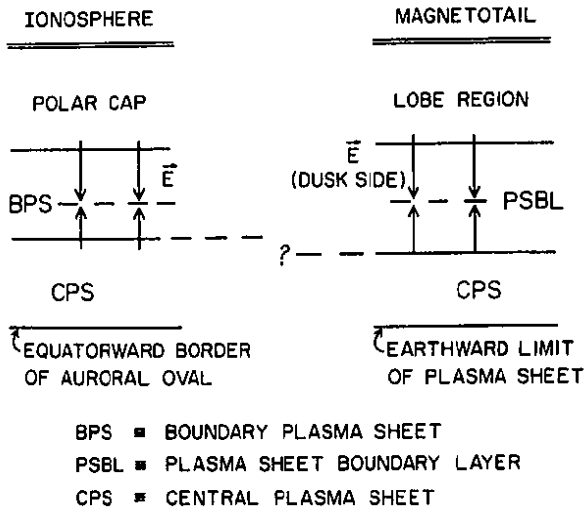

Figure 53. A schematic illustration showing the mapping of ionospheric regions to the plasma sheet.

is called the Harang discontinuity (Heppner, 1972). The Harang discontinuity is the location of upward field-aligned current predominantly due to closure of a fraction of the Hall current flowing in the electrojets (Kunkel *et al.*, 1986). The auroral substorm expansion begins with the formation of a westward-travelling surge on the most equatorward auroral arc within the Harang discontinuity (Nielsen and Greenwald, 1979). The substorm current wedge also forms at this time with its westward edge originating in the surge (Baumjohann, 1983). Advocates of the PSBL dynamics model believe their model explains these facts and that the NENL model does not.

The right-hand panel of Fig. 53 shows a portion of the transverse cross section of the magnetotail and the assumed correspondence with ionospheric features. The polar cap maps to the tail lobe. The BPS maps to the PSBL and the CPS to itself. This mapping implies that there is an electric field reversal imbedded in the middle of the PSBL.

Additional assumptions of the PSBL model are illustrated by the equatorial projection presented in Fig. 54. The low-latitude boundary layers (LLBL) are defined as layers of tailward-flowing plasma threaded by closed field lines on the dawn and dusk sides of the magnetotail. These layers become detached from the magnetopause where they first encounter the distant neutral line. They continue flowing tailward, but diverge inward, flowing towards the centre of the tail bounded on the outside by the neutral line and on the inside by a boundary with the CPS. The neutral line is taken as a parabola opening earthward (not tailward as is suggested by the observations of Slavin and Kamide, 1986). The flows eventually turn earthward producing the electric field transitions through velocity shears at the inside edges of the boundary layers. The electric field transitions and the neutral line join at the centre of the tail.

With the foregoing geometry, closed field lines map the LLBLs out of the distant neutral sheet along the top and bottom of the plasma sheet. Tailward-flowing plasma thus maps to the high-latitude portion of the PSBL and to the corresponding location in the ionospheric BPS. Similarly the electric field transitions produced by the flow reversals map along closed field lines in the interior of the PSBL. However, the electric field transitions do not define the boundary between the PSBL and the CPS as is suggested by the equatorial projection. Instead, the transitions map to the middle of the PSBL to correspond with the ionospheric observations (see Fig. 53). Because this model allows tailward-flowing plasma to penetrate all the way to the centre of the tail, the electric field transitions produced by the reversal of the boundary layer flows also meet in the centre of the tail.

Although not discussed by the advocates of the model, this mapping implies that the low-latitude portion of the PSBL maps into the distant

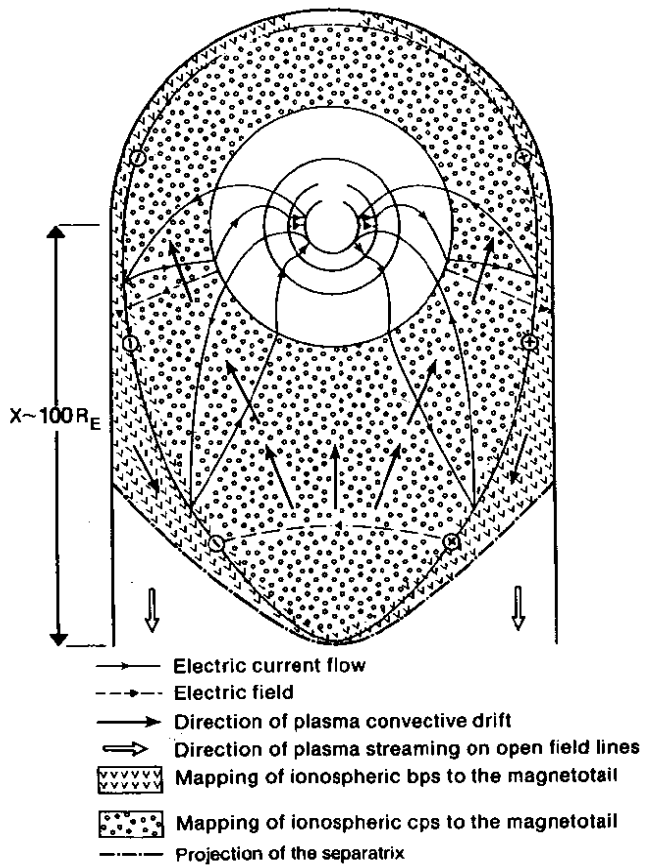

Figure 54. An equatorial cross-section of the magnetosphere showing the mapping of ionospheric regions into the equatorial plane. These lines show the Region 1–2 field-aligned current system.

CPS just earthward of the electric field transitions. However, according to Rostoker and Eastman (1987), '...bps and PSBL particles are found on common field lines which, further downtail, are seen to populate the velocity shear zone between the LLBL and the CPS'. This seems to imply that the line representing the electric field transition in Fig. 54 is actually of wide areal extent. If this inference is correct, then it is not clear what physical process creates the boundary between the CPS and BPS. However, the authors note that 'during the process of entrainment (of LLBL plasma in CPS), parallel electric fields accelerate the low-energy LLBL electrons to CPS energy levels'. Where along the field lines, and why this acceleration

occurs is not specified. However, we note that DeCoster and Frank (1979) originally explained the distribution function for ions in the PSBL by parallel electric field acceleration in the distant tail. Cowley (1980) has pointed out that the Speiser mechanism will produce such a distribution provided there is some pitch angle scattering of the particles ejected from the current sheet. Presumably the earthward edge of the region of particle acceleration is the beginning of the CPS.

In the PSBL dynamics model, the high-latitude, Region 1 field-aligned currents are assumed to map to the velocity shear zones between the CPS and LLBL. On the dawn side the electric field diverges from this shear zone

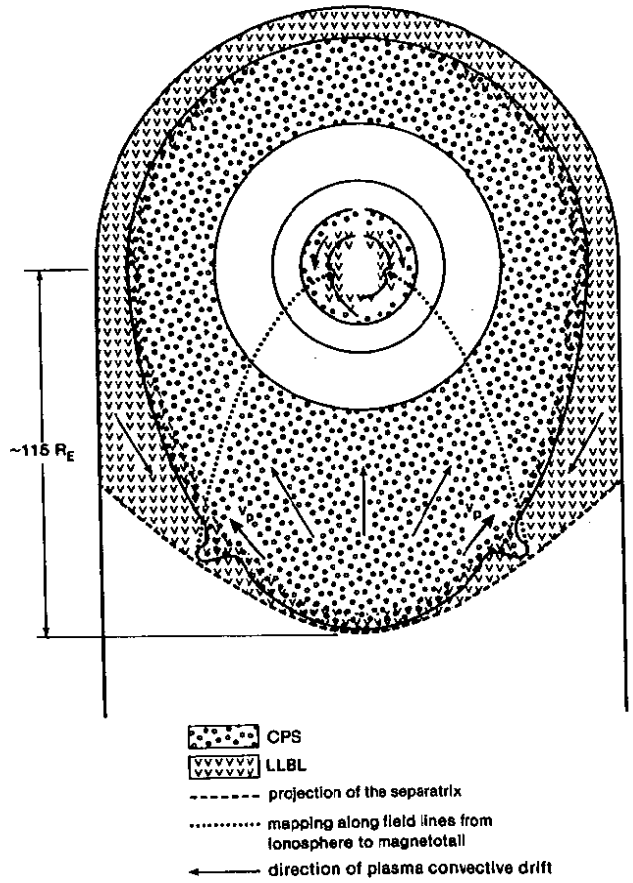

Figure 55. An equatorial view showing the mapping of K–H waves into the Harang discontinuity and drifting omega bands.

indicating an accumulation of positive space charge. Region 1 currents flow earthward from this region. On the dusk side the electric field converges to the shear zone corresponding to negative space charge into which the Region 1 currents return. Because the dawn and dusk shear zones are assumed to meet in the centre of the distant tail, Region 1 field-aligned currents are expected to be present in the ionosphere all the way to local midnight. The low-latitude Region 2 currents are assumed to map to the inner edge of the plasma sheet.

An essential feature of the PSBL dynamics model is the mapping of the Harang discontinuity illustrated in Fig. 55. Because the Harang discontinuity is an electric field reversal, and because it is oriented from northwest to southeast in the premidnight sector, it is assumed to be an ionospheric projection of the dusk flank velocity shear. But in the PSBL dynamics model this shear is furthest from the Earth at local midnight so that the most equatorward portion of the Harang discontinuity is mapped to the most distant tail. But a portion of the eastward and westward electrojet currents closes upward along field lines originating in the Harang discontinuity (Kamide and Vickerey, 1983; Kamide and Rostoker, 1977; Kunkel *et al.*, 1986). Thus these field-aligned currents must map to the distant velocity shear. Now, as noted above, auroral substorm expansions are initiated as a westward surge in the Harang discontinuity near midnight, so this mapping requires that the physical process causing the auroral expansion must take place at the centre of the distant tail near the contact between the velocity shear and the neutral line. Also, since the westward edge of the substorm current wedge flows out of the westward surge, this current must map to the distant shear as well. But then the substorm current wedge is colocated with the closure of currents in the driven system. Therefore, the substorm current wedge must be a perturbation of the driven system.

4.4.2 *The substorm expansion phase*

In the PSBL dynamics model the substorm expansion phase is initiated by a sudden burst of reconnection at the distant neutral line. The burst injects a plug of energized plasma into the CPS and forces it earthward with high velocity. The plug of plasma flows up the centre of the tail enhancing the velocity shears on the dawn and dusk sides of the plasma sheet. On the dusk side the increased velocity contrast between the LLBL and the CPS is sufficient to destabilize the Kelvin–Helmholtz instability in a limited azimuthal sector. A wave grows in the shear zone causing the CPS plasma to intrude into the LLBL as illustrated in Fig. 55. When this distortion is

mapped to the ionosphere by field lines it produces a surge-like auroral form. Propagation of the distortion earthward at the plasma convection velocity causes the surge to appear to move westward. Growth of the Kelvin–Helmholtz instability causes a parallel electric field to develop in the centre of the magnetospheric disturbance. This field draws additional ionospheric current out of the surge in an attempt to limit the growth of the wave. This produces a localized enhancement of the sheet of field-aligned current normally linking the velocity shear to the ionosphere. Rostoker and Eastman (1987) suggest that this enhancement is accomplished by reducing the outward current at slightly later local times rather than by increasing the earthward field-aligned current postmidnight.

The interaction of the earthward-moving plasma with the dawn shear zone is apparently quite different from its interaction with the dusk shear zone. Instead of a single intrusion, a series of waves (a vortex street) develops. This sequence of earthward-moving waves is projected on the ionosphere as a sequence of eastward-drifting omega bands. Alternating sheets of concentrated and weakened, earthward-directed, field-aligned current flow from the shear to the ionosphere. Magnetic perturbations from the closure of these currents produce Ps 6 (pulsations substorm) disturbances on the ground.

A fundamental postulate of the PSBL dynamics model is that southward magnetic fields in the plasma sheet can often be explained as edge effects of the field-aligned current from the westward surge. A schematic illustration of how this might happen is shown in Fig. 56. The top panel depicts the field-aligned currents produced by the driven system as projected in the dawn–dusk plane of the tail. Magnetic perturbations from these currents are parallel to the edges of the PSBLs. Since these layers are closest together in the centre of the tail, the current sheets are tilted. Because of this tilt the vertical component of the perturbation magnetic field is slightly negative everywhere in the CPS. We point out, however, that because field lines of the CPS curve upward through the neutral sheet with a positive vertical component the total vertical component probably remains positive.

The bottom panel of Fig. 56 depicts the expansion phase current wedge as represented graphically by Rostoker and Eastman (1987). Concentrated field-aligned current flows outward in the PSBL on the dusk side and inward on the dawn side. Everywhere outside the current wedge vertical magnetic perturbations are generally negative while everywhere inside they are positive. The strongest negative perturbations occur in the PSBL at the edges of the outward current. Somewhat weaker perturbations are seen at the eastern edge of the current wedge.

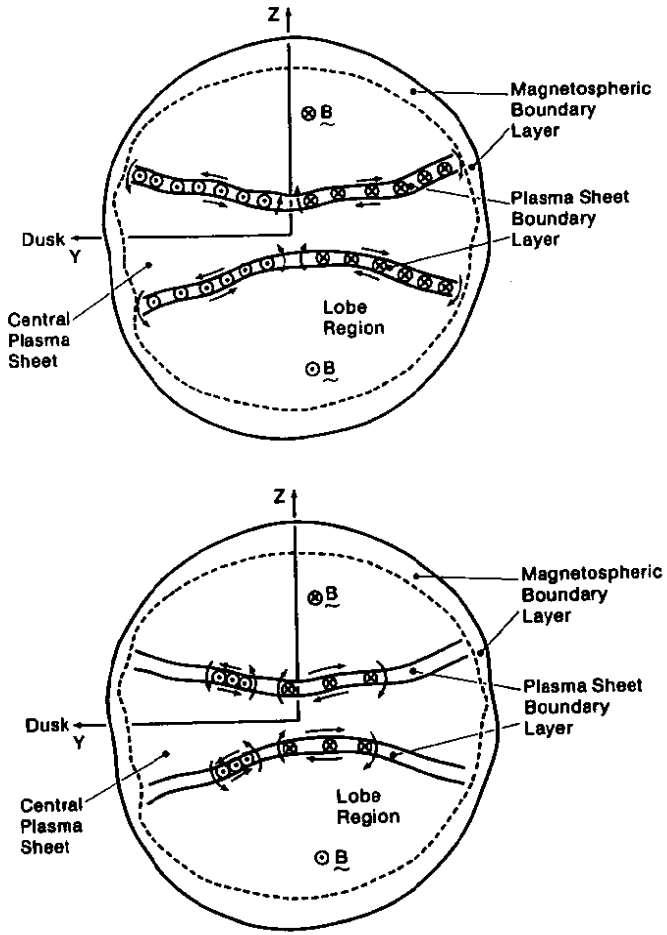

Figure 56. The configuration of field-aligned currents in the PSBL. Top panel shows the driven system and the bottom panel shows the unloading system.

4.4.3 Comments on the PSBL dynamics model

Advocates of the PSBL dynamics model claim that their model accounts for fundamental features of the magnetospheric substorm which the NENL model does not. For example, Rostoker and Eastman (1987) state '...we do claim our framework to be superior in several respects'. These include:

(1) The PSBL dynamics model recognizes that the plasma sheet is made up of two distinct regions, the PSBL and the CPS. In the NENL model '...those differences seem much less relevant'.

(2) The PSBL dynamics model deals with the ramifications of field-aligned current (FAC) flowing out of the westward-travelling surge, while the NENL model '...does not call on substorm FAC to produce any observable perturbations in the magnetotail magnetic field'.
(3) In the PSBL dynamics model the unloading system of FAC represents a perturbation of the driven system in the region of the Harang discontinuity. In contrast the NENL model '...does not take account of this important phenomenological feature'.

Also, according to these authors the NENL model has two major drawbacks:

(1) 'Signatures used to identify one's position with respect to the NENL do not seem to be repeatable'.
(2) 'The NENL model provides an explanation only for the loading–unloading component of substorm activity'.

First we do not believe that the drawbacks of the NENL model actually exist. The NENL model is primarily a phenomenological model developed from numerous studies of the plasma and magnetic field within the tail. It would not have been possible to develop this model if the phenomena did not occur with some regularity. In fact, the model explains a lack of regularity as the consequence of variations in the azimuthal and radial location at which the localized neutral line forms. However, another factor which contributes to an apparent lack of regularity is not properly appreciated. Space observations of substorms are necessarily made along satellite trajectories. These trajectories are such that outbound and inbound passes occur at quite different latitudes and local times. Furthermore, successive passes are not slightly displaced replicas of each other. Because the orbital period of the spacecraft is some non-integer multiple of the Earth's rotation period, the magnetic field configuration on successive orbits is quite different. For example, on the ISEE spacecraft the orientation of the Earth's dipole is approximately the same every fifth orbit. This time corresponds to approximately 2 weeks or 15° in local time. The localization of substorms phenomena in the tail is sufficient that nearly every orbit in a given year represents a unique path through the substorm disturbance.

The second drawback of the NENL model listed by the PSBL dynamics model advocates appears to be a misunderstanding of the model. In the NENL model the growth phase of a substorm is a manifestation of the driven system. Furthermore, it is the growth phase that establishes conditions that lead to the formation of the near-Earth x-line. As summarized in the following section, dayside reconnection combined with the viscous

interaction produces a two-celled convection system that drives field-aligned and ionospheric currents. Because reconnection at the distant neutral line does not immediately increase to match the dayside merging rate, flux accumulates in the tail lobes (loading). The magnetosphere becomes increasingly distorted with an inward extension and thinning of the tail current sheet. This thinning reduces the vertical component of the magnetic field through the plasma sheet leading to the onset of ion tearing and the creation of an azimuthally localized pair of x- and o-type neutral lines. A plasmoid is initiated during the growth phase because the x-line forms inside the CPS on closed field lines, which when reconnected form loops around the o-line. Reduction in tail lobe flux (unloading) begins only when the last closed field line connected to the distant neutral line is severed and lobe field lines begin to reconnect. But then the high Alfvén velocity of the tail lobes causes an explosive increase in the rate of reconnection and the onset of the expansion phase. Also when lobe field lines reconnect they form a sling around the closed loops of the plasmoid and their tension pulls the plasmoid down the tail. Apparently, advocates of the PSBL dynamics model do not accept this sequence of events as part of the NENL model. It does, however, explain many of the phenomena seen prior to expansion onset.

The advocates of the PSBL dynamics model claim that the NENL model does not take into account the PSBL. This is not entirely true. The boundary layers exist in the NENL model and are produced by the Speiser mechanism. Plasma mantle particles drifting vertically across the tail lobes enter the distant current sheet and are energized by serpentine motion along the cross tail electric field. They are ejected when their gyration about B_z brings their trajectories into near alignment with a magnetic field line passing through the sheet. They are subsequently reflected at the ionosphere and counterstream through inward directed ion beams ejected closer to the Earth. Also these layers cary field-aligned currents flowing to the ionosphere out of the distant current sheet. It is true, however, that in the NENL model no particular role in the expansion phase onset has been attributed to the PSBL.

Proponents of the PSBL dynamics model also claim that the NENL model does not take account of the field-aligned currents flowing out of the westward surge. This is clearly not the case. A fundamental feature of the NENL model is the substorm current wedge which forms at expansion onset. The westward edge of this current wedge is located in the westward surge. The model attributes the wedge to a diversion of the cross-tail current through the ionosphere as a segment of westward electrojet. This diversion occurs because the total current in the tail must decrease to produce the x-line geometry for reconnection.

The effects of the expansion current wedge are also included in the NENL model. The dipolarization of the synchronous orbit magnetic field (rotation toward more dipole orientation), the D-spikes there (an FAC signature) and mid-latitude positive bays are all consequences of this current system. Azimuthal expansion of the current wedge is seen as delays in the occurrence of dipolarization on the ground and at synchronous orbit.

The third way in which the PSBL dynamics model is claimed to be superior is that it collocates the field-aligned currents of the driven system and the substorm current wedge. In fact, it claims the wedge current is simply a perturbation of the driven system. The latter is almost certainly true, although we agree that it is not explained in the current version of the NENL model. In fact, the current wedge is usually presented in the NENL model as an entirely new current system that forms close to the earth interior to the CPS. We note, however, that at the time the wedge forms, the near-earth x-line has just become connected to the distant neutral line though severance of the last closed field lines over a limited azimuthal sector. The rather peculiar topology of the field at this time may account for the apparent collocation. We address this point later in our discussion of outstanding questions. We note in ending this discussion of the PSBL dynamics model that we are very doubtful of magnetic field mapping which connects the equatorward edge of the Harang discontinuity to the distant neutral line though closed field lines. In summary, our objections to the PSBL dynamics model include:

(1) No physical explanation is given for the cause of the parallel electric fields that generate earthward-streaming plasma in the PSBL.
(2) The model requires plasma to travel earthward in the CPS for 100 R_e after expansion onset, when observations show that it travels tailward.
(3) The model predicts that earthward streaming plasma will be associated with strong negative B_z since strong negative B_z are seen in the PSBL west of the outward field-aligned current from the surge, and their boundary layer only contains earthward- or counterstreaming beams. But actually most strong negative B_z are observed in association with tailward-streaming plasma.
(4) The model predicts that positive B_z perturbations will be seen everywhere along the central meridian of substorm disturbances out to 100 R_e, and negative perturbations will be seen west of the surge longitude, or somewhere east of the closure of the wedge. In observations, negative B_z are most frequently found near the midnight meridian, not west of typical surges which form on the average at 22–23 LT, or east of midnight in the omega band region.

(5) The model provides no explanation for the observed thinning of the plasma sheet. Since it attributes thinning to a growth phase effect of the IMF it should not be correlated with expansion onset as observed.
(6) The model provides no explanation for thickening of the plasma sheet in substorm recovery phase.
(7) Because plasma energization and injection occurs at the distant neutral line it does not account for the injection of plasma at synchronous orbit immediately after expansion onset.
(8) The model connects the equatorward edge of the Harang discontinuity to the last closed field line connected to the distant neutral line. This is physically implausible.

4.5 Summary of the near-Earth neutral line (NENL) model

4.5.1 Reconnection of the dayside magnetic field

Studies of solar-wind coupling have consistently shown that substorms occur when the interplanetary magnetic field is antiparallel to the Earth's field near the subsolar point (see papers in book edited by Kamide and Slavin, 1986). Only one physical mechanism is known which accounts for this relation—magnetic reconnection. Reconnection occurs in collisionless plasmas wherever oppositely directed fields are driven together and the infinite conductivity approximation of MHD breaks down (Cowley, 1985). This can happen as a result of 'anomalous resistivity' produced by wave turbulence or as a result of finite gyroradius effects in regions of strong field gradients (Vasyliunas, 1975). Whatever the underlying process a small region develops in the interface between the oppositely magnetized plasmas that allows their magnetic fields to diffuse into each other. The importance of reconnection to substorms is severalfold. First, it provides a mechanism for introducing the solar-wind electric field into the tail lobes and the polar caps. The momentum transfer caused by this electric field drives the internal convection system that transports plasma and magnetic flux through the magnetosphere and creates the extended tail. Second, it simplifies the entry of solar wind particle into the magnetic field of the Earth. These particles provide a substantial fraction of the magnetospheric plasma. Third, it creates topologically distinct regions of the magnetic field within which the total magnetic flux is constantly changing. Magnetic flux transported from the day side to the tail lobes provides a reservoir in which energy extracted from the solar wind can be stored for short intervals of time.

There is evidence that steady state reconnection of the type illustrated in Figs 28 and 37 occurs infrequently (Sonnerup *et al.*, 1981; Sonnerup, 1984). More typically as shown in Fig. 29, localized, transient reconnection called flux transfer events (FTE) transports small bundles of flux from the day to night side (Russell and Elphic, 1978; Cowley, 1982a,b; Sonnerup, 1984; Baumjohann and Haerendel, 1987; Elphic, 1990). As demonstrated by Berchem and Russell (1984), these events only occur when the magnetosheath magnetic field is southward. The frequency of occurrence and typical size are sufficient to create an average effect as large as is typically observed in polar-cap electric fields (Cowley, 1985).

Many studies (Kamide and Slavin, 1986) of the relation between the solar wind magnetic field and substorm and storm activity have established that the magnetopause acts as a rectifier of the solar wind electric field (e.g. Burton *et al.*, 1975). Only when this field points from dawn to dusk, i.e. when the IMF is antiparallel to the Earth's magnetic field, does magnetic activity occur. This activity is typically delayed by about an hour after a southward turning of the IMF. A system analysis using linear prediction filters shows that isolated substorms are characterized by a bimodal response function (Clauer *et al.*, 1981; Bargatze *et al.*, 1985; McPherron *et al.*, 1988). This result implies that there are two components to magnetic activity. One which responds rapidly to the solar wind within about 20 min and is apparently directly driven by the solar wind (Akasofu, 1981a,b). Another which is delayed about an hour and represents the unloading of stored energy (Baker *et al.*, 1984; Baumjohann, 1986b).

4.5.2 Erosion of the magnetopause

For reconnection to occur at the subsolar point magnetic flux must flow towards the x-line from both sides of the magnetopause. Within the magnetosphere the rate at which this can happen is controlled by the ionospheric conductivity at the feet of the magnetospheric field lines (Coroniti and Kennel, 1973). Initially magnetospheric field lines bulge outward, trying to flow towards the x-line. This produces a kink in the field lines which propagates to the ionosphere as an Alfvén wave (Southwood, 1987). Accompanying this wave is a field-aligned current that closes through the ionosphere. The interaction of this current with the ionospheric magnetic field produces a force that accelerates the ionospheric plasma poleward. The final velocity of this plasma is determined by an opposing force produced by collisions of drifting ions with neutral particles in the ionosphere. The geometry of this current is illustrated in Fig. 57. Its sense is that obtained by diverting a fraction of the dawn-to-dusk magnetopause current normally flowing through the subsolar region along field

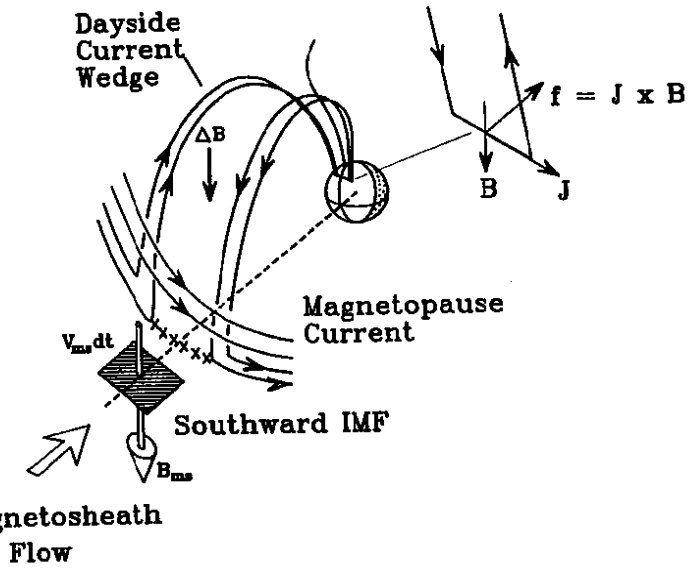

Figure 57. A highly idealized model of field-aligned currents expected for steady-state merging at subsolar point. Magnetopause current diverted through the ionosphere provides the x-line geometry, the magnetic perturbation needed to balance pressure at the magnetopause, and force required to accelerate ionospheric plasma.

lines. This current flows down on the morningside of the polar cusp, then eastward through the ionosphere, and finally upward on the afternoon side of the polar cusp. It should be noted that the localized decrease in magnetopause current will produce an x-type magnetic configuration of finite length near the subsolar point. Furthermore, the perturbation magnetic field interior to this current system is southward and hence reduces the total magnetic field of the dipole and magnetopause.

Attempts have been made to detect the ground effects of a large-scale current system such as that shown in Fig. 57 without success (Clauer, personal communication). This can be understood if FTEs are the dominant form of dayside reconnection. Typical FTEs of 1 R_e dimension would have an ionospheric footprint of about 100 km. Field-aligned currents separated by only this amount would not be observable far from the foot of a reconnecting flux tube. However, Southwood (1987) has suggested that directly under the tube a twin vortex pattern of ionospheric current and flow should be observable. Several recent reports describe such current systems (Todd *et al.*, 1986; Lanzerotti *et al.*, 1987; Friis-Christensen *et al.*, 1988; Glassmeier *et al.*, 1989). However, the authors and others have noted that

these events appeared to be associated with northward IMF and changes in solar-wind dynamic pressures rather than southward IMF (Sibeck *et al.*, 1989).

The dayside current wedge described above has a large inductance and the ionospheric closure a finite resistance. Together they establish an inductive time constant $\tau = L/R$ which is of the order of 15 min. Because of this inductive delay the rate at which magnetospheric flux flows into the dayside reconnection region is initially less than that at which magnetosheath flux arrives. But the net flux into the x-line on the two sides must be equal. This is achieved by moving the magnetopause and x-line earthward. In a coordinate system moving with the x-line, equal amounts of flux arrive from either side. The result of this process is 'erosion' of the dayside magnetopause. Successive layers of the Earth's closed field lines are opened to the solar wind becoming part of the polar cap. Satellite observations provide evidence that this phenomenon occurs during substorms (Aubry *et al.*, 1970; Burch, 1973; Holzer and Slavin, 1978, 1979). In general, the magnetopause moves inward, and the polar cusp moves equatorward during the substorm growth phase.

Earthward displacement of the magnetopause seems to violate the pressure balance condition which determines the location of the magnetopause. In the absence of reconnection the dynamic pressure of the solar wind is balanced by the sum of the magnetic fields of the Earth and the magnetopause current. But as the boundary moves earthward the magnetic pressure inside increases as a result of the stronger field closer to the Earth. Since the pressure outside does not necessarily change in a corresponding way it seems that pressure will not balance across the magnetopause. However, the magnetic perturbations of the dayside current wedge and the tail current are oriented such that they reduce the total magnetic field inside the dayside magnetopause. Thus adjustments of the strength or locations of these two current systems can maintain pressure balance.

4.5.3 *Transport of magnetic flux to the tail*

Magnetic flux cut and reconnected at the subsolar x-line is initially ejected away from the equatorial plane by the forces present around the x-line. As soon as the field lines leave the diffusion region they again satisfy the approximations of MHD and their respective plasmas and fields are frozen together. In the magnetosheath the flow velocity gradually increases as the plasma leaves the reconnection region. As shown in Fig. 58, the segments of newly opened field lines frozen in the magnetosheath plasma are transported over the polar caps and along the magnetotail boundaries. The segment within the magnetopause current layer is initially strongly kinked

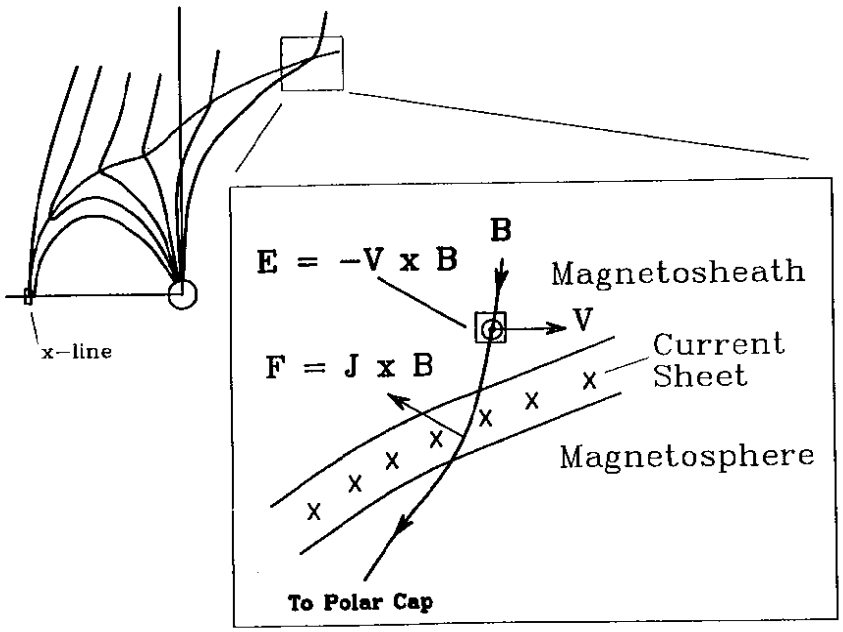

Figure 58. Configuration of reconnected field lines as they pass through the polar cusp. Open field lines passing through the magnetopause current sheet create a force which retards the solar-wind flow, and apply its electric field to the polar cap.

with the fields on the two sides, making an acute angle with each other. As this segment passes through the polar cusp the kink opens and tailward of the poles it makes an obtuse angle through the boundary. The component of magnetic field which points through the magnetotail current sheet produces a retarding force on the solar wind and transfers momentum to field lines within the magnetosphere (see insert).

According to MHD a moving plasma polarizes producing an electric field $E = v \times B$ observable in a frame at rest relative to the plasma. For the configuration shown in Fig. 58 the magnetosheath electric field is directed out of the plane of the diagram, as shown in the inset. Magnetic field lines are virtually perfect conductors so this electric field is transmitted through the magnetopause along field lines to the ionosphere. Since by definition all open field lines map to the polar cap this electric field appears as an eastward or dawn-to-dusk polar-cap potential drop. The expected magnitude of the polar-cap electric field depends on a number of theoretical considerations based on reconnection theory. Generally speaking, a faster wind, a stronger IMF and a more southerly orientation should produce a stronger potential.

Reiff *et al.* (1981) have tested linear relations between hourly averages of various solar-wind coupling parameters and satellite observations of polar cap potential drops. Their results show that there is a high degree of correlation between parameters suggested by reconnection theory and the polar-cap potential. The highest empirical correlations are produced by the rectified solar-wind electric field ($r \sim 0.81$), and the Perreault and Akasofu (1978) epsilon parameter ($r \sim 0.89$). However, to obtain good correlations it was necessary to amplify and limit the magnetosheath field to a value given by $\alpha = (7B_{sw}/60)$ nT < 1. The factor $7B_{sw}$ is a consequence of bow-shock compression of the solar wind IMF followed by depletion of plasma from field lines stagnating near the subsolar point. The factor 60 comes from the requirement that the external magnetic field cannot exceed the internal field and maintain pressure balance at the magnetopause. Wygant *et al.* (1983) have made an independent assessment of these relations and while confirming that the correlations are consistent with reconnection, obtain somewhat different results. They conclude first that parameters with electric field dimensionality show the best relation to the IMF. Second they find that the polar-cap potential depends on the solar wind for at least 4 h before a measurement. Finally, they conclude that 100% of the southward flux incident on a 30 R_e magnetopause reconnects until the polar-cap potential saturates at about 100 keV. Both authors find a residual potential not related to the IMF. For Reiff *et al.* (1981) this value was about 35 keV. Wygant *et al.* (1983) argue that much of this residual is a consequence of not accounting for the decay of the potential from previous hours. They estimate the value to be less than 20 keV. Both studies support the view that the composite magnetosphere is driven by a combination of reconnection and viscous interaction as presented in earlier sections.

4.5.4 *Accumulation of flux in the magnetotail lobes*

Information about the start of dayside reconnection will be transported along the magnetotail boundary with the velocity of the magnetosheath plasma. Tailward of the Earth this is nearly the solar-wind velocity. Thus the kink associated with the first reconnected field line in a new episode of southward IMF will reach the location of the distant neutral line at 120 R_e in about 30 min. However, from the argument in the preceding section a fraction of the solar-wind electric field is present across the polar cap and hence the tail lobes. This causes field lines to drift across the lobes towards the neutral sheet. In the absence of any other effects it would take them about 1.5–2.0 h to reach the neutral sheet.

Coupling studies mentioned above indicate that rapid reconnection does not begin in the tail for about an hour after the IMF turns southward. At

least 30 min of this delay can be attributed to the time it takes the solar wind to carry the discontinuity associated with a new front of reconnection to the distance neutral line. Close to the Earth, magnetic flux begins to accumulate in both tail lobes because of this delay. But according to Faraday's law, an increasing magnetic flux through a circuit induces an electric field. Since the flux is increasing, this field is parallel to the electrostatic field at the outside boundaries of the lobes and antiparallel to it at the plasma sheet boundaries. Depending on the relative strength of these fields, there may be no drift of field lines at all near the plasma sheet. Thus it seems likely there is initially nothing to bring the antiparallel fields together and initiate merging. Instead magnetic flux simply accumulates in the lobes. Furthermore, because the magnetotail boundaries are parallel to the magnetosheath flow the lobe magnetic pressure must balance the thermal pressure in the magnetosheath. But this pressure does not change so that there can be no change in the internal field strength. Thus, newly added flux can only increase the size of the distant tail lobes.

Closer to the Earth the situation is quite different as discussed by Coroniti and Kennel (1972a). Here the magnetopause flares from zero diameter at the subsolar point to its final downstream diameter. Wherever the boundary is not parallel to the magnetosheath flow it intercepts some fraction of its dynamic pressure. Internally, the magnetic field pressure must balance both this and the thermal pressure of the magnetosheath. As magnetic flux is eroded from the day side, the cross-section of the near-Earth magnetosphere decreases in proportion to the decreasing subsolar standoff distance. However, the shrinking magnetopause must merge continuously with the growing size of the distant tail. As illustrated schematically in Fig. 59 the angle the near-Earth magnetopause makes with the magnetosheath flow increases as the day side shrinks. This requires a corresponding increase in the magnetic field strength within the near-Earth tail lobes. If there were no change in tail diameter at these distances the field would increase simply because the total flux increases. Since the cross-section decreases the field strength must increase even more. Thus, near the Earth the cross-tail current creating the lobe field must also increase. These changes continue for more than 30 min before the front of newly reconnected field lines ever reaches the downstream location of the distant neutral line.

During isolated substorms there is ample evidence that magnetic flux accumulates in the tail lobes. Spacecraft in the near tail ($X_{GSM} < 25\ R_e$) have consistently observed increases in the field magnitude prior to the onset of the expansion phase (Fairfield and Ness, 1970; Aubry and McPherron, 1971; McPherron, 1972; McPherron *et al.*, 1973; Caan *et al.*, 1973; Nishida and Nagayama, 1973). Statistical studies indicate that this

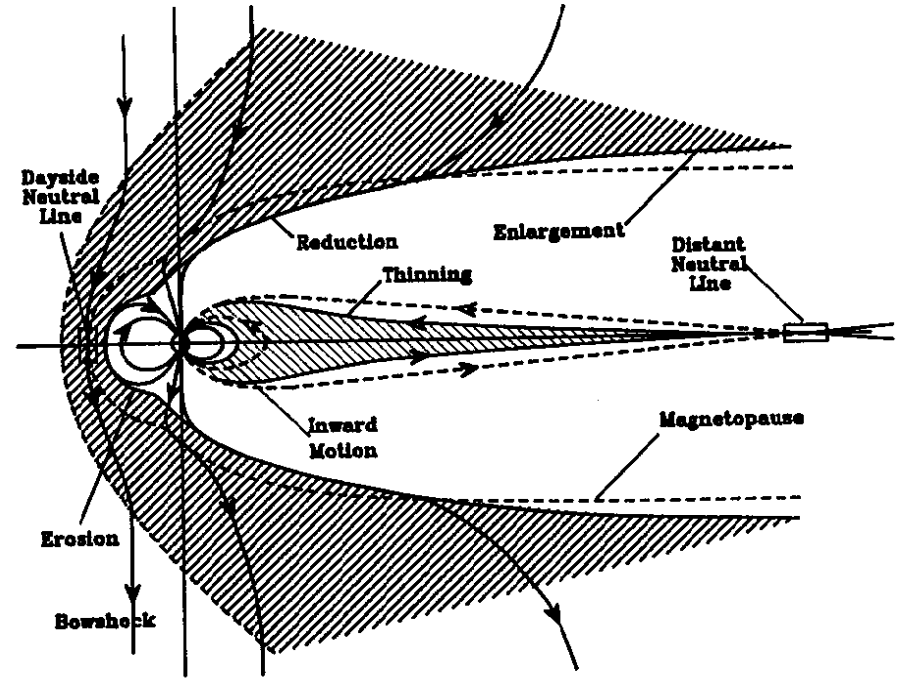

Figure 59. Changes in the magnetospheric configuration induced by a southward turning of the IMF. These include dayside magnetopause erosion, accumulation of magnetic flux in lobes, alteration of shape of magnetopause, thinning of the plasma sheet and inward motion of current sheet.

effect is most pronounced when the substorm onset is associated with a well-defined mid-latitude positive bay (Caan *et al.*, 1975, 1978). In some cases, however, spacecraft are within or close to the plasma sheet and it is impossible to decide whether the field increases without good plasma data. During continuous activity it becomes too difficult to identify onsets, and in fact it seems likely that the lobe field might reach equilibrium between flux storage and release, so there would be no large changes in field magnitude.

Spacecraft in the distant tail also provide evidence of flux accumulation during substorm growth phase. Maezawa (1975) used Explorer 33 data to study distant magnetopause crossings in relation to mid-latitude substorm onset. He found that the boundary moves outward during the growth phase, and inward during the expansion phase. The ISEE-3 spacecraft made similar observations at distances from 60–220 R_e (Baker *et al.*, 1984a,b, 1987a,b). Both individual events and superposed epoch analysis

demonstrate that the radius of the tail increases by as much as 2–4 R_e during substorm growth phase.

Ground observations provide additional evidence that the amount of open flux increases during substorms. For example, the well-known increase in size of the auroral oval at higher levels of activity (Feldstein and Starkov, 1967) supports this idea if it is assumed that field lines poleward of the oval are open. Meng (1979) has reviewed a variety of ground observations which show that this increase is caused by a southward IMF. Dynamical studies exhibit the same pattern seen in the tail. The oval expands in the growth phase after a southward turning, and decreases in the expansion phase. Frank and Craven (1988) illustrate this beautifully (their Fig. 21) using auroral images from the DE-1 spacecraft.

4.5.5 *Earthward movement of the tail current*

Once reconnection has begun there is a normal component of magnetic field through the magnetotail boundary. The interaction of this field with the tail current produces a force retarding the solar wind. By Newton's law the solar wind exerts an equal and opposite force on the tail boundary. This force provides the 'tangential drag' by which the solar wind pulls the dipole field antisunward creating the tail. Integrated over the entire boundary of the magnetotail this force of the solar wind is substantial and must be balanced by an equal and opposite force of the Earth on the magnetotail. As shown by Siscoe (1966) this force $\boldsymbol{F}$ is created by the interaction of the Earth's dipole moment $\boldsymbol{\mu}$ with the fringing field $\boldsymbol{B}_t$ of the earthward edge of the tail current system according to the relation $\boldsymbol{F} = \nabla (\boldsymbol{\mu} \cdot \boldsymbol{B}_t)$. Since the dipole moment $\boldsymbol{\mu}$ is constant the field gradient at the Earth must change. This is accomplished by the tail current moving closer to the Earth. As discussed earlier this motion is a natural consequence of particle drift in an enhanced convection electric field.

Data that most clearly illustrate this process are provided by synchronous spacecraft. During the growth phase of a substorm a synchronous spacecraft in the magnetic equatorial plane observes a continuous decrease in the magnetic field magnitude and z component (parallel to dipole axis) (McPherron and Coleman, 1969). Spacecraft at higher synchronous latitudes usually observe an increase in magnitude as in the lobes, and also an increasing inclination toward more tail-like field (Coleman and McPherron, 1976; Kokubun and McPherron, 1981). Synchronous particle data respond to these field changes with pitch angle distributions becoming increasingly peaked parallel to the field during the growth phase (Baker *et al.*, 1978; Baker, 1984). Often, just before expansion onset the fluxes of energetic electrons completely disappear as if the spacecraft had passed into

the tail lobes (Baker and McPherron, 1990). Kauffman (1987) has pointed out that the tail-like fields observed during the growth phase require intense equatorial sheets of current immediately outside synchronous orbit. Tsyganenko (1989) suggests this sheet is a consequence of the inductive electric field produced by loading flux into the tail lobes.

4.5.6 *Thinning of the near-Earth current sheet*

Coincident with the earthward motion of the tail current is a thinning of the current sheet. At least two factors contribute to this thinning. The first is increased magnetic pressure in the tail lobes resulting from flux storage. The second is loss of magnetic flux from the central plasma sheet to the return flow created by dayside reconnection. As plasma and flux are withdrawn from the nightside plasma sheet the normal component of magnetic field crossing the sheet decreases and the sheet thins. Simultaneously, the total current carried by the sheet is increasing as required by the increasing lobe field strength. Figure 59 shows these changes schematically as changes in the spatial locations of various nightside boundaries.

While there is experimental evidence for growth phase thinning of the tail current sheet (McPherron *et al.*, 1987), it is less clear how much the thickness of the plasma sheet decreases. Data show that fluxes of energetic particles ($E > 30$ keV) decrease as the structure of the plasma sheet magnetic field changes (Walker *et al.*, 1976; Pytte *et al.*, 1976). However, the dimensions of the region occupied by plasma ($E \sim 1$ keV) may remain relatively constant while the change in magnetic field structure alters the drifts of particles such that the current density increases most rapidly at the centre of the plasma sheet. Such a change would in effect move a spacecraft from the CPS to the PSBL. Since the magnetic field in the boundary layer is very nearly the same as in the lobe a magnetometer would observe an apparent thinning of the plasma sheet.

4.5.7 *Enhancement of convection*

The first effect of dayside reconnection is to start ionospheric plasma flowing towards the night side, adding newly opened magnetic flux to the polar cap. As the flux is added to the top of the lobes it creates a magnetic pressure gradient that forces a flow across the lobes. The solar-wind electric field is mapped along open field lines to the polar cap. Here it drives a Pedersen current that diverges along field lines in the regions of the dawn and dusk velocity shears. This current continuously forces the plasma to drift against the counteracting force of collisions with neutrals. Within a

short time a rarefaction wave produced by flow into the dayside reconnection region propagates around the Earth in the equatorial plane and reaches the plasma sheet. This wave starts the plasma flowing sunward within the near-Earth plasma sheet returning magnetic flux and plasma to the dayside. The electric field produced by polarization of this flow is mapped into the nightside auroral oval and causes an increased flow of ionospheric plasma towards the day side.

The effect of these changes is the well known DP2, twin-vortex convection pattern in the polar cap (Iijima and Nagata, 1972). Friis-Christensen and Wilhjelm (1975) and Friis-Christensen *et al.* (1985) used polar-cap magnetometers to show particularly well how this current vanishes when the IMF turns northward. Also they show that IMF-B_y controls the location of the foci of the vortices. In the northern hemisphere the convection pattern is shifted towards dawn or dusk, opposite to the direction of the IMF-B_y component. Ionospheric radars reveal similar patterns (Foster, 1984), as do data from polar orbiting spacecraft (Heppner, 1977; Heelis and Hanson, 1980; Heppner and Maynard, 1987).

A consequence of the increased convection electric field is a change in the location of the separatrix (plasmapause in steady state). Since the separatrix is produced by a balance between convection and corotation electric fields, an enhancement of convection causes the separatrix to move earthward (Nishida, 1966). But then, plasma originally on closed drift paths within the plasmasphere is on open drift paths as illustrated in Fig. 60. If the enhanced electric field remains steady for 8 h or longer, the plasma originally inside the plasmapause eventually drifts through the magnetosphere and is lost to the magnetosheath (Grebowsky and Chen, 1975). Meanwhile, plasma drifting sunward from the CPS approaches closer to the Earth than it did before. Particles with finite energy in the distant plasma sheet depart from the convection drift paths of the cold plasma due to gradient and curvature drift in the near-Earth magnetic field (Kavanagh *et al.*, 1968; Chen, 1970). On the night side this drift has a component across the equipotentials in the direction of the magnetospheric electric field. On the night side the drifts are such that both ions and electrons gain energy.

If the convection electric field were to remain steady, particles energized on the night side lose energy as they drift against the total electric field on the day side. However, the convection electric field eventually decreases and the energy dependent separatrices for particles of different energy move away from the Earth. This leaves those particles energized from drift through the night side inside their new separatrices. They become trapped inside regions 'forbidden' to entry from the night side, or at least forbidden during quiet conditions. Such fluctuations in the convection electric field

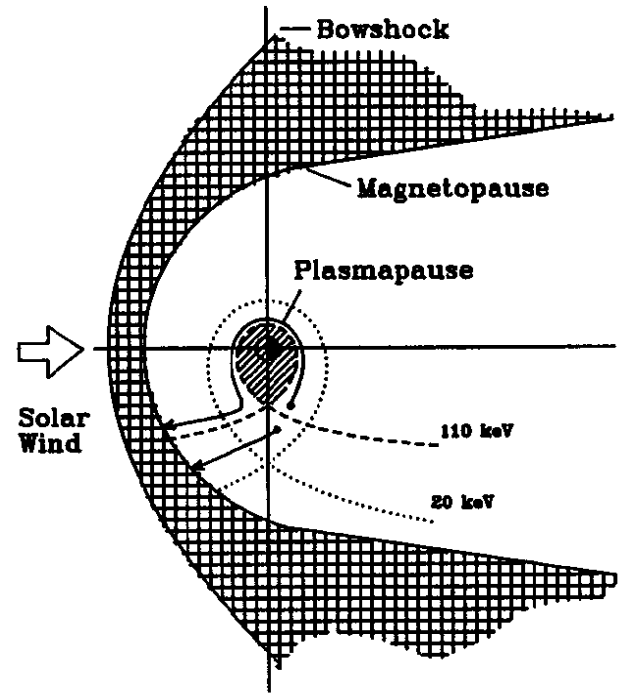

Figure 60. Erosion of the plasmasphere as a result of enhancement of the convection electric field. The separatrix between open and closed drift paths is shown for quiet times (dots—20 keV) and for disturbed times (dashes—110 keV).

are the primary mechanism for trapping particles in the outer radiation belts. A subsequent enhancement of the convection electric field will further energize the half of these particles which happen to be drifting through the night side. Those on the day side will lose energy, but there will always be some particles that gain additional energy with each enhancement (Lyons and Schulz, 1989).

Drift of particles through the entire magnetosphere can take many hours for low-energy particles. Consequently, the configuration of particles in the magnetosphere cannot adjust immediately to changes in the convection electric field. An important consequence of this is a breakdown in the shielding of the plasmasphere. As discussed in §3.1.5, the separatrices for energetic particle drift are not symmetric with respect to the noon–midnight axis. Generally speaking, electrons approach closer to the Earth on the dawn side than do positive ions, producing a region of negative space charge there. Similarly, ions approach closer to the Earth on the dusk side. The electric field resulting from this polarization is normally opposite

to the convection electric field and nearly cancels it inside the plasmasphere. However, the enhancement of convection penetrates the region interior to the new cold plasma separatrix distorting the closed drift paths within. With time, particles drift inward from the tail re-establishing the polarization and shielding. While this is in progress a fraction of the convection electric field is present inside the plasmasphere and ionospheric drifts are substantially different from those of quiet times.

4.5.8 *Increase in field-aligned currents*

An enhancement of convection increases the strength of field-aligned currents. Both the Region 1 and Region 2 systems discussed in §3.1.3 become stronger in response to the increased electric field. The reason for this is current continuity. Ohm's law requires that an increase in ionospheric electric field produce an increase in current. However, wherever there is a divergence in the ionospheric electric field, or a gradient in electrical conductivity the ionospheric current must diverge along field lines. Since the ionospheric current increases the field-aligned currents must also increase.

These increases are well documented by polar-orbiting spacecraft. Iijima and Potemra (1976) show statistically that the Region 1–2 currents are present for all levels of activity. Both currents increase almost linearly with increasing magnetic activity. Region 1 currents are strongest on the day side, while Region 2 currents are strongest on the night side. Total integrated current strengths are of order 2×10^6 A for moderate activity. Iijima and Potemra (1978) show that as activity increases the location of the Region 1–2 currents expands equatorward with the aurora oval, widening and growing in strength.

A second reason for the increase in field-aligned currents is an increase in ionospheric conductivity with activity (Spiro, *et al.*, 1982; Hardy *et al.*, 1987). For a constant convection electric field an increase in conductivity will produce a larger current, which when it diverges, increases the field-aligned currents. The increase in conductivity is a consequence of inward motion of the tail current. The diffuse aurora and the corresponding ionization are produced by particle precipitation from the central plasma sheet. As the tail current moves closer to the Earth to balance solar-wind drag the precipitation rate increases (Southwood and Wolf, 1978). This is a result of several factors. First, more particles are lost because their loss cone increases as the ratio of equatorial to ionospheric magnetic field increases. Second, the length of field lines become shorter allowing particles on them to reach the ionosphere sooner. Third, and somewhat less certain, particles are more frequently scattered by enhanced wave–particle interactions, or scattered by the sharp bend in the growing tail-like magnetic field.

4.5.9 *Increase in ionospheric currents*

The increases in ionospheric electric field and conductivity enhance the ionospheric Pedersen and Hall currents. Magnetic perturbations from these currents are recorded on the ground, and are in fact, a primary tool for deducing convection patterns as discussed above. Improvements in techniques for inverting these data are producing ever increasing resolution of the details of magnetospheric convection. A recent example of such improvements is the AMIE (Assimilative Mapping of Ionopheric Electrodynamics) technique developed by Richmond and Kamide (1988) and applied to a substorm during a moderate magnetic storm by Knipp *et al.* (1989). As noted by Knipp *et al.* the instantaneous patterns can differ substantially from the average patterns obtained with radars or satellites.

The enhancement of the twin vortex current system is responsible for the magnetic perturbations of the substorm growth phase (McPherron, 1970). It also produces the initial departure of the *AU* and *AL* indices from their quiet backgrounds. Allen and Kroehl (1975) have shown that the stations which most frequently contribute to the *AU* and *AL* indices are respectively located at 1730 and 0315 MLT. These times are a consequence of the twin vortex system having maximum eastward and westward current densities at these locations. Today this current system is usually referred to as the 'convection electrojet'.

4.5.10 *Reconnection in the central plasma sheet (CPS)*

The close relation between the orientation of the IMF and a variety of magnetospheric phenomena related to geomagnetic activity is the primary reason for asserting that magnetic reconnection occurs on the dayside magnetopause. If it occurs on the day side then it must also occur on the night side. If not, there would be a flux catastrophe in which either all the magnetic flux on the day side would be transported to the magnetotail, or more likely, all closed flux in the plasma sheet would flow to the day side to be reconnected and transported to the tail. Various models of substorms differ in where they place nightside reconnection. The NENL model assumes it begins within 20–30 R_e of the Earth, sometimes as close as 10 R_e (McPherron *et al.*, 1973; Russell and McPherron, 1973; Hones *et al.*, 1973; Nishida and Nagayama, 1973). It is this assumption that gives the model its name. The model also assumes that when reconnection begins there is a second, inactive neutral line at distances greater than 100 R_e as illustrated in Fig. 61.

The simultaneous presence of two neutral lines in the tail imposes topological constraints on the reconnection process. One of these is the requirement that near-Earth reconnection begin on closed field lines

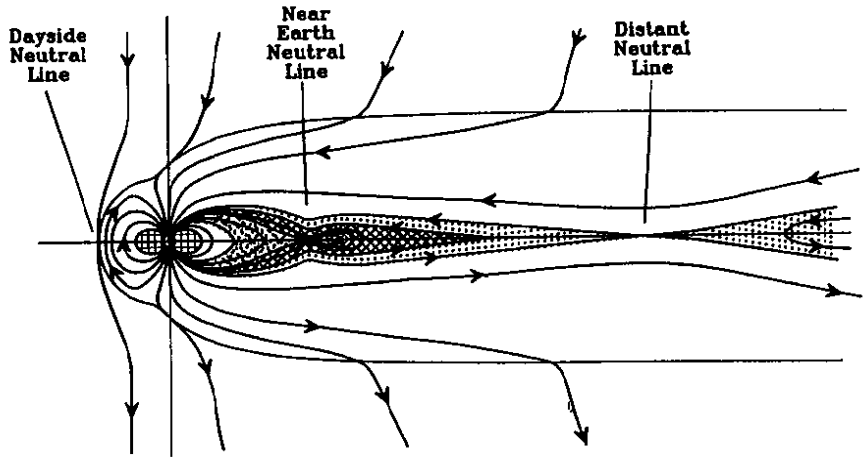

Figure 61. An approximate scale drawing showing the formation of a near-Earth neutral line within the CPS during the late growth phase.

passing through the neutral sheet (Russell and McPherron, 1973). There are currently two views as to how this might happen. The original model illustrated by Fig. 61 assumes that reconnection begins in the CPS. In this case closed field lines are loaded with hot plasma and the field is weak, so that the Alfvén velocity is low. Since the reconnection rate is proportional to the Alfvén velocity reconnection is initially slow (Coroniti, 1985). As reconnection proceeds, more and more field lines are cut. Earthward of the neutral line the field lines collapse sunward flowing around the Earth. Tailward, the field lines collapse into closed loops disconnected from the Earth. These loops, and the newly energized plasma which populates them are initially held to the Earth by tension of closed field lines which cross the neutral sheet tailward of the disconnected loops. This growing bubble of plasma and magnetic field line has been named a plasmoid (Hones, 1977).

4.5.11 Development of a plasmoid

If reconnection continues within the CPS long enough, field lines in the plasma sheet boundary layer eventually begin to reconnect. Since the Alfvén velocity in this region is higher than the CPS the reconnection rate increases. Eventually, reconnection severs the last closed field lines which define the boundary of the plasma sheet and map to the distant neutral line. Then the low density of the magnetotail lobes causes a dramatic increase in the Alfvén velocity and the reconnection rate. Also, the topology of

reconnection changes suddenly as the bubble of closed field lines and plasma generated by reconnection of closed field lines becomes disconnected from the Earth. This instant is generally assumed to be the onset of the substorm expansion phase.

An alternative model of where nightside reconnection begins has been suggested by Lyons and Nishida (1988). Ground observations show that the onset of the auroral substorm occurs on the most equatorward discrete arc which is located just poleward of the diffuse aurora. Since discrete arcs are thought to be associated with the PSBL, and diffuse aurora with the CPS (Akasofu, 1977; Lyons and Evans, 1984), this suggests that the neutral line forms at the location of this boundary in the plasma sheet. Figure 61 is drawn with this boundary beyond 20–30 R_e, somewhat further than the region usually referred to as the near-Earth neutral plasma sheet. However, the location of this boundary is determined by the magnitude of cross-tail electric field, and it is possible that during intense southward IMF it is closer to the Earth. For this to be true, most of the CPS would have to be withdrawn to the inner magnetosphere at expansion onset, and the plasmoid would be constructed entirely of boundary layer plasma (Nishida, 1988). In other respects, this alternative model of plasmoid formation does not differ from the earlier model.

As noted above, the onset of the expansion phase is attributed to the severance of the last closed field lines and the beginning of the retreat of the plasmoid. For this to be true, reconnection must begin during the substorm growth phase. It is a major difficulty of the NENL model that there seems to be no observational support for this phenomenon. Perhaps the initial region in which the plasmoid forms is very localized. Possibly the reconnection rate is too slow to cause observable effects until boundary layer field lines become involved. Baker and McPherron (1990) suggest the possibility that the extreme dropouts of energetic particles at synchronous orbit are a result of growth phase reconnection. They argue that slow reconnection in the CPS might divert tail current earthward producing the extreme tail-like fields seen at synchronous orbit late in the growth phase.

4.5.12 Loss of a plasmoid

The fate of the plasmoid after expansion onset is illustrated in Fig. 62. As soon as the last closed field line is severed, subsequent reconnection cuts open field lines of the tail lobes. As lobe field lines reconnect, segments of field lines earthward of the neutral line close, connecting to the Earth through the plasma sheet. Tailward of the neutral line the field line segments connect only to IMF lines. However, because they are sharply kinked where they cross the neutral sheet they form a sling around the

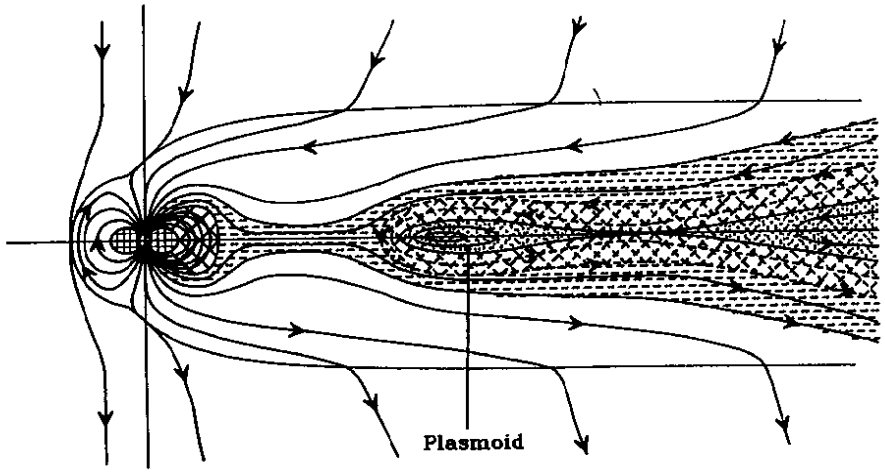

Figure 62. A schematic illustration of the loss of a large-scale plasmoid during the expansion phase. Tension of IMF field lines around the bubble pull it from the centre of the tail.

plasmoid. Tension in these field lines accelerates the plasmoid away from the earth as they begin to straighten. Also the normal pressure gradient in the pre-existing plasma sheet, and the ram pressure of plasma ejected from NENL provide additional forces on the plasmoid.

As the plasmoid leaves the near-Earth region it takes with it the plasma and magnetic field of the original plasma sheet. Thus, earthward of the retreating plasmoid the plasma sheet collapses into a very thin current sheet separating the reconnecting fields of the north and south tail lobes. The x-line, however, remains close to the Earth, reconnecting the magnetic flux stored in the tail lobes. As reconnection continues, open field lines of the lobe are converted to closed field lines earthward of the x-line, and to open field lines tailward of it. If the IMF remains southward so that reconnection continues on the day side, the reconnected flux will flow around the Earth. Otherwise, it is added to the night side of the magnetosphere, eventually forcing the nightside x-line to retreat down the tail.

The NENL model is primarily based on observations taken immediately after expansion onset. If a spacecraft is in the tail lobe the field magnitude suddenly stops increasing and begins to decrease. Often, the slope of the vertical component changes as well (McPherron *et al.*, 1973; Nishida and Nagayama, 1973). Before onset B_z usually decreases throughout the growth phase, indicating increasing flaring of the magnetopause as erosion adds dayside flux to the tail lobes (Fairfield, 1985). After onset, reconnection at the NENL converts the open flux of the lobes to closed field lines, returning

them to the day side. This decreases the total flux in the lobe and changes both the magnitude and slope of the lobe field.

If the spacecraft is initially inside the plasma sheet, but near the edge, the behaviour is quite different. The field magnitude will suddenly increase from weak and turbulent to strong and steady values. Often there will be substantial azimuthal B_y perturbations suggestive of field-aligned currents (Aubry *et al.*, 1972; Fairfield, 1973; Elphic *et al.*, 1985; Ohtani *et al.*, 1988). The vertical component B_z frequently decreases, indicating the magnetic field has rotated slightly due to a thicker plasma sheet tailward of the spacecraft (Pytte *et al.*, 1976). Plasma observations show that the changes in magnetic field are caused by a sudden disappearance or thinning of the plasma sheet (Hones *et al.*, 1971; Hones and Schindler, 1979). Usually, there is a brief burst of tailward-flowing plasma as the edge of the thinning plasma sheet passes over the spacecraft (Hones and Schindler, 1979). Occasionally the boundary of the plasma sheet moves temporarily over the spacecraft, revealing that a thin residual plasma sheet remains and that it still contains tailward-flowing plasma (Hones *et al.*, 1986).

In the less frequent event that the spacecraft is located near the CPS at expansion onset, there is additional evidence that a neutral line forms earthward of the spacecraft. An example is the substorm studied during the sixth Coordinated Data Analysis Workshop (CDAW-6) (McPherron and Manka, 1985). Effects of a substorm expansion were observed at 13 R_e, 4 min after onset, and 1 min after the neutral sheet crossed upward over one of two ISEE spacecraft. A transient burst of high-speed tailward flow (~ 500 km s^{-1}) was accompanied by a strong southward magnetic field ($B_z < -50$ nT) (Paschmann *et al.*, 1985). Both the plasma and magnetic data show that the spacecraft was very close to the neutral sheet at this time. The second ISEE spacecraft was somewhat tailward and higher, and observed a weaker magnetic effect after a delay consistent with the measured plasma velocity. Lin *et al.* (1990) have done a detailed study of this event and show that the magnetic changes at the two spacecraft are consistent with a 'mini-plasmoid' moving tailward. A similar structure with comparable dimensions (3 R_e long and 1 R_e high) was seen a few minutes later. Subsequently, a very thin current sheet of thickness less than 1000 km apparently remained stable as it moved upward, crossing the second spacecraft 8 min later. For 24 min after the expansion onset both spacecraft were embedded in a weak tailward-flowing plasma with characteristics similar to that of the PSBL. Lin *et al.* (1990) demonstrate that energetic electrons and protons continuously streamed tailward throughout this interval.

The CDAW-6 event is not an example of a large-scale plasmoid of the type pictured in Fig. 62. Instead it is interpreted as small-scale structure in the current sheet earthward of the retreating plasmoid. The size of the true

plasmoid is determined by the distance between the NENL and the distant neutral line (Slavin *et al.*, 1989). Typically this is 60–80 R_e. Although the plasmoid model has been developed by observations in the near-Earth environment, the triumph of this model is its ability to explain substorm observations in the deep tail made by the ISEE-3 spacecraft.

The ISEE-3 observations provide convincing proof that the plasmoid model is basically correct. Nishida *et al.* (1988) have studied ISEE-3 data at intermediate distances near the Moon. They find that it is not possible to identify a PSBL at this location. They suggest this is because the current sheet acceleration region which creates the boundary layer is located in this part of the plasma sheet. Their evidence is a lack of field-aligned anisotropy in energetic particles when the spacecraft enters the plasma sheet. On exit (a thinning) the flow is mostly tailward. They find, furthermore, that earthward anisotropy is mostly associated with quiet times, and tailward anisotropy with substorm onset in the *AL* index. They conclude that some process occurs earthward of 60 R_e which after expansion onset creates ions with energies an order of magnitude higher than those created by ionospheric acceleration mechanisms. A few minutes after onset the plasma sheet at 60 R_e expands, engulfing a spacecraft initially in the lobe in tailward streaming ions. As this occurs, the magnetic field usually remains constant in direction before dipping southward and becoming weak and turbulent. A short time later, the spacecraft re-enters the high steady field of the lobe. The data are interpreted as the result of being somewhere above the centre of a large-scale plasmoid like, for example, near the point labelled 'plasmoid' in Fig. 62. Initial filling of the plasmoid by near-Earth reconnection causes the expansion. Subsequent tailward motion causes thinning and reorientation of the magnetic field similar to that seen near the Earth on the earthward side of the retreating plasmoid.

Observations by ISEE-3 at greater distances provide even more convincing proof of the plasmoid model. At distances of 220 R_e, the spacecraft is well beyond the distant neutral line and hence the region where the plasmoid forms (Zwickl *et al.*, 1984). Thus there are substantial delays of order 20–40 min between expansion onset and arrival at ISEE-3 (Baker *et al.*, 1987a,b). When the plasmoid passes ISEE-3 the magnetic and plasma signatures are consistent with the plasmoid model illustrated in Fig. 63. A spacecraft in the magnetosheath enters the tail lobe (Baker *et al.*, 1984a,b). A spacecraft in the high north lobe observes a travelling compression region (TCR) (Slavin *et al.*, 1989). When a TCR passes, the lobe magnetic field rotates first upward then downward as might be expected for a bubble of closed field lines passing beneath. The field magnitude rises then falls with a maximum at the centre of the accompanying rotation. Both the magnetopause crossing and the TCR are expected consequences of a large bubble locally swelling the cross-section of the tail as explained by Slavin *et al.*, (1989). A spacecraft somewhat lower in the lobe is engulfed in the plasmoid as it passes by (Hones *et al.*, 1984).

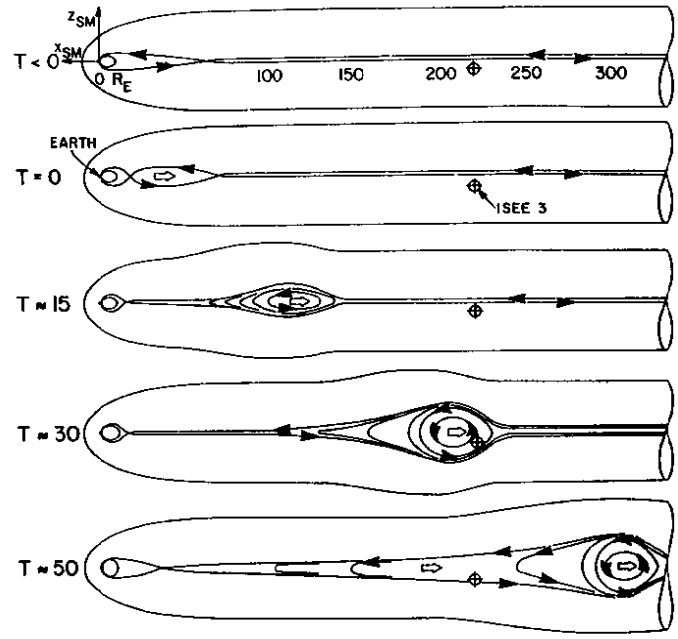

Figure 63. Effects of the large-scale plasmoid as it travels down the tail (Hones *et al.*, 1984). These include expansion of the magnetopause, travelling compression regions and engulfment of a spacecraft within the plasmoid where it observes characteristic field and plasma variations.

4.5.13 Development of the substorm current wedge

Concurrent with the loss of the plasmoid there develops a field-aligned current system called the substorm current wedge (Clauer and McPherron, 1974). This three-dimensional current system shown in Fig. 64 appears at the onset of the substorm expansion phase and is normally centred near midnight (Akasofu and Meng, 1969; Meng and Akasofu, 1969). As illustrated in the diagram, the current is produced by a diversion of a fraction of the cross-tail current along field lines to the ionosphere. Within the ionosphere the current flows westward, enhancing the westward electrojet (Bonnevier *et al.*, 1970). As the expansion phase progresses, the azimuthal extent and intensity of the diverted current increase. Within the ionosphere this westward current accelerates plasma equatorward, providing the

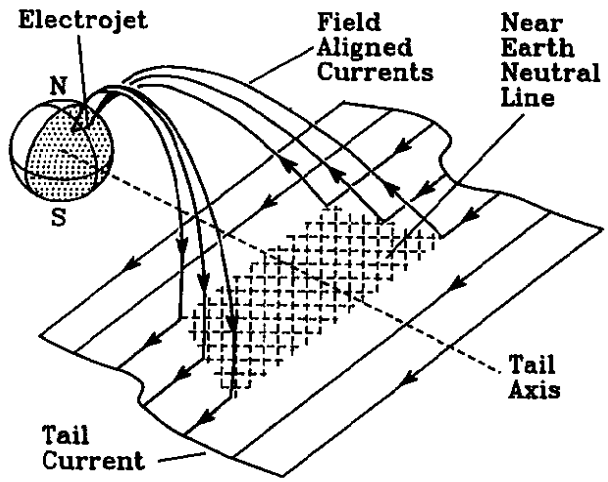

Figure 64. The diversion of the tail current through the ionosphere during the substorm expansion phase.

momentum required to start the return of plasma along the auroral oval to the day side.

The existence of this current system seems to be related to the finite azimuthal extent of the near-Earth x-line. Figure 65 presents an equatorial view of the magneotail during the growth phase depicted earlier in Fig. 59. The figure indicates that an x-line of finite length requires a connected o-type neutral line. Creation of this pair of separator lines requires a diversion of the tail current away from the region where the field lines disconnected by reconnection close downward through the current sheet. If the diversion occurs in the equatorial plane it might explain both the o-line (which requires enhanced current), and the earthward extension of the tail current in the equatorial plane (Baker and McPherron, 1990). If the diversion is along field lines it can account for the substorm current wedge.

This can be understood in the following way. At the end of the growth phase, prior to the formation of the x-line, the tail magnetic field consists of two regions of antiparallel magnetic field separated by a thin current sheet as depicted in Fig. 66a. To a first approximation this can be modelled by an infinite uniform sheet current. To produce an x-line field geometry, the total current across the sheet in the region of the x-line must be reduced. One way of doing this is to add an oppositely directed line current as shown in Fig. 66b. The reduction in total cross-tail current causes the field lines to bulge towards the neutral sheet, producing an x-type configuration. If we require that the x-type field configuration have finite

azimuthal extent, then we must terminate the opposing line current in some manner. This can be accomplished by introducing field-aligned currents at the ends of the line current and closing them in the Earth's ionosphere as illustrated in Fig. 66c.

Although the existence of a wedge-like current was suspected for some time, ground data alone were insufficient to determine its magnetospheric closure. However, when synchronous spacecraft reported observations of the same magnetic perturbations as recorded at mid-latitude ground observatories it became clear that the currents flow on field lines above the spacecraft (McPherron, 1972; McPherron *et al.*, 1973a). The first observations of this current system were made by ATS-1 in the magnetic equatorial plane. Subsequent observations above the equator by ATS-6 clearly confirmed the initial interpretation (McPherron *et al.*, 1975; McPherron and Barfield, 1980; Kokubun and McPherron, 1981).

The pattern of ground magnetic perturbations produced by the substorm current wedge was discussed in §2.4.2, and illustrated in Fig. 9. This pattern of magnetic perturbations is a persistent feature of isolated substorms, and is often seen during major substorms in highly disturbed

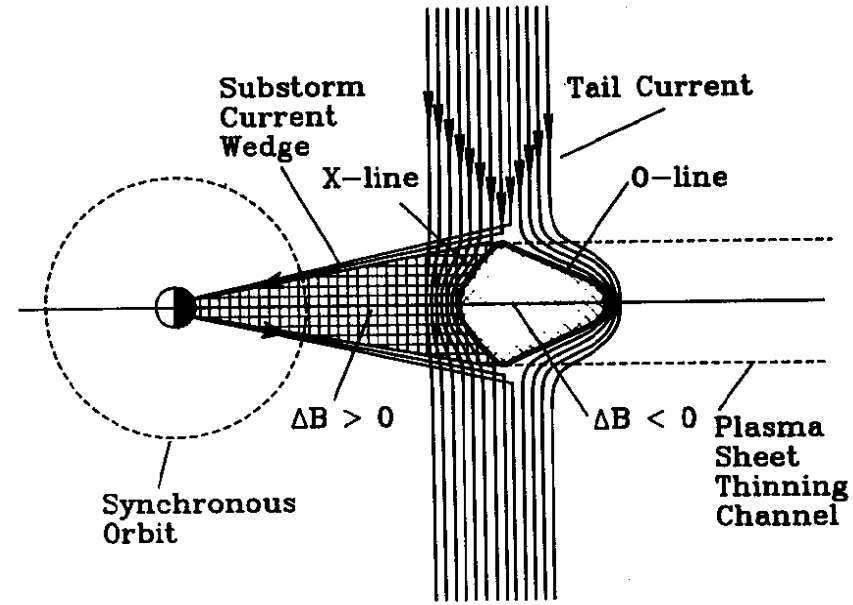

Figure 65. A schematic illustration of the formation of a connected pair of x- and o-type neutral lines in the CPS through current diversion. Dashed lines are the channel within which the plasma sheet collapses during loss of the plasmoid.

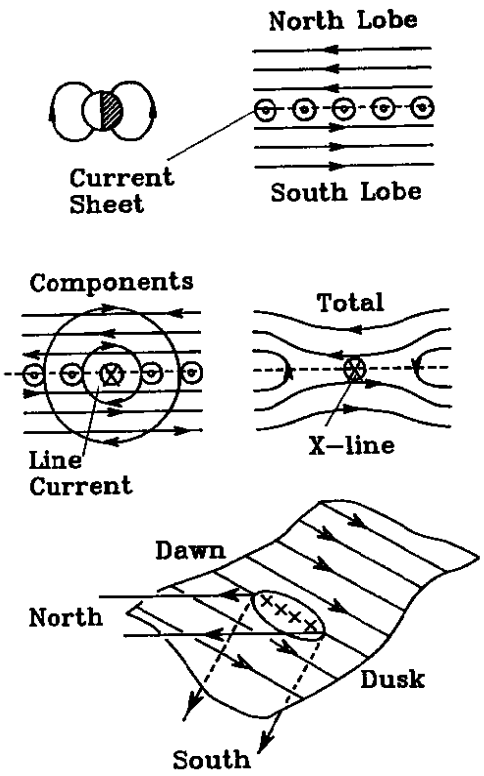

Figure 66. A schematic illustration showing how vacuum superposition of effects of tail and line current produces x-line field geometry. Top panel shows uniform field produced by a sheet current. Middle panel shows perturbation and total field produced by superposing an opposing line current. Bottom panel shows how localization requires current diversion from the region of the x-line.

periods. It provides additional evidence favouring the NENL model, since the formation of the plasmoid requires some kind of current diversion. It is interesting to note that if steady-state reconnection were to occur on the dayside magnetopause, one would expect to see a similar current system of opposite sense centred near noon. The fact that we do not argues strongly that reconnection on the day side is random and localized.

Auroral zone observations with latitude chains of magnetometers show that the development of the westward electrojet during the expansion phase is not steady. Kisabeth and Rostoker (1971) found that it occurs as a sequence of discrete intensifications. Additional filaments of westward current are added quasiperiodically every 10–20 min at the poleward edge

of the pre-existing electrojet. Mid-latitude observations clearly show the same effect with westward enhancement of positive H and D bays occurring quite frequently (Clauer and McPherron, 1974; Pytte *et al.*, 1976). Although there is a general tendency for successive filaments to be added poleward and westward of preceding filaments as suggested by Weins and Rostoker (1975), there are contrary examples as discussed by Clauer and McPherron (1974) and Pytte *et al.* (1976). Rostoker *et al.* (1987) have recently confirmed this using VIKING images of substorm intensifications.

Data from synchronous magnetometers have been particularly valuable in proving that step-like intensifications of the expansion phase are a common occurrence. Two spacecraft separated by only a few hours of local time observe quite different magnetic perturbations at the time of expansion onset (McPherron and Barfield 1980; Nagai, 1982a,b; Barfield *et al.*, 1985). Frequently, one spacecraft will observe a sudden dipolarization of the magnetic field produced by the perturbation field inside the current wedge, while one nearby will see continued development of tail-like field indicating that it is outside the wedge. Nagai (1982a,b) finds that the D perturbation generated by the current wedge starts at the onset of the mid-latitude positive bay, but the dipolarization (rotation in the meridian plane) begins only when D reaches its maximum, that is when the meridian containing the field-aligned current passes the spacecraft. There is a systematic increase in the delay of the time of dipolarization for spacecraft located away from 2300 LT. Taken together, these results show the wedge is initially localized and then with time expands azimuthally towards dawn and dusk.

There is growing evidence that the shape of the substorm current wedge is more complex than previously thought. At times the field-aligned currents creating the wedge can apparently flow inside synchronous orbit (Barfield *et al.*, 1985; Nagai *et al.*, 1987). In the event studied by Nagai *et al.* it appears that multiple sheets of current were flowing on magnetic shells on both sides of the GOES spacecraft at synchronous orbit, and the SCATHA satellite 1 R_e further out. In an accompanying statistical study Nagai (1987) finds that just before midnight the D perturbations at the ground and the satellite may have different sign. In this case the D perturbation at the ground is always positive, while at the satellite it is negative. Nagai proposes that this is caused by a solenoidal current system. The downward current on the dawn side of the current wedge consists of a sheet oriented to the west northwest, perhaps parallel to the Harang discontinuity. Similarly the upward current consists of sheet of upward current somewhat further towards dusk. In the region between the two sheets the magnetic perturbation points west northwest. When a synchronous spacecraft is in between the sheets it should observe negative D variations.

Ground stations are sensitive only to the location of the central moments of these two current distributions. To explain the observations a ground station in the satellite meridian must always be west of the central meridian of the net current system. Nagai suggests this could happen if the outward current is stronger that the inward current sheet moving the central meridian on the ground east of the geometric centre of the current wedge.

Additional evidence supporting the proposed wedge-current system can be found in the analysis of the CDAW-6 substorm by Clauer and Kamide (1985). In their study of the different time developments of the DP1 and DP2 current system they calculated field-aligned current patterns at expansion onset. The calculated currents had exactly the form described by Nagai. Incidentally, Barfield *et al.* (1985) noted that the synchronous *D* perturbations at the same time were consistent with moving though a field-aligned current sheet to a region of negative *D* perturbation. Hughes and Singer (1985) studied an isolated Pi 2 burst which occurred several hours earlier than the CDAW-6 substorm and also noted this pattern.

Pi 2 pulsation data obtained with the AFGL mid-latitude magnetometer chain has been used in conjunction with synchronous magnetometer data to study the development of the current wedge (Lester *et al.*, 1984; Hughes and Singer, 1985; Gelpi *et al.*, 1985, 1987). For simple substorm onsets, Pi 2 polarization azimuths define the same central meridian as do the ground *D* perturbations. Later intensifications identified by additional Pi 2 bursts may have different central meridians indicating that new current systems are being added to the initial system. There appears to be no consistent pattern defining where the subsequent intensifications are centred. The data show the substorm current wedge is asymmetric with the upward current being more localized than the downward current. The upward current appears to flow directly out of the westward travelling surge.

The foregoing reports demonstrate that the current wedge becomes observable only after the onset of the substorm expansion phase. As discussed above this is the time that the last closed field lines are severed and the plasmoid begins down the tail. We noted, however, that formation of the plasmoid initially requires reconnection of field lines that close across the neutral sheet. Only if this happens will a plasmoid consisting of closed magnetic loops be formed. We are forced to one of two conclusions. One possibility is that the formation of the loops of the plasmoid happens so rapidly that the details can not be resolved within the accuracy of present determinations of expansion onset. Another possibility is that the initial diversion of current that creates the connected *x*-line and *o*-line occurs only in the plane of the neutral sheet. That is, the diversion is some combination of earthward and tailward meanders similar to those suggested in Fig. 65. In the latter case one would expect distinct patterns in the B_y component

of the plasma sheet field which might reveal the existence of these meanders.

In the NENL model, expansion onset occurs when the last closed field lines at the edge of the plasma sheet are cut and the plasmoid is released. When this happens there is a sudden change in geometry of the neutral line that separates the solar wind and Earth's magnetic fields. In Fig. 29 (§3.2.1) this line was pictured as an ellipse in the equatorial plane. Results from ISEE-3 suggest that the cross-tail segment of the neutral line is a parabola concave away from the Earth as illustrated in Fig. 39. At plasmoid release the localized near-Earth *x*-line is connected to the distant *x*-line by the field lines that originally defined the boundary of the plasma sheet. This connection is schematically illustrated by dashed lines parallel to the central axis of the plasma sheet in Fig. 65. As the plasmoid retreats from the Earth it leaves behind a channel across which the magnetic field points southward. On either side, plasma sheet field lines point northward. The extended *x*-type neutral line separates these regions which are part of the earth's field from the central channel which now consists of IMF. The plasma sheet thinning studies show that the plasma and current sheets within this channel are very thin, while on either side the plasma sheet remains thicker.

Let us suppose that the channel walls created by the retreat of the plasmoid provide a barrier to the cross-tail current, and that a fraction of this current is diverted along field lines to the ionosphere. If 10% of a cross-tail current of typical strength 20 mA m^{-1} is diverted, then more than 80 R_e of tail would be required to produce a 10^6 A current wedge. A current of this magnitude flowing along the channel walls would constitute a current wedge of exactly the type described by Rostoker and Eastman (1987) and discussed in §4.4.2. Its effect would be positive magnetic perturbations along the entire central axis of the tail. Exactly the opposite is seen both in case histories and statistical studies (Fairfield, 1987). It seems more likely that most of the current wedge is diverted from the inner magnetosphere. Diversion from this region explains the field perturbations seen at synchronous orbit reviewed above, and also removes the earthward extensions of the tail current created in the substorm growth phase. Also, as noted by Kauffman (1987) the sheet current strength in this region is more like 200 mA m^{-1} and the entire sheet is destroyed during the expansion phase.

4.5.14 Current wedge and the Harang discontinuity

An important and valid objection to the NENL model is that it does not explain how neutral line formation is related to the large-scale current

system driven by convection. It is well known that the auroral expansion begins near midnight on the most equatorward discrete arc (Akasofu, 1968). Furthermore, this arc is usually located within the Harang discontinuity (Nielsen and Greenwald, 1979). As the substorm expansion proceeds, the brightened arc develops a large propagating fold called the westward-travelling surge. The surge is the location of intense energetic electron precipitation (Reme and Bosqued, 1973; Meng *et al.*, 1978) and the outward field-aligned current forming the westward edge of the substorm current wedge (Kisabeth and Rostoker, 1973; Rostoker and Hughes, 1979; Tighe and Rostoker, 1981). As the expansion proceeds the westward-travelling surge carries the head of the westward electrojet towards dusk along the poleward side of the eastward electrojet, that is along the Harang discontinuity (Akasofu *et al.*, 1966, 1969). Thus the substorm current wedge is intimately associated with the Harang discontinuity and the ionospheric and field-aligned currents which flow in this region.

A diagram summarizing the distribution of current expected in the Harang discontinuity is shown in Fig. 67. The nightside auroral oval is drawn as two semicircles. Crosses at the edges of the auroral oval denote

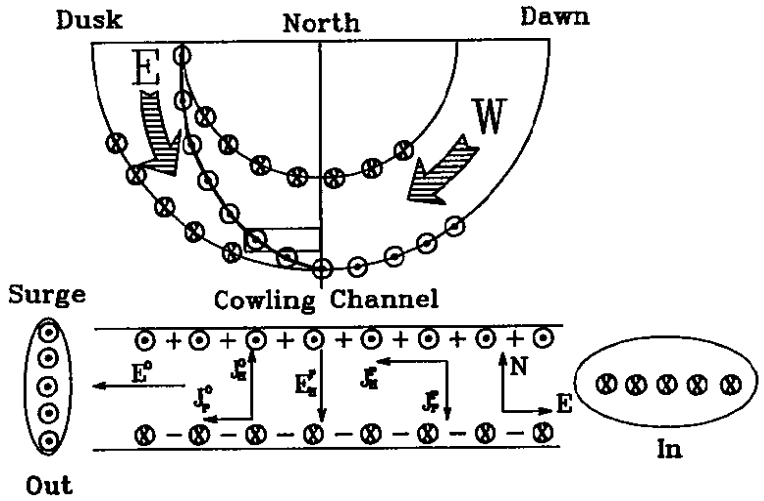

Figure 67. A schematic illustration of a possible relation between the field-aligned current (FAC) from the Harang discontinuity and the substorm expansion current wedge. Top panel shows the FAC which bound the auroral oval and the convection electrojets. Bottom panel shows an expanded view of the Cowling channel which forms at expansion onset. A localized FAC from the westward surge forms the west edge of the wedge.

downward field-aligned currents while circles represent upward currents. Pedersen currents which are not shown connect these field-aligned currents north–south across the oval. The Harang discontinuity is indicated by a heavy line starting at midnight and trending to the west northwest. The eastward and westward electrojets meet at the Harang discontinuity. Because of the difference in Hall conductivity in the oval and polar cap, some of the electrojet current closes upward along field lines rooted in the Harang discontinuity (see §3.1.3). But this is the region in which the dusk-side Region 1 current and the dawnside Region 2 current are also upward (Kamide and Rostoker, 1977). Thus it is expected that there is substantial outward current into the magnetosphere along the discontinuity.

Our mapping of the Harang discontinuity into the magnetospheric equatorial plane was discussed in Fig. 50 (§3.4). From the work of Maynard (1974) and Fairfield and Mead (1975) we project this discontinuity into the near-Earth plasma sheet. However, because the Fairfield–Mead model represents an average field we expect that as one moves to higher latitudes the actual location of the Harang discontinuity will be progressively further from the Earth than that indicated by the model. Recall that our mapping connects the high-latitude end of the Harang discontinuity to the centre of the dusk convection cell, rather than to the distant neutral line at midnight as does the PSBL dynamics model. For sake of discussion we estimate that our mapping locates the terminus of the Harang discontinuity no further than half ($\sim$50–100 R_e) the distance to the distant neutral line, which at the magnetopause is $\sim$100–200 R_e downstream.

Ionospheric observations place the auroral expansion onset 1–2 h before midnight just south of the Harang discontinuity in a region dominated by a northwestward electric field (Baumjohann, 1983). This location projects somewhere between 6–20 R_e behind the Earth somewhat before midnight. Spacecraft observations place the onset typically 15–20 R_e behind the Earth (Hones, 1977) a location consistent with this projection.

During the initial brightening of a substorm onset energetic electron precipitation rapidly enhances the conductivity along a narrow east–west channel as shown in the bottom panel of Fig. 67. According to Baumjohann (1983) the typical dimensions of such a channel a few minutes after auroral activation are 1000 km E–W, and 100–200 km N–S. An idealized channel of this type is shown in the top panel as an east–west rectangle. The westward component of the ionospheric electric field (^0E) drives a primary Pedersen current (^0J_P) westward along this channel, and a primary Hall current (^0J_H) northward. Since the channel is of finite length it must be fed by downward field-aligned currents in the east, and drained by an upward current in the west. These field-aligned currents are the substorm current wedge and the Cowling channel is its ionospheric closure.

Baumjohann *et al.* (1981) have modelled an auroral break-up using simultaneous two-dimensional electric and magnetic field data. Their results show that the upward current is localized in the westward-travelling surge while the downward current is more distributed to the east.

Because of the conductivity contrast at the edges of the channel, the northward Hall current cannot close through the ionosphere, so field-aligned sheet currents form at the poleward and equatorward edges of the channel. These sheets are not able to carry all of the Hall current, so polarization charges accumulate at the edges of the channel. These charges produce an equatorward electric field (${}^{P}E$) that drives a secondary Pedersen current (${}^{P}J_{P}$) southward. This current cancels the fraction of the north–south Hall current that is unable to close through the sheet currents. It also drives a secondary Hall current (${}^{P}J_{H}$) westward, augmenting the primary Pedersen current. The total westward current is called a Cowling current (Coroniti and Kennel, 1972b). Because of the polarization the total current is much stronger than the Pedersen current alone and creates an intense magnetic disturbance on the ground. The westward current in the channel is dissipative since the westward electric field and total current are parallel $({}^{0}J_{P} + {}^{P}J_{H}) \cdot {}^{0}\mathbf{E} > 0$. Note, however, that the energy added to the ionosphere by dissipation of ${}^{P}J_{H}$ is balanced by energy lost from the ionosphere in the north–south Hall-current generator $({}^{P}J_{P} \cdot {}^{P}E < 0)$ (Rothwell *et al.*, 1989).

The questions which must be answered include: 'How does the Cowling channel project into the magnetospheric equatorial plane?; and 'How is the channel related to the NENL?' A recent model which suggests a possible answer to the first question is that of Rothwell *et al.* (1989). In their model the Cowling channel is projected to the near tail as a rectangular block with its longer dimension east–west across the midnight meridian. The westward current is assumed to be generated by some unspecified magnetospheric process. They also assume that the current sheets at the poleward and equatorward edges of the channel are connected in the equatorial plane by an earthward current sheet flowing across the projected rectangle. This closure produces a $\boldsymbol{J} \times \boldsymbol{B}$ force on magnetospheric plasma which accelerates it towards dawn.

To complete their model the authors assume that outward field-aligned currents develop field-aligned potential drops with electric fields pointed away from the ionosphere. These potential structures accelerate electrons towards the ionosphere and ions away from it, enhancing the field-aligned currents. The accelerated electrons bombard the ionosphere causing discrete auroral arcs and regions of enhanced conductivity. Polar-orbiting spacecraft passing through the structures observe a characteristic increase in electron energy followed by a decrease (inverted-V) (Frank and

Ackerson, 1971). In the Cowling channel, outward field-aligned currents are located at the western end, and poleward edge of the channel. The westward surge is attributed to luminosity produced by a potential structure in the return path of the westward current to the tail. Similarly, a bright arc at the poleward edge of the auroral bulge is produced by a potential structure in the current sheets, diverting the northward Hall current into the tail.

The various current segments, electric fields, and Hall and Pedersen conductivities, are linked by highly non-linear relations. For example, the ratio of Hall and Pedersen conductivities in the ionosphere depends on the energy of the electrons precipitated by the field-aligned potential structures. Changes in these parameters alter the currents in the channel. But a change in conductivity alters the field-aligned closure currents and the polarization electric fields. This changes the potential structures in a feedback loop which the authors argue is unstable.

In the model of Rothwell *et al.* (1989) it is possible for the field-aligned potential drop in the poleward current sheet to exceed the potential drop N–S across the channel due to polarization. When this happens the polarization electric field projected into the tail reverses sign. In the absence of field-aligned potentials the equatorward ionospheric electric field projects as an earthward-pointing field. This is in the same direction as the closure of the Hall-current sheet in the equator, implying that the plasma sheet is then a load on the ionospheric Hall-current generator ($\mathbf{J}_{He} \cdot \boldsymbol{E}_{Pe} > 0$). For an earthward electric field the $\boldsymbol{E} \times \boldsymbol{B}$ plasma drift is eastward towards dawn. Presumably this drift is a consequence of the acceleration due to the $\boldsymbol{J} \times \boldsymbol{B}$ force. On the other hand, if the plasma drift is initially towards dusk, the projected electric field must be tailward to correspond to the drift. Then, the plasma sheet is also a generator in the circuit ($\boldsymbol{J}_{He} \cdot \boldsymbol{E}_{Pe} < 0$). In this case the eastward acceleration of the $\boldsymbol{J} \times \boldsymbol{B}$ force decreases the westward drift velocity. The energy extracted from the east–west flow helps maintain the field-aligned potential drop.

Rothwell *et al.* (1989) do not consider the relation of the Cowling channel as mapped to the magnetosphere to the mapping of the Harang discontinuity. In fact the work of Baumjohann *et al.* (1981) does not specify the relation of the east end of the channel to the discontinuity. In Fig. 67 we assumed the channel runs east–west across the ionospheric flow. Also the west end of the channel with its outward field-aligned current was placed in the Harang discontinuity where outward current is already present. We do not consider it a coincidence that the outward current of the wedge is colocated with outward current of the convection electrojets. In fact, it is possible that an instability of the current flowing outward from the Harang discontinuity initiates the substorm expansion. Instability leads

to field-aligned potential drop in a localized part of this current. This accelerates electrons downward into the westward surge, increasing conductivity and drawing more current through the ionosphere. As this happens the tail magnetic field collapses into an x-line configuration in the region from which the diversion is occurring. Reconnection begins, accelerating plasma both earthward and tailward. The polarization field from the substorm electrojet gives this plasma a strong acceleration towards dawn.

The foregoing discussion is highly speculative. It is extremely difficult to visualize the consequences of the interaction between the various parts of the system. In a recent paper, Kaufmann and Larson (1989) attempted to map the Cowling channel quantitatively to the magnetosphere. Their results shown in Fig. 68 are extremely dependent on the field-aligned current system. These currents are so strong that they significantly modify the shape of the field lines on which they flow. The mapped flows bear little resemblance to those shown in Fig. 50. The lesson to be learned from this work is that a simple dipole projection of ionospheric features to the magnetospheric tail are likely to be wrong. However, we feel that the underlying idea that the expansion phase depends in some way on complex, non-linear feedback with the ionosphere is correct.

There is growing evidence that the inner magnetosphere is the location where substorm expansions are initiated. The AMPTE spacecraft with apogee at 8.8 R_e has probed the equatorial region just beyond synchronous orbit. Takahashi *et al.* (1987) report that very strong negative B_z fluctuations at 8.1 R_e are correlated with a Pi 2 burst. Another such event was reported by Lui *et al.* (1988) who argue that the current sheet disruption diverts current into the ionosphere, but the process is turbulent and does not develop an x-line geometry. Lopez *et al.* (1988a,b) show that substorm reconfigurations of the magnetic field are extremely frequent outside synchonous orbit. He has found several unique events for which there appears to be evidence that the disruption and diversion of current begins close to synchronous and propagates outward (Lopez *et al.*, 1988c, 1990). Since this interpretation depends crucially on the relative locations of spacecraft in the ill-defined magnetic field it is difficult to know where the events really begin. We point out that in the extremely well-documented CDAW-6 substorm the first observed disturbance was the onset of synchronous particle flux recovery at 1052 UT. The ground onset was 1054 UT, and the ISEE spacecraft onset at 13 R_e was 1058 UT.

These results from the AMPTE-CCE spacecraft are difficult to reconcile with the reports of infrequent neutral lines inside the apogee of the ISEE spacecraft ($\sim$22 R_e) (Huang and Frank 1986; Cattell and Mozer, 1984). Huang's statistical study has been criticized by Cattell and Elphic (1987),

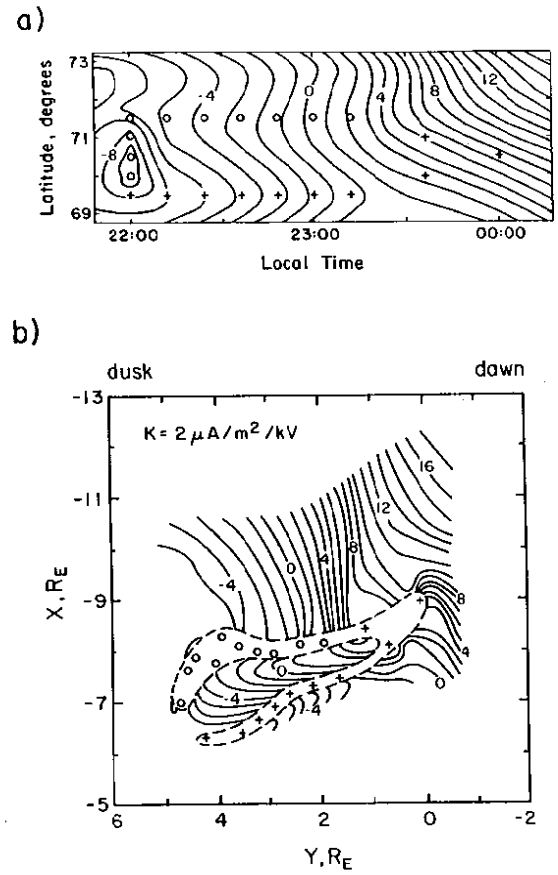

Figure 68. A quantitative model extrapolating the Cowling channel from the ionosphere to the magnetosphere (Kaufmann and Larson, 1989). Equipotentials within the channel are severely distorted by the twisting introduced by the field-aligned currents, and by the polarization charges within the channel.

but Baumjohann *et al.* (1989) obtain similar results with the AMPTE-IRM spacecraft plasma detector. Thus we have the situation where activity seems to begin at synchronous orbit, but very little passes outward at ISEE-1/2 ($\sim$20 R_e), yet large plasmoids are frequently seen at 200 R_e. Clearly something is wrong with our understanding of the data. Perhaps the most fundamental question of substorm physics at this time is to understand the relation of reconnection to the disturbances seen at synchronous orbit and how they map into the electrodynamics of the Harang discontinuity.

4.5.15 *Retreat of the NENL*

Eventually, NENL retreats tailward. The cause of this retreat is not well understood, but the model suggests it may be a consequence of the inability of the reconnected magnetic flux to flow earthward from the x-line. For example, isolated substorms are created by short intervals of southward IMF. Once the IMF turns northward there is no longer demand for closed flux on the day side of the magnetosphere. However, there is still flux stored in the tail lobes waiting to be reconnected. The simplest way to deal with this situation is for the x-line to move tailward, adding excess flux to the nightside plasma sheet as it does. This process is the inverse of dayside erosion and might be called flux accretion. Even if the IMF does not turn northward there is no reason to assume that the rate of nightside reconnection exactly balances the return flow to the day side. In such a case the neutral line may move either earthward or tailward to adjust the rate of earthward flow of reconnected flux.

Soon after the IMF turns northward, most auroral zone phenomena begin to recover. However, there is considerable evidence that activity persists for some time at higher latitudes. In fact it has been suggested (Hones, 1985, 1986), and highly contested (Rostoker, 1986) that there is a sudden poleward leap of activity. Regardless of how activity spreads to higher latitudes in the ionosphere it is observed that eventually all ionospheric phenomena begin to decrease in intensity, and most boundaries tend to move back to their presubstorm locations. By definition, the end of the substorm expansion phase occurs when all ionospheric phenomena reach their maximum poleward extent and begin to decrease in intensity. Somewhat before this time, about when the aurora and electrojets begin to disappear at lower latitudes, the plasma sheet in the near-Earth region suddenly expands and is found to be filled with much hotter plasma. The NENL model explains this expansion and energization by tailward motion of an active neutral line. Earthward of the neutral line the plasma is constrained by the rate at which it can flow around the Earth. Unable to move out of the region of the x-line fast enough, the plasma fills and expands the plasma sheet. Tailward of the neutral line there is an unlimited region for the plasma to flow into, and the feet of the reconnected field lines are not connected to the resistive ionosphere which slows the rate of flow away from the x-line. Consequently, the sheet remains thin. Eventually the x-line retreats far down the tail to its typical location at $120\,R_e$ filling the entire plasma sheet behind it as it travels.

Once the x-line reaches this location it appears that reconnection ceases in the plasma sheet. This does not mean that the x-line vanishes, only that no magnetic flux and plasma flows through the neutral line. Tailward of this static neutral line the lobe field lines are separated by a current sheet

across which there is no field line closure. Open field lines remaining in the lobe remain open and stretch as the IMF discontinuity between southward and northward IMF travels away from the Earth. As long as the IMF remains northward there will be no further substorms. However, convection does not cease. The viscous interaction between the solar wind and Earth continues to drag closed field lines tailward releasing them to flow sunward again in the plasma sheet. Low-level currents continue to flow in the ionosphere as a result of this convection.

5 IMPORTANT QUESTIONS IN SUBSTORM PHYSICS

In preparing this review the author encountered a number of questions he was unable to answer. Clearly some of these are simply due to a lack of familiarity with the relevant work. However, in some cases where theory seems to suggest an answer, the data seem ambiguous or contradictory. For example, four high-latitude convection cells are expected during northward IMF. Some authors claim to have seen them, but others argue that what actually occurs is a highly distorted two- or three-cell system (Heelis *et al.*, 1986; Heppner and Maynard, 1987). Is this a consequence of lack of measurement resolution, not accounting for IMF-B_y effects, or is it some consequence of continuity? Maybe it is simply not possible to make continuous transitions from two-celled to four-celled convection.

Much of this chapter has been presented as though it was established fact. In practice there is considerable argument concerning what has actually been observed. Interpretations are even more controversial than the facts on which they are based. As an example of questions about a fact it has been claimed that tailward flows in the near-Earth plasma sheet at substorm expansion onset reported by Hones (1979a,b) are not bulk flows, but are instead accelerated ionospheric ions, or counterstreaming boundary layer ion beams (Lui *et al.*, 1983). An example of different interpretations of the same fact is that negative B_z in the plasma sheet are attributed to fringing fields of a field-aligned current as opposed to evidence for a closed loop in a plasmoid (Rostoker and Eastman, 1987).

A major problem in substorm research is the absence of global measurements. It is almost always necessary to use statistical procedures to infer three-dimensional structure from a few point measurements. These techniques are necessarily model dependent, and there may be alternative models that explain the same observations. This is particularly true if one uses only a subset of the available data. Many models of substorms fail in that they do not account for important observations. For example, how does the thermal catastrophe model account for the distant tail observations made by ISEE-3? Experiments with multiple spacecraft such as the

forthcoming ISTP mission will be of great value. However, many questions could be quickly answered if high-resolution time and space images of the magnetosphere could be obtained (Williams, 1990).

Another problem is related to topology and visualization. The magnetospheric system consists of a complex, three-dimensional collection of regions and boundaries which are constantly changing. Very few can describe this system in a manner which makes it possible for the uninitiated to understand the various linkages. In teaching graduate classes in magnetospheric physics, the author finds that much of his time is spent in trying to produce images of the magnetosphere in student minds. This problem is made more difficult by the fact that we do not presently have a good model of the Earth's magnetic field! Without such a model it is possible for the advocates of the PSBL dynamics model to map the Harang discontinuity at midnight to the distant neutral line while the NENL advocates map it to synchronous orbit. These locations are over 100 R_e apart! We believe that one of the most outstanding problems of substorm physics is producing a good magnetic field model. Such a model will require far greater detail in representing substorm distortions than have previous models of the average field. Once this is available we will require an equally good electric field model.

The magnetosphere is a highly interactive, non-linear feedback system. Such systems are exceedingly difficult to describe mathematically. Probably it is as complex as the atmospheric system responsible for surface weather and climate. If it ever becomes necessary to predict space weather accurately, we must question whether it will be possible to make a sufficient number of measurements to calculate the consequence of a given solar-wind input. Possibly the system is sufficiently chaotic that no precise calculation is possible (Baker *et al.*, 1990).

The following subsections present lists of questions that have occurred to the author while preparing this review. These questions may be of interest in as much as they show where the author is less certain than the previous presentation might suggest. Also, it is hoped that they may stimulate further research leading to a better understanding of the causes of geomagnetic activity.

5.1 Solar-wind–magnetosphere coupling

(1) Is the relation of the magnetic activity to the solar wind deterministic, or is it chaotic?
(2) What is the best observable measure of the strength of solar-wind coupling?

(3) Can the known relations between the solar-wind and activity indices be improved?
(4) Can internal magnetospheric parameters be used to infer the state of the solar wind?

5.2 The magnetopause and tangential drag

(1) What is the relative importance of viscous and reconnection processes? Does this depend on the state of the solar wind?
(2) What types of reconnection occur on the dayside magnetopause? What properties of the solar wind control the type of reconnection?
(3) How are the average properties of reconnection determined by solar-wind coupling studies related to details of the reconnection process?
(4) Why is the average effect of reconnection like a half-wave rectifier with the Earth's magnetic equatorial plane so important?
(5) What is the ionospheric signature of dayside reconnection?
(6) Do pressure pulses and surface waves play a role in creating tangential drag?
(7) What physical processes provide drag in the low-latitude boundary layer?

5.3 The polar cap

(1) Do the open field lines of the polar cap ever completely close?
(2) Where are the boundaries between antisunward convecting open and closed field lines?
(3) What is the form of a front of enhanced convection propagating across the polar cap?
(4) How does the convection pattern associated with southward IMF evolve into that for a northward IMF?
(5) Do closed field lines of the plasma sheet bulge up into the lobes to create a transpolar arc?
(6) What is the topology of magnetic field lines from the polar cap several hours after a transition from south to north IMF?

5.4 The distant neutral line

(1) Is the distant neutral line always present in the magnetotail?
(2) Is the inferred parabolic shape and location of this neutral line correct?

Slavin, J. A., Baker, D. N., Craven, J. D., Elphic, R. C., Fairfield, D. H., Frank, L. A., Galvin, A. B., Hughes, W. J., Manka, R. H., Mitchell, D. G., Richardson, I. G., Sanderson, T. R., Sibeck, D. J., Smith, E. J. and Zwickl, R. D. (1989). CDAW 8 observations of plasmoid signatures in the geomagnetic tail: An assessment. *J. Geophys. Res.* **94**(A11), 15 153–15 175.

Smith, P. H., Bewtra, N. K. and Hoffman, R. A. (1981). Inference of the ring current ion composition by means of charge exchange decay. *J. Geophys. Res.* **86**(A5), 3470–3480.

Smith, R. A., Goertz, C. K. and Grossman, W. (1986). Thermal catastrophe in the plasma sheet boundary layer. *J. Geophys. Res.* **13**(13), 1380–1383.

Snyder, C. W., Neugeauer, M. and Rao, U. R. (1963). The solar wind velocity and its correlation with cosmic-ray variations and with solar and geomagnetic activity. *J. Geophys. Res.* **68**(24), 6361–6370.

Sonnerup, B. U. O. (1980). Theory of the low-altitude boundary layer. *J. Geophys. Res.* **85**(A5), 2017–2026.

Sonnerup, B. U. O. (1984). Magnetic field reconnection at the magnetopause: An overview. In *Magnetic Reconnection in Space and Laboratory Plasma* (ed. E. W. Hones, Jr), pp. 92–103. Geophysical Monograph 30, American Geophysical Union, Washington, D.C.

Sonnerup, B. U. O., Paschmann, G., Papamastorakis, I., Sckopke, N., Haerendel, G., Bame, S. J., Asbridge, J. R., Gosling, J. T. and Russell, C. T. (1981). Evidence for magnetic field reconnection at the Earth's magnetopause. *J. Geophys. Res.* **86**(A12), 10 049–10 067.

Southwood, D. J. (1987). The ionospheric signature of flux transfer events. *J. Geophys. Res.* **92**(A4), 3207–3213.

Southwood, D. J. and Wolf, R. A. (1978). An assessment of the role of precipitation in the magnetospheric convection. *J. Geophys. Res.* **83**(A11), 5227–5232.

Speiser, T. W. (1965). Particle trajectories in model current sheets: 1. Analytical solutions. *J. Geophys. Res.* **70**(17), 4219–4226.

Speiser, T. W. (1967). Particle trajectories in model current sheets 2. Applications to auroras using a geomagnetic tail model. *J. Geophys. Res.* **72**, 3219.

Spiro, R. W., Reiff, P. H. and Maher, L. J. Jr (1982). Precipitating electron energy flux and auroral zone conductances—an empirical model. *J. Geophys. Res.* **87**(A10), 8215–8227.

Sugiura, M. (1964). Hourly values of equatorial Dst for the IGY. *Ann. Int. Geophys. Year*, **35**, 9.

Takahashi, K. and Hones, E. W. Jr (1988). ISEE 1 and 2 observations of ion distribution at the plasma sheet–tail lobe boundary. *J. Geophys. Res.* **93**(A8), 8558–8582.

Takahashi, K., Zanetti, L. J., Lopez, R. E., McEntire, R. W., Potemra, T. A. and Yumoto, K. (1987). Disruption of the magnetotail current sheet observed by AMPTE/CCE. *Geophys. Res. Lett.* **14**(10), 1019–1022.

Tighe, W. G. and Rostoker, G. (1981). Characteristics of westward travelling surges during magnetospheric substorms. *J. Geophys.* **50**, 51–67.

Todd, H., Bromage, B. J. I., Cowley, S. W. H., Lockwood, M., van Eyken, A. P. and Wilis, D. M. (1986). EISCAT observations of bursts of rapid flow in the high latitude dayside ionosphere. *Geophys. Res. Lett.* **13**, 909–912.

Tsyganenko, N. A. (1989). On the redistribution of the magnetic field and plasma

in the near nightside magnetosphere during a substorm growth phase. *Planet. Space Sci.* **37**(2), 183–192.

Vasyliunas, V. M. (1968). A survey of low-energy electrons in the evening sector of the magnetosphere with OGO-1 and OGO-3. *J. Geophys. Res.* **73**(9), 2839–2884.

Vasyliunas, V. M. (1975). Theoretical models of magnetic field line merging. 1. *Rev. Geophys. Space Phys.* **13**(1), 303–336.

Vasyliunas, V. M. (1984). Steady state aspects of magnetic field line merging. In *Magnetic Reconnection in Space and Laboratory Plasmas*, pp. 25–31. Geophysical Monographs 30, American Geophysical Union, Washington, D.C.

Walker, R. J., Erickson, K. N., Swanson, R. L. and Winckler, J. R. (1976). Substorm-associated particle boundary motion at synchronous orbit. *J. Geophys. Res.* **81**(31), 5541–5550.

Weins, R. G. and Rostoker, G. (1975). Characteristics of the development of the westward electrojet during the expansive phase of magnetospheric substorms. *J. Geophys. Res.* **80**(16), 2109–2128.

Westcott, E. M., Stolarik, J. D. and Heppner, J. P. (1969). Electric field in the vicinity of auroral forms from motions of barium vapor releases. *J. Geophys. Res.* **74**(14), 3469–3487.

Wilcox, J. M., Schatten, K. H. and Ness, N. F. (1967). Influence of interplanetary magnetic field and plasma on geomagnetic activity during quiet-sun conditions. *J. Geophys. Res.* **72**(1), 19–26.

Williams, D. J. (1990). Why we need global observation.

Winningham, J. D., Yasuhara, F., Akasofu, S.-I. and Heikkila, W. J. (1975). The latitudinal morphology of 10-eV to 10-keV electron fluxes during magnetically quiet and disturbed times in the 2100–0300 MLT sector. *J. Geophys. Res.* **80**(22), 3148–3171.

Wygant, J. R., Torbert, R. B. and Mozer, F. S. (1983). Comparison of S3-3 polar cap potential drops with the interplanetary magnetic field and models of magnetpause reconnection. *J. Geophys. Res.* **88**(A7), 5727–5735.

Zwickl, R. D., Baker, D. N., Bame, S. J., Feldman, W. C., Gosling, J. T., Hones, E. W. Jr, McComas, D. J., Tsurutani, B. T. and Slavin, J. A. (1984). Evolution of the earth's distant magnetotail: ISEE 3 electron plasma results. *J. Geophys. Res.* **89**(A12), 11 007–11 012.

Teresawa, T. and Tsurutani, B. (1988). Assessment of the boundary layer model of the magnetospheric substorm. *J. Geophys. Res.* **93**(A6), 5579–5588.
Ohtani, S., Kokubun, S., Elphic, R. C. and Russell, C. T. (1988). Field-aligned current signatures in the near-tail region, 1, ISEE observations in the plasma sheet boundary layer. *J. Geophys. Res.* **93**(A9), 9709–9720.
Olson, W. P. (1969). The shape of the tilted magnetopause. *J. Geophys. Res.* **74**(24), 5642–5651.
Park, C. G. (1970). Whistler observations of the interchange of ionization between the ionosphere and the protonsphere. *J. Geophys. Res.* **75**(22), 4249–4260.
Parks, G. K., Coroniti, F. V., McPherron, R. L. and Anderson, K. A. (1968). Studies of magnetospheric substorms, I. Characteristics of modulated energetic electron precipitation occurring during auroral substorms. *J. Geophys. Res.* **73**(5), 1685–1696.
Paschmann, G., Sckopke, N. and Hones, E. W. Jr (1985). Magnetotail plasma observations during the 1054 UT substorm on March 22, 1979 (CDAW 6). *J. Geophys. Res.* **90**(A2), 1217–1229.
Paschmann, G., Sonnerup, B. U. O., Papamastorakis, I., Sckopke, N., Haerendel, G., Bame, S. J., Asbridge, J. R., Gosling, J. T., Russell, C. T. and Elphic, R. C. (1979). Plasma acceleration at the earth's magnetopause: Evidence for reconnection. *Nature* **282**, 243.
Paulikas, G. A. (1974). Tracing of high-latitude magnetic field lines by solar particles. *Rev. Geophys. Space Phys.* **12**(1), 117–128.
Perreault, P. and Akasofu, S.-I. (1978). A study of geomagnetic storms. *Geophys. J. R. Astr. Soc.* **54**, 547–573.
Petschek, H. E. (1964). Magnetic field annihilation. In *AAS-NASA Symposium on the Physics of Solar Flares*, pp. 425–439. NASA SP-50, Scientific and Technical Information Division NASA, Washington, D.C.
Pilipp, W. G. and Morfill, G. (1978). The formation of the plasma sheet resulting from plasma mantle dynamics. *J. Geophys. Res.* **83**(A12), 5670–5678.
Pytte, T., McPherron, R. L. and Kokubun, S. (1976). The ground signatures of the expansion phase during multiple onset substorms. *Planet. Space Sci.* **24**, 1115–1132.
Pytte, T., McPherron, R. L., Hones, E. W. Jr and West, H. I. Jr (1978). Multiple-satellite studies of magnetospheric substorms: Distinction between polar magnetic substorms and convection-driven negative bays. *J. Geophys. Res.* **83**(A2), 663–679.
Rasmussen, C. E. and Schunk, R. W. (1988). Ionospheric convection inferred from interplanetary magnetic field-dependent Birkeland currents. *J. Geophys. Res.* **93**(A3), 1909–1921.
Reiff, P. H., Spiro, R. W. and Hill, T. W. (1981). Dependence of polar cap potential drop on interplanetary parameters. *J. Geophys. Res.* **86**(A9), 7639–7648.
Reme, H. and Bosqued, J. M. (1973). Rocket observations of electron precipitation in a westward-traveling surge. *J. Geophys. Res.* **78**(25), 5553–5558.
Richmond, A. D. and Kamide, Y. (1988). Mapping electrodynamic features of the high-latitude ionosphere from localized observations: Techniques. *J. Geophys. Res.* **93**(A6), 5741–5759.
Roederer, J. G. and Hones, E. W. Jr (1974). Motion of magnetospheric particle clouds in a time-dependent electric field model. *J. Geophys. Res.* **79**(10), 1432–1438.
Rosenbauer, H., Grunwaldt, H., Montgomery, M. D., Paschmann, G. and

Sckopke, N. (1975). Heos 2 plasma observations in the distant polar magnetosphere: The plasma mantle. *J. Geophys. Res.* **80**(19), 2723–2737.
Rostoker, G. (1972). Geomagnetic indices. *Rev. Geophys. Space Phys.* **10**(4), 935–950.
Rostoker, G. (1986). Comment on 'The poleward leap of the auroral electrojet as seen in auroral images' by Edward W. Hones, Jr. *J. Geophys. Res.* **91**(A5), 5879–5880.
Rostoker, G. and Eastman, T. (1987). A boundary layer model for magnetospheric substorms. *J. Geophys. Res.* **92**(A11), 12 187–12 201.
Rostoker, G. and Hughes, T. J. (1979). A comprehensive model current system for high-latitude magnetic activity—II. The substorm component. *Geophys. J. R. Astr. Soc.* **58**, 571–581.
Rostoker, G., Jones, A. V., Gattinger, R. L., Anger, D. D. and Murphree, J. S. (1987). The development of the substorm expansive phase: The 'eye' of the substorm. *Geophys. Res. Lett.* **14**(4), 399–402.
Rostoker, G., Akasofu, S.-I., Foster, J., Greenwald, R. A., Kamide, Y., Kawasaki, K., Lui, A. T. Y., McPherron, R. L. and Russell, C. T. (1980). Magnetospheric substorms—definition and signatures. *J. Geophys. Res.* **85**(A4), 1663–1668.
Rothwell, P. L., Block, L. P., Silevitch, M. B. and Falthammar, C.-G. (1989). A new model for auroral breakup during substorms. *IEEE Trans. Plasma Sci.* **17**(2), 150–157.
Russell, C. T. (1972). The configuration of the magnetosphere. *Critical Problems of Magnetospheric Physics*, pp. 1–16. National Academy of Science.
Russell, C. T. and Brody, K. (1967). Some remarks on the position and shape of the neutral sheet. *J. Geophys. Res.* **72**(23), 6104–6106.
Russell, C. T. and Elphic, R. C. (1978). Initial ISEE magnetometer results: Magnetopause observations. *Space Sci. Rev.* **22**(681).
Russell, C. T. and McPherron, R. L. (1972). The magnetotail and substorms. *Space Sci. Rev.* **11**, 111–122.
Russell, C. T. and McPherron, R. L. (1973). Semiannual variation of geomagnetic activity. *J. Geophys. Res.* **78**(1), 92–108.
Schatten, K. H. and Wilcox, J. M. (1967). Response of the geomagnetic activity index Kp to the interplanetary magnetic field. *J. Geophys. Res.* **72**(21), 5185–5191.
Schield, M. A., Freeman, J. W. and Dessler, A. J. (1969). A source for field-aligned currents at auroral latitudes. *J. Geophys. Res.* **74**(1), 247–255.
Sckopke, N. and Paschmann, G. (1978). The plasma mantle. A survey of magnetotail boundary layer observations. *J. Atmos. Terrest. Phys.* **40**, 261–278.
Sibeck, D. G., Baumjohann, W. and Lopez, R. E. (1989). Solar wind dynamic pressure variations and transient magnetospheric signatures. *Geophys. Res. Lett.* **16**(1), 13–16.
Siscoe, G. L. (1966). A unified treatment of magnetospheric dynamics with applications to magnetic storms. *Planet. Space Sci.* **14**, 947–967.
Slavin, J. A. and Kamide, Y. (1986). Solar wind-magnetosphere coupling: Introduction. In *Solar Wind-Magnetosphere Coupling* (ed. Y. Kamide and J. Slavin), pp. ix–xii. Terra Scientific, Tokyo and Reidel, Dordrecht.
Slavin, J. A., Smith, E. J., Sibeck, D. G., Baker, D. N., Zwickl, R. D. and Akasofu, S.-I. (1985). An ISEE 3 study of average and substorm conditions in the distant magnetotail. *J. Geophys. Res.* **90**(A11), 10 875–10 895.

Maezawa, K. (1976). Magnetospheric convection induced by the positive and negative Z components of the interplanetary magnetic field: Quantitative analysis using polar cap magnetic records. *J. Geophys. Res.* **81**(13), 2289–2303.

Maezawa, K. and Murayama, T. (1985). In *Solar Wind Velocity Effects on the Auroral Zone Magnetic Disturbances*, pp. 59–83. Terra Scientific Publishing Co., Tokyo.

Matsushita, S. and Campbell, W. H. (1967a). *Physics of Geomagnetic Phenomena*, Vol. 1. Academic Press, New York.

Matsushita, S. and Campbell, W. H. (1967b). *Physics of Geomagnetic Phenomena*, Vol. 2. Academic Press, New York.

Mayaud, P. N. (1980). *Derivation, Meaning and Use of Geomagnetic Indices*. Geophysical Monograph 22, American Geophysical Union, Washington, D.C.

Maynard, N. C. (1974). Electric field measurements across the Harang discontinuity. *J. Geophys. Res.* **79**(31), 4620–4631.

McDiarmid, I. B., Burrows, J. R. and Wilson, M. D. (1980). Comparison of magnetic field perturbations and solar electron profiles in the polar cap. *J. Geophys. Res.* **85**(A3), 1163–1170.

McPherron, R. L. (1970). Growth phase of magnetospheric substorms. *J. Geophys. Res.* **75**(28), 5592–5599.

McPherron, R. L. (1972). Substorm related changes in the geomagnetic tail: The growth phase. *Planet. Space Sci.* **20**, 1521–1539.

McPherron, R. L. (1979). Magnetospheric substorms. *Rev. Geophys. Space Phys.* **17**(4), 657–681.

McPherron, R. L. (1987). The Earth's magnetic field. *Encyclopedia Britannica*, pp. 545–558.

McPherron, R. L. and Barfield, J. N. (1980). A seasonal change in the effect of field-aligned currents at synchronous orbit. *J. Geophys. Res.* **85**(A12), 6743–6746.

McPherron, R. L. and Coleman, P. J. Jr (1969). *Magnetic Field Variations at ATS-1*, pp. 119–144. ESRO Pub. No. SP-60, ESRO Colloquium, Lyngby, Denmark.

McPherron, R. L. and Manka, R. H. (1985). Dynamics of the 1054 UT, March 22, 1979 substorm event: CDAW-6. *J. Geophys. Res.* **90**(A2), 1175–1190.

McPherron, R. L., Parks, G. K. and Coroniti, F. V. (1967). *Relation of Correlated Magnetic Micropulsations and Electron Precipitation to the Auroral Substorm*. ESSA Tech. Mem. IERTM-ITSA. pp. III-4.1–4.15.

McPherron, R. L., Russell, C. T. and Aubry, M. (1973a). Satellite studies of magnetospheric substorms on August 15, 1968, 9. Phenomenological model for substorms. *J. Geophys. Res.* **78**(16), 3131–3149.

McPherron, R. L., Parks, G. K., Colburn, D. S. and Montgomery, M. D. (1973b). Satellite studies of magnetospheric substorms on August 15, 1968, 2. Solar wind and outer magnetosphere. *J. Geophys. Res.* **78**(16), 3054–3061.

McPherron, R. L., Russell, C. T., Kivelson, M. G. and Coleman, P. J. Jr (1973c). Substorms in space: The correlation between ground and satellite observations of the magnetic field. *Radio Science* **8**(11), 1059–1076.

McPherron, R. L., Coleman Jr, P. J. and Snave, R. C. (1975). ATS-6 UCLA Flexgate magnetometer. *IEEE Trans. Aerospace Electr. Sys.*, **AES-11(6)**, 1110–1117.

McPherron, R. L., Nishida, A. and Russell, C. T. (1987). Is near-earth current sheet the cause of auroral substorm expansion onset? (extended abstract). In *Quantitative Modeling of Magnetosphere–Ionosphere Coupling Processes* (eds Y. Kamido and R. A. Wolf), pp. 252–257, Kyoto Samgyo University, Japan.

McPherron, R. L., Baker, D. N., Bargatze, L. F., Clauer, C. R. and Holzer, R. E. (1988). IMF control of geomagnetic activity. *Adv. Space Res.* **8**(9–10), 71–86.

Mead, G. D. (1964). Deformation of the geomagnetic field by the solar wind. *J. Geophys. Res.* **69**(7), 1181–1195.

Mead, G. D. and Beard, D. B. (1964). Shape of the geomagnetic field solar wind boundary. *J. Geophys. Res.* **69**(7), 1169–1179.

Meng, C.-I. (1979). Polar cap variations and the interplanetary magnetic field. In *Dynamics of the Magnetosphere* (ed. S.-I. Akasofu), pp. 23–46. D. Reidel Pub. Co.

Meng, C.-I. and Akasofu, S.-I. (1969). A study of polar magnetic substorms, 2. Three-dimensional current system. *J. Geophys. Res.* **74**(16), 4035–4053.

Meng, C.-I., Holzworth, R. H. and Akasofu, S.-I. (1977). Auroral circle—delineating the poleward boundary of the quiet auroral belt. *J. Geophys. Res.* **82**(1), 164–172.

Meng, C.-I., Snyder, A. L. Jr and Kroehl, H. W. (1978). Observations of westward traveling surges and electron precipitations. *J. Geophys. Res.* **83**(A2), 575–585.

Mihalov, J. D., Colburn, D. S., Currie, R. G. and Sonett, C. P. (1968). Configuration and reconnection of the geomagnetic tail. *J. Geophys. Res.*, **73**(3), 943–959.

Nagai, T. (1982a). Observed magnetic substorm signatures at synchronous altitude. *J. Geophys. Res.* **87**(A6), 4405–4417.

Nagai, T. (1982b). Local time dependence of electron flux changes during substorms derived from multi-satellite observations at synchronous orbit. *J. Geophys. Res.* **87**(A5), 3456–3468.

Nagai, T. (1987). Field-aligned currents associated with substorms in the vicinity of synchronous orbit 2. GOES 2 and GOES 3 observations. *J. Geophys. Res.* **92**(A3), 2432–2446.

Nagai, T., Singer, H. J., Ledley, B. G. and Olsen, R. C. (1987). Field-aligned currents associated with substorms in the vicinity of synchronous orbit 1. The July 5, 1979, substorm observed by SCATHA, GOES 3, and GOES 2. *J. Geophys. Res.* **92**(A3), 2425–2431.

Ness, N. F. (1965). The earth's magnetic tail. *J. Geophys. Res.* **70**(13), 2989–3005.

Ness, N. F. (1987). Magnetotail research: The early years. In *Magnetotail Physics*, pp. 11–20. John Hopkins University Press, Baltimore.

Nielsen, E. and Greenwald, R. A. (1979). Electron flow and visual aurora at the Harang discontinuity. *J. Geophys. Res.* **84**(A8), 4189–4200.

Nishida, A. (1966). Formation of the plasmapause, or magnetospheric plasma knee, by the combined action of magnetospheric convection and plasma escape from the tail. *J. Geophys. Res.* **71**(23), 5669–5679.

Nishida, A. (1988). Critical issues in the solar wind/magnetosphere coupling and the magnetotail dynamics, Solar-terrestrial energy program: major scientific problems. pp. 31–51. XXVII COSPAR Plenary Meeting.

Nishida, A. and Nagayama, N. (1973). Synoptic survey for the neutral line in the magnetotail during the substorm expansion phase. *J. Geophys. Res.* **78**(19), 3782–3798.

Nishida, A., Bame, S. J., Baker, D. N., Gloeckler, G., Scholer, M., Smith, E. J.,

Johnson, F. S. (1960). The gross character of the geomagnetic field in the solar wind. *J. Geophys. Res.* **65**(10), 3049–3051.

Kamide, Y. and Rostoker, G. (1977). The spatial relationship of field-aligned currents and auroral electrojets to the distribution of nightside auroras. *J. Geophys. Res.* **82**(35), 5589–5608.

Kamide, Y. and Slavin, J. A. (eds) (1986). *Solar Wind–Magnetosphere Coupling*. Terra Scientific Publishing Company, Tokyo and D. Reidel Publishing Company, Dordrecht.

Kamide, Y. and Vickerey, J. F. (1983). Variability of the Harang discontinuity as observed by the Chatanika radar and the IMS Alaska magnetometer chain. *Geophys. Res. Lett.* **10**, 159–162.

Kaufmann, R. L. and Larson, D. J. (1989). Electric field mapping and auroral birkeland currents. *J. Geophys. Res.* **94**(A11), 15 307–15 319.

Kavanagh, L. D. Jr, Freeman, J. W. Jr and Chen, A. J. (1968). Plasma flow in the magnetosphere. *J. Geophys. Res., Space Phys.* **73**(17), 5511–5519.

Kawasaki, K. and Akasofu, S.-I. (1971). Low-latitude DS component of geomagnetic storm field. *J. Geophys. Res.* **76**(10), 2396–2405.

Khorosheva, O. V. (1962). The diurnal drift of the closed auroral ring. *Geomag. Aeron.* **2**(5), 696–705.

Kisabeth, J. L. and Rostoker, G. (1971). Development of the polar electrojet during polar magnetic substorms. *J. Geophys. Res.* **76**(28), 6815–6828.

Kisabeth, J. L. and Rostoker, G. (1973). Current flow in auroral loops and surges inferred from ground-based magnetic observations. *J. Geophys. Res.* **78**(25), 5573–5584.

Kivelson, M. G., Kaye, S. M. and Southwood, D. J. (1980). The physics of plasma injection events. In *Dynamics of the Magnetosphere*, pp. 385–405. Reidel, Dordrecht.

Knipp, D. J. (1989). *Quantifying and Reducing Uncertainty in the Assimilative Mapping of Ionospheric Dynamics*. Unpublished dissertation, Department of Atmospheric Sciences, University of California Los Angeles, Los Angeles, CA 90024.

Knipp, D. J., Richmond, A. D., Crowley, G., de La Beaujardiere, O., Friis-Christensen, E., Evans, D. S., Foster, J. C., McCrea, I. W., Rich, F. J. and Waldock, J. A. (1989). Electrodynamic patterns for September 19, 1984. *J. Geophys. Res.* **94**(A12), 16 913–16 923.

Kokubun, S. and McPherron, R. L. (1981). Substorm signatures at synchronous altitude. *J. Geophys. Res.* **86**(A13), 11 265–11 277.

Kokubun, S., McPherron, R. L. and Russell, C. T. (1977). Triggering substorms by solar wind discontinuities. *J. Geophys. Res.* **82**(1), 74–86.

Kunkel, T., Baumjohann, W., Untiedt, J. and Greenwald, R. W. (1986) Electric fields and currents at the Harang discontinuity: a case study. *J. Geophys.* **59**, 73–86.

Lanzerotti, L. J., Hunsucker, R. D., Rice, D., Lee, L. C., Wolfe, A., Maclennan, C. G. and Medford, L. V. (1987). Ionosphere and ground-based response to field-aligned currents near the magnetospheric cleft regions. *J. Geophys. Res.* **92**(A7), 7739–7743.

Lester, M., Hughes, J. and Singer, H. J. (1984). Longitudinal structure in Pi 2 pulsations and the substorm current wedge. *J. Geophys. Res.* **89**(A7), 5489–5494.

Lin, N., Walker, R. J., McPherron, R. L. and Kivelson, M. G. (1990). Magnetic islands in the near geomagnetic tail and its implications for the mechanism of

1054 UT CDAW 6 substorm. In *AGU Monograph on Physics of Magnetic Flux Ropes* (ed. C. T. Russell), pp. 641–654. American Geophysical Union, Washington, D.C.

Lincoln, J. V. (1967). Geomagnetic indices. In *Physics of Geomagnetic Phenomena*, Vol. I (ed. S. Matsushita and W. H. Campbell), pp. 67–100. Academic Press, New York.

Lopez, R. E. and Lui, A. T. Y. (1990). A multi-satellite study of the expansion of a subatom current wedge in the near-earth magnetotail. *J. Geophys. Res.* **85**(A6), 8009–8017.

Lopez, R. E., Baker, D. N., Lui, A. Y. T., Sibeck, D. G., Belian, R. D., McEntire, R. W., Potemra, T. A. and Krimigis, S. M. (1988a). The radial and longitudinal propagation characteristics of substorm injections. *Adv. Space Res.* **8**(9–10), (9)91–(9)95.

Lopez, R. E., Lui, A. T., Sibeck, D. G., McEntire, R. W., Zanetti, L. J., Potemra, T. A. and Krimigis, S. M. (1988b). The longitudinal and radial distribution of magnetic reconfigurations in the near-earth magnetotail as observed by AMPTE/CCE. *J. Geophys. Res.* **93**(A2), 997–1001.

Lopez, R. E., Sibeck, D. G., Lui, A. T., Takahashi, K., McEntire, R. W. and Potemra, T. A. (1988c). Substorm variations in the magnitude of the magnetic field: AMPTE/CCE observations. *J. Geophys. Res.* **93**(A12), 14 444–14 452.

Lopez, R. E., Baker, O. N., Beliam, R. D., McEntire, R. W. and Potemra, T. A. (1990). A case study of a radially antisunward propagating local substorm onset. *Planet. Space Sci.* **38**, 771–784.

Lui, A. T. Y. and Anger, C. D. (1973). A uniform belt of diffuse auroral emission seen by the ISIS-2 scanning photometer. *Planet. Space Sci.* **21**(5), 799–809.

Lui, A. T. Y., Anger, D. D., Venkatesan, D., Sawchuk, W. and Akasofu, S.-I. (1975). The topology of the auroral oval as seen by the ISIS 2 scanning auroral photometer. *J. Geophys. Res.* **80**(13), 1795–1804.

Lui, A. T. Y., Eastman, T. E., Williams, D. J. and Frank, L. A. (1983). Observations of ion streaming during substorms. *J. Geophys. Res.* **88**(A10), 7753–7764.

Lui, A. T. Y., Lopez, R. E., Krimigis, S. M., McEntire, R. W., Zanetti, L. J. and Potemra, T. A. (1988). A case study of magnetotail current sheet disruption and diversion. *Geophys. Res. Lett.* **15**(7), 721–724.

Lyons, R. L. (1984). Electron energization in the geomagnetic tail current sheet. *J. Geophys. Res.* **89**(A7), 5479–5487.

Lyons, L. R. and Evans, D. S. (1984). An association between discrete aurora and energetic particle boundaries. *J. Geophys. Res.* **89**(A4), 2395–2400.

Lyons, L. R. and Nishida, A. (1988). Description of substorms in the tail incorporating boundary layer and neutral line effects. *Geophys. Res. Lett.* **15**(12), 1337–1340.

Lyons, L. R. and Schulz, M. (1989). Access of energetic particles to stormtime ring current through enhanced radial diffusion. *J. Geophys. Res.* **94**(A5), 5491–5496.

Lyons, L. R. and Speiser, T. W. (1982). Evidence for current sheet acceleration in the geomagnetic tail. *J. Geophys. Res.* **87**, 2276–2286.

Lyons, L. R. and Williams, D. J. (1984). *Quantitative Aspects of Mangetospheric Physics*. Reidel, Dordrecht.

Maezawa, K. (1975). Magnetotail boundary motion associated with geomagnetic substorms. *J. Geophys. Res.* **80**(25), 3543–3548.

triggered response to sudden changes in the solar wind. *Geophys. Res. Lett.* **15**(3), 253–256.
Garrett, H. B. and DeForest, S. E. (1979). An analytical simulation of the geosynchronous plasma environment. *Planet. Space Sci.* **27**, 1101–1109.
Gelpi, C., Singer, H. J. and Hughes, W. J. (1987). A comparison of magnetic signatures and DMSP auroral images at substorm onset: three case studies. *J. Geophys. Res.* **92**(A3), 2447–2460.
Gelpi, C., Hughes, W. J., Singer, H. J. and Lester, M. (1985). Mid-latitude Pi 2 polarization pattern and synchronous orbit magnetic activity. *J. Geophys. Res.* **90**(A7), 6451–6458.
Glassmeier, K., Honisch, M. and Untietd, J. (1989). Ground-based and satellite observations of traveling magnetospheric convection twin vortices. *J. Geophys. Res.* **94**(A3), 2520–2528.
Goertz, C. K. and Smith, R. A. (1989). Thermal catastrophe model of substorms. *J. Geophys. Res.* **94**, 6581.
Grebowsky, J. M. and Chen, A. J. (1975). Effects of convection electric field on the distribution of ring current type protons. *Planet. Space Sci.* **23**(7), 1045–1052.
Harang, L. (1946). The mean field of disturbance of polar geomagnetic storms. *Terr. Magn. Atmos. Elec.* **51**, 353–380.
Hardy, D. A., Gussenhoven, M. S. and Raistrick, R. (1987). Statistical and functional representations of the pattern of auroral energy flux, number flux, and conductivity. *J. Geophys. Res.* **92**(A11), 12 275–12 294.
Harel, M., Wolf, R. A., Spiro, R. W., Reiff, P. H., Chen, C.-K., Burke, W. J., Rich, F. J. and Smiddy, M. (1981). Quantitative simulation of a magnetospheric substorm 2. Comparison with observations. *J. Geophys. Res.* **86**(A4), 2242–2260.
Heelis, R. A. and Hanson, W. B. (1980). High-latitude ion convection in the nighttime F region. *J. Geophys. Res.* **85**(A5), 1995–2002.
Heelis, R. A., Reiff, P. H., Winningham, J. D. and Hanson, W. B. (1986). Ionospheric convection signature observed by DE 2 during northward interplanetary magnetic field. *J. Geophys. Res.* **91**(A5), 5817–5830.
Heppner, J. P. (1954). *A Study of Relationships Between the Aurora Borealis and the Geomagnetic Disturbances Causes by Electric Currents in the Ionosphere.* Unpublished Ph.D. dissertation, California Institute of Technology, Pasadena, CA.
Heppner, J. P. (1972). The Harang discontinuity in auroral belt ionospheric currents. *Geophys. Norv.* **29**, 105.
Heppner, J. P. (1977). Empirical models of high-latitude electric fields. *J. Geophys. Res.* **82**(7), 11 115–11 256.
Heppner, J. P. and Maynard, N. C., (1987) Empirical high-latitude electric field models. *J. Geophys. Res.* **92**(A5), 4467–4489.
Holzer, R. E. and Slavin, J. A. (1978). Magnetic flux transfer associated with expansions and contractions of the dayside magnetosphere. *J. Geophys. Res.* **83**(A8), 3831–3839.
Holzer, R. E. and Slavin, J. A. (1979). A correlative study of magnetic flux transfer in the magnetosphere. *J. Geophys. Res.* **84**(A6), 2573–2578.
Holzworth, R. H. and Meng, C.-I. (1975). Mathematical representation of the auroral oval. *Geophys. Res. Lett.* **2**(9), 377–380.
Holzworth, R. H. and Meng, C.-I. (1984). Auroral boundary variations and the interplanetary magnetic field. *Planet. Space Sci.* **32**(1), 25–29.

Hones, E. W. Jr (1977). Substorm processes in the magnetotail: Comments on 'On hot tenuous plasmas, fireballs, and boundary layers in the earth's magnetotail' by L. A. Frank, K. L. Ackerson, and R. P. Lepping. *J. Geophys. Res.* **82**(35), 5633–5640.
Hones, E. W. Jr (1979a). Plasma flow in the magnetotail and its implications for substorm theories. In *Dynamics of Magnetosphere* (ed. S.-I. Akasofu), pp. 542–562, Reidel, Dordrecht.
Hones, E. W. Jr (1979b). Transient phenomena in the magnetotail and their relation to substorms. *Space Sci. Rev.* **23**, 393.
Hones, E. W. Jr (1985). The poleward leap of the auroral electrojet as seen in auroral images. *J. Geophys. Res.* **90**(A6), 5333–5337.
Hones, E. W. Jr (1986). Reply. *J. Geophys. Res.* **91**(A5), 5881–5884.
Hones, E. W. Jr and Bergeson, J. E. (1965). Electric field generated by a rotating magnetized sphere. *J. Geophys. Res.* **70**(19), 4951–4958.
Hones, E. W. Jr and Schindler, K. (1979). Magnetotail plasma flow during substorms: A survey with IMP 6 and IMP 8 satellites. *J. Geophys. Res.* **84**(A12), 7155–7169.
Hones, E. W. Jr, Asbridge, J. R. and Bame, S. J. (1971). Time variations of the magnetotail plasma sheet at 18 Re determined from concurrent observations by a pair of Vela satellites. *J. Geophys. Res.* **76**(19), 4402–4419.
Hones, E. W. Jr, Asbridge, J. R., Bame, S. J. and Singer, S. (1973). Substorm variations of the magnetotail plasma sheet from Xsm = −6 Re to Xsm = −60 Re. *J. Geophys. Res.* **78**(1), 109–132.
Hones, E. W. Jr, Fritz, T. A., Birn, J., Cooney, J. and Bame, S. J. (1986). Detailed observations of the plasma sheet during a substorm on April 24, 1979. *J. Geophys. Res.* **91**(A6), 6845–6859.
Hones, E. W. Jr, Baker, D. N., Bame, S. J., Feldman, W. C., Gosling, J. T., McComas, D. J., Zwickl, R. D., Slavin, J. A., Smith, E. J. and Tsurutani, B. T. (1984). Structure of the magnetotail at 220 Re and its response to geomagnetic activity. *Geophys. Res. Lett.* **11**(1), 5–7.
Huang, C. Y. and Frank, L. A. (1986). A statistical study of the central plasma sheet: Implications for substorm models. *Geophys. Res. Lett.* **13**(7), 652–655.
Hughes, T. J. and Rostoker, G. (1977). Current flow in the magnetosphere and ionosphere during periods of moderate activity. *J. Geophys. Res.* **82**(16), 2271–2282.
Hughes, W. J. and Singer, H. J. (1985). Mid-latitude Pi 2 pulsations, geosynchronous substorm onset signatures and auroral zone currents on March 22, 1979: CDAW 6. *J. Geophys. Res.* **90**(A2), 1297–1304.
Iijima, T. and Nagata, T. (1972). Signatures for substorm development of the growth phase and expansion area. *Planet. Space Sci.* **20**, 1095–1112.
Iijima, T. and Potemra, T. A. (1976). The amplitude distribution of field-aligned currents at northern high latitudes observed by triad. *J. Geophys. Res.* **81**(13), 2165–2174.
Iijima, T. and Potemra, T. A. (1978). Large-scale characteristics of field-aligned currents associated with substorms. *J. Geophys. Res.* **83**(A2), 599–615.
Iijima, T. and Shibaji, T. (1987). Global characteristics of northward IMF-associated (NBZ) field-aligned currents. *J. Geophys. Res.* **92**(A3), 2408–2424.
Jelley, D. and Brice, N. (1967). Association between increased radiation in the outer belt and polar auroral substorms (abstract). *Trans. Am. Geophys. Union* **48**, 180.

Cowley, S. W. H. (1980). Plasma populations in a simple open model magnetosphere. *Space Sci. Rev.* **26**, 217–275.
Cowley, S. W. H. (1982a). The causes of convection in the earth's magnetosphere: A review of developments during the IMS. *Rev. Geophys. Space Phys.* **20**(3), 531–565.
Cowley, S. W. H. (1982b). Substorms and the growth phase problem. *Nature* **295**, 365–366.
Cowley, S. (1985). Magnetic reconnection. In *Solar System Magnetic Fields*. pp. 121–155. Reidel, Dordrecht.
Crooker, N. U. and Siscoe, G. L. (1974). Model geomagnetic disturbance from asymmetric ring current particles. *J. Geophys. Res.* **79**(4), 589–594.
Crooker, N. U. and Siscoe, G. L. (1981). Birkeland currents as the cause of the low-latitude asymmetric disturbance field. *J. Geophys. Res.* **86**(A13), 11 201–11 210.
Crooker, N. U. and Siscoe, G. L. (1986). The effect of the solar wind on the terrestrial environment. In *Physics of the Sun, Vol. III* (ed. A. Sturrock), pp. 193–249. Reidel, Dordrecht.
Davis, L. Jr (1947). Stellar electromagnetic fields. *Phys. Rev.* **72**(7), 632–633.
Davis, L. Jr (1948). Stellar electromagnetic fields (abstract). *Phys. Rev.* **73**, 536.
Davis, T. N. (1962). The morphology of the auroral displays of 1957–1958, 2. Detail analysis of Alaska data and analysis of high-latitude data. *J. Geophys. Res.* **67**, 75.
Davis, T. N. and Parthasarathy, R. (1967). The relationship between polar magnetic activity DP and growth of the geomagnetic ring current. *J. Geophys. Res.* **72**(23), 5825–5836.
Davis, T. N. and Sugiura, M. (1966). Auroral electrojet activity index AE and its universal time variations. *J. Geophys. Res.* **71**(3), 785–801.
DeCoster, R. J. and Frank, L. A. (1979). Observation pertaining to the dynamics of the plasma sheet. *J. Geophys. Res.* **84**(A9), 5099–5121.
Dessler, A. J. and Parker, E. N. (1959). Hydromagnetic theory of magnetic storms. *J. Geophys. Res.* **64**(12), 2239–2259.
Dungey, J. W. (1953). Conditions for the occurrence of electrical discharge in astrophysical systems. *Phil. Mag.* **44**, 725.
Dungey, J. W. (1961). Interplanetary magnetic field and the auroral zones. *Phys. Res. Lett.* **6**, 47–48.
Dungey, J. W. (1963). The structure of the exosphere or adventures in velocity space. In *Geophysics. The Earth's Environment*. Gordon and Breach, New York.
Eastman, T. E. and Frank, L. A. (1984). The plasma sheet boundary layer. *Geophys. Res.* **89**(A3), 1553–1572.
Eastman, T. E., Frank, L. A. and Huang, C. Y. (1985). The boundary layers as the primary transport regions of the earth's magnetotail. *J. Geophys. Res.* **90**(A10), 9541–9560.
Eastman, T. E., Rostoker, G., Frank, L. A., Huang, C. Y. and Mitchell, D. G. (1988). Boundary layer dynamics in the description of magnetospheric substorms. *J. Geophys. Res.* **93**(A12), 14 411–14 432.
Elphic, R. C. (1990). Observations of flux transfer events: Are FTE's flux ropes, islands, or surface waves? In *AGU Monograph on Physics of Magnetic Flux Ropes* (ed. C. T. Russell), pp. 455–471. American Geophysical Union, Washington, D.C.

Elphic, R. C., Mutch, P. A. and Russell, C. T. (1985). Observations of field-aligned currents at the plasma sheet boundary: an ISEE-1 and 2 survey. *Geophys. Res. Lett.* **12**(10), 631–634.
Elvey, C. T. (1957). *Proc. Nat. Acad. Sci.* **43**, 63.
Fairfield, D. H. (1973). Magnetic field signatures of substorms on high-latitude field lines in the nighttime magnetosphere. *J. Geophys. Res.* **78**(10), 1553–1562.
Fairfield, D. H. (1985). Solar wind control of magnetospheric pressure (CDAW 6). *J. Geophys. Res.* **90**(A2), 1201–1204.
Fairfield, D. H. (1987). Structure of the geomagnetic tail. In *Magnetotail Physics*, pp. 23–33. John Hopkins University Press.
Fairfield, D. H. and Cahill, L. J. Jr (1966). Transition region magnetic field and polar magnetic disturbances. *J. Geophys. Res.* **71**(1), 155–169.
Fairfield, D. H. and Mead, G. D. (1975). Magnetospheric mapping with a quantitative geomagnetic field model. *J. Geophys. Res.* **80**(4), 535–542.
Fairfield, D. H. and Ness, N. F. (1970). Configuration of the geomagnetic tail during substorms. *J. Geophys. Res.* **75**(34), 7032–7047.
Fairfield, D. H. and Scudder, J. D. (1985). Polar rain: Solar coronal electrons in the earth's magnetosphere. *J. Geophys. Res.* **90**(A5), 4055–4068.
Feldstein, Y. I. (1963). Some problems concerning the morphology of auroras and magnetic disturbances at high latitudes. *Geomagn. Aeron.* **3**(2), 183–192.
Feldstein, Y. I. and Starkov, G. V. (1967). Dynamics of auroral belt and polar geomagnetic disturbances. *Planet. Space Sci.* **15**(2), 209–229.
Forbes, T. G., Hones, E. W. Jr, Bame, S. J., Asbridge, J. R., Paschmann, G., Sckopke, N. and Russell, C. T. (1981). Substorm-related plasma sheet motions as determined from differential timing of plasma changes at the ISEE satellites. *J. Geophys. Res.* **86**(A5), 3459–3469.
Foster, J. C. (1984). Ionospheric signatures of magnetospheric convection. *J. Geophys. Res.* **89**(A2), 855–865.
Foster, J. C., Fuller-Rowell, T. and Evans, D. S. (1989). Quantitative patterns of large scale field-aligned currents in the auroral ionosphere. *J. Geophys. Res.* **94**(A3), 2555–2564.
Frank, L. A. and Ackerson, K. L. (1971). Observations of charged particle precipitation into the aurora zone. *J. Geophys. Res.* **76**(16), 3612–3643.
Frank, L. A. and Craven, J. D. (1988). Imaging results from dynamics explorer 1. *Rev. Geophys.* **26**(2), 249–283.
Frank, L. A., Craven, J. D. and Rairden, R. L. (1985). Images of the earth's aurora and geocorona from the dynamics explorer mission. *Adv. Space Res.* **5**(4), 53–68.
Frank, L. A., Craven, J. D., Burch, J. L. and Winningham, J. D. (1982). Polar views of the earth's aurora with Dynamics Explorer. *Geophys. Res. Lett.* **9**(9), 1001–1004.
Friis-Christensen, E. and Wilhjelm, J. (1975). Polar cap currents for different directions of the interplanetary magnetic field in the Y–Z plane. *J. Geophys. Res.* **80**(10), 1248–1260.
Friis-Christensen, E., Kamide, Y., Richmond, A. D. and Matsushita, S. (1985). Interplanetary magnetic field control of high-latitude electric fields and currents determined from greenland magnetometer data. *J. Geophys. Res.* **90**(A2), 1325–1338.
Friis-Christensen, E., McHenry, M. A., Clauer, C. R. and Vennerstrom, S. (1988). Ionospheric traveling convection vortices observed near the polar cleft: A

Baumjohann, W. (1986b). Some recent progress in substorm studies. *J. Geomagn. Geolelectr.* **38**, 633–651.

Baumjohann, W. and Haerendel, G. (1987). Entry and dissipation of energy in the earth's magnetosphere. *Space Astronomy and Solar System Exploration: Proceedings of Summer School, Alpbach. Austria*, pp. 121–130.

Baumjohann, W., Paschmann, G. and Cattell, C. A. (1989). Average plasma properties in the central plasma sheet. *J. Geophys. Res.* **94**(A6), 6597–6606.

Baumjohann, W., Pellinen, W. R., Opgenoorth, H. J. and Nielsen, E. (1981). Joint two-dimensional observations of ground magnetic and ionospheric electric fields associated with auroral zone currents: Current systems associated with local auroral break-ups, *Planet. Space Sci.* **29**(4), 431–447.

Behannon, K. W. (1970). Geometry of the geomagnetic tail. *J. Geophys. Res.* **75**(4), 743–753.

Berchem, J. and Russell, C. T. (1984). Flux transfer events on the magnetopause: Spatial distribution and controlling factors. *J. Geophys. Res.* **89**(A8), 6689–6703.

Birkeland, K. (1908). *The Norwegian Aurora Polaris Expedition 1902–1903*, Vol. 1. 1st sec. Aschhoug, Christiania.

Birkeland, K. (1913). *The Norwegian Aurora Polaris Expedition 1902–1903*, Vol. 1. 2nd sec. Aschhoug, Christiania.

Birmingham, T. J. and Jones, F. C. (1968). Identification of moving magnetic field lines. *J. Geophys. Res.* **73**(17), 5505–5510.

Bonnevier, B., Bostrom, R. and Rostoker, G. (1970). A three-dimensional model current system for polar magnetic substorms. *J. Geophys. Res.* **75**(1), 107–122.

Brice, N. (1964). Fundamentals of very low frequency emission generation mechanisms. *J. Geophys. Res.* **69**(21), 4515–4522.

Brice, N. (1967a). *Morphology of Elementary Magnetospheric Substorms*. ESSA Tech. Mem. IERTM-ITSA 72.

Brice, N. M. (1967b). Bulk motion of the magnetosphere. *J. Geophys. Res.* **72**(21), 5193–5211.

Burch, J. L. (1973). Rate of erosion of dayside magnetic flux based on a quantitative study of the dependence of polar cusp latitude on the interplanetary magnetic field. *Radio Sci.* **8**(11), 955–961.

Burke, W. J., Kelley, M. C., Sagalyn, R. C., Smiddy, M. and Lai, S. T. (1979). Polar cap electric field structures with a northward interplanetary magnetic field. *Geophys. Res. Lett.* **6**, 21.

Burton, R. K., McPherron, R. L. and Russell, C. T. (1975). An empirical relationship between interplanetary conditions and Dst. *J. Geophys. Res.* **80**(31), 4204–4214.

Bythrow, P. F., Potemra, T. A. and Zanetti, L. J. (1983). Variation of the auroral Birkeland current pattern associated with the north-south component of the IMF. *Magnetospheric Currents Geophys. Monogr.* **28**, 131–136.

Caan, M. N., McPherron, R. L. and Russell, C. T. (1973). Solar wind and substorm-related changes in the lobes of the geomagnetic tail. *J. Geophys. Res.* **78**(34), 8087–8093.

Caan, M. N., McPherron, R. L. and Russell, C. T. (1975). Substorm and interplanetary magnetic field effects on the geomagnatic tail lobes. *J. Geophys. Res.* **80**(1), 191–194.

Caan, M. N., McPherron, R. L. and Russell, C. T. (1978). The statistical magnetic signature of magnetospheric substorms. *Planet. Space Sci.* **26**(90), 269–279.

Cattell, C. A. and Elphic, R. C. (1987). Comment on 'A statistical study of the central plasma sheet: Implications for substorm models'. *Geophys. Res. Lett.* **14**(7), 773–775.

Cattell, C. A. and Mozer, F. S. (1984). Substorm electric fields in the earth's magnetotail. In *Magnetic Reconnection in Space and Laboratory Plasmas* (ed. E. W. Hones, Jr), pp. 208–215. American Geophysical Union, Washington, D.C.

Cauffman, D. P. and Gurnett, D. A. (1972). Satellite measurements of high latitude convection electric fields. *Space Sci. Rev.* **13**, 369.

Chapman, S. (1967). Perspective. In *Physics of Geomagnetic Phenomena*, Vol. 1 (ed. S. Matsushita and W. H. Campbell), pp. 3–28. Academic Press, New York.

Chapman, S. and Bartels, J. (1962). *Geomagnetism*, Vol. 1, 542 pp. Clarendon Press, Oxford.

Chapman, S. and Ferraro, V. C. A. (1930). A new theory of magnetic storms. *Nature* **126**, 129–130.

Chapman, S. and Ferraro, V. C. A. (1931a). A new theory of magnetic storms. Part I. The initial phase. *Terr. Magn. Atmosph. Elec.* **36**, 77–97.

Chapman, S. and Ferraro, V. C. A. (1931b). A new theory of magnetic storms. *Terr. Magn. Atmosph. Elec.* **36**, 171–186.

Chapman, S. and Ferraro, V. C. A. (1932). A new theory of magnetic storms. *Terr. Magn. Atmosph. Elec.* **37**, 147–156.

Chen, A. J. (1970). Penetration of low-energy protons deep into the magnetosphere. *J. Geophys. Res.* **75**(13), 2458–2467.

Clauer, C. R. and Kamide, Y. (1985). DP 1 and DP 2 current systems for the March 22, 1979 substorms. *J. Geophys. Res.* **90**(A2), 1343–1354.

Clauer, C. R. and McPherron, R. L. (1974). Mapping the local time-universal time development of magnetospheric substorms using mid-latitude magnetic observations. *J. Geophys. Res.* **79**(19), 2811–2820.

Clauer, C. R., McPherron, R. L. and Searls, C. (1983). Solar wind control of the low-latitude asymmetric magnetic disturbance field. *J. Geophys. Res.* **88**(A4), 2123–2130.

Clauer, C. R., McPherron, R. L., Searls, C. and Kivelson, M. G. (1981). Solar wind control of auroral zone geomagnetic activity. *Geophys. Res. Lett.* **8**(8), 915–918.

Coleman, P. J. Jr and McPherron, R. L. (1976). *Substorm Observations of Magnetic Perturbations and ULF Waves at Synchronous Orbit by ATS-1 and ATS-6*, pp. 345–365. Reidel, Dordrecht.

Coroniti, F. V. (1985). Explosive tail reconnection: The growth and expansion phases of magnetospheric substorms. *J. Geophys. Res.* **90**(A8), 7427–7447.

Coroniti, F. V. and Kennel, C. F. (1972a). Changes in magnetospheric configuration during the substorm growth phase. *J. Geophys. Res.* **77**(19), 3361–3370.

Coroniti, F. V. and Kennel, C. F. (1972b). Polarization of the auroral electrojet. *J. Geophys. Res.* **77**(16), 2835–2850.

Coroniti, F. V. and Kennel, C. F. (1973). Can the ionosphere regulate magnetospheric convection. *J. Geophys. Res.* **78**(16), 2837–2851.

Coroniti, F. V., McPherron, R. L. and Parks, G. K. (1968). Studies of the magnetospheric substorm: 3. Concept of the magnetospheric substorm and its relation to electron precipitation and micropulsations. *J. Geophys. Res.* **73**(5), 1715–1722.

REFERENCES

Akasofu, S.-I. (1964). The development of the auroral substorm. *Planet. Space Sci.* **12**(4), 273–282.

Akasofu, S.-I. (1968). *Polar and Magnetospheric Substorms*. Reidel, Dordrecht.

Akasofu, S.-I. (1974). A study of auroral displays photographed from the DMSP-2 satellite and from the Alaska meridian chain of stations. *Space Sci. Rev.* **16**, 617–725.

Akasofu, S.-I. (1976). Recent progress in studies of DMSP auroral photographs. *Space Sci. Rev.* **19**, 169–215.

Akasofu, S.-I. (1977). *Physics of Magnetospheric Substorms*. Reidel, Dordrecht.

Akasofu, S.-I. (1979a). What is a magnetospheric substorm? In *Dynamics of the Magnetosphere* (ed. S.-I. Akasofu), pp. 447–460. Reidel, Hingam, MA.

Akasofu, S.-I. (1979b). Interplanetary energy flux associated with magnetospheric substorms. *Planet. Space Sci.* **27**, 425–431.

Akasofu, S.-I. (1981a). Energy coupling between the solar wind and the magnetosphere. *Space Sci. Rev.* **28**, 121–190.

Akasofu, S.-I. (1981b). Magnetospheric substorms: A newly emerging model, *Planet. Space Sci.* **29**(10), 1069–1078.

Akasofu, S.-I. and Chapman, S. (1961). The ring current, geomagnetic disturbance, and the Van Allen radiation belts. *J. Geophys. Res.* **66**(5), 1321–1350.

Akasofu, S.-I. and Chapman, S. (1964). On the asymmetric development of magnetic storm fields in low and middle latitudes. *Planet. Space Sci.* **12**(6), 607–626.

Akasofu, S.-I. and Meng, C.-I. (1969). A study of polar magnetic substorms, *J. Geophys. Res.* **74**(1), 293–313.

Akasofu, S.-I., Chapman, S. and Meng, C.-I. (1965). The polar electrojet. *J. Atmos. Terr. Phys.* **27**(11/12), 1275–1305.

Akasofu, S.-I., Eather, R. H. and Bradbury, J. N. (1969). The absence of the hydrogen emission (Hbeta) in the westward traveling surge. *Planet. Space Sci.* **17**(7), 1409–1412.

Akasofu, S.-I., Meng, C.-I. and Kimball, D. S. (1966). Dynamics of the Aurora-IV: Polar magnetic substorms and the westward traveling surge. *J. Atmos. Terr. Phys.* **28**, 489–496.

Allen, J. H. and Kroehl, H. W. (1975). Spatial and temporal distributions of magnetic effects of auroral electrojets as derived from AE indices. *J. Geophys. Res.* **80**(25), 3667–3677.

Angerami, J. J. and Thomas, J. O. (1964). Studies of planetary atmospheres 1. The distribution of electrons and ions in the earth's exosphere. *J. Geophys. Res.* **69**(21), 4537–4560.

Aubry, M. P. and McPherron, R. L. (1971). Magnetotail changes in relation to the solar wind magnetic field and magnetospheric substorms. *J. Geophys. Res.* **76**(19), 4381–4401.

Aubry, M. P., Kivelson, M. G., McPherron, R. L., Russell, C. T. and Colburn, D. S. (1972). Outer magnetosphere near midnight at quiet and disturbed times. *J. Geophys. Res.* **77**(28), 5487–5502.

Aubry, M. P., Russell, C. T. and Kivelson, M. G. (1970). Inward motion of the magnetopause before a substorm. *J. Geophys. Res.* **75**(34), 7018–7031.

Axford, W. I. (1964). Viscous interaction between the solar wind and the earth's magnetosphere. *Planet. Space Sci.* **12**, 45–53.

Axford, W. I. and Hines, C. O. (1961). A unifying theory of high-latitude geophysical phenomena and geomagnetic storms. *Can. J. Phys.* **39**, 1433–1464.

Baker, D. N. (1984). *Particle and Field Signatures of Substorms in the Near Magnetotail*, pp. 193–202. American Geophysical Union, Geophysical Monograph 30, Washington, D.C.

Baker, D. N. and McPherron, R. L. (1990). Extreme energetic particle decreases near geostationary orbit: A manifestation of current diversion within the inner plasma sheet. *J. Geophys. Res.*, **95**(A5), 6591–6599.

Baker, D. N., Higbie, P. R., Hones, E. W. Jr and Belian, R. D. (1978). High-resolution energetic particle measurements at 6.6 Re. 3. Low-energy electron anisotropies and short-term substorm predictions. *J. Geophys. Res.* **83**(A10), 4863–4868.

Baker, D. N., Akasofu, S.-I., Baumjohann, W., Bieber, J. W., Fairfield, D. H., Hones, E. W. Jr, Mauk, B., McPherron, R. L. and Moore, T. E. (1984a). Substorms in the magnetosphere, Chapter 8 pp., NASA Scientific and Technical Information branch, NASA Reference Pub. 1120.

Baker, D. N., Bame, S. J., Belian, R. D., Feldman, W. C., Gosling, J. T., Higbie, P. R., Hones, E. W. Jr, McComas, D. J. and Zwickl, R. D. (1984b). Correlated dynamical changes in the near-earth and distant magnetotail regions: ISEE-3. *J. Geophys. Res.* **89**(A6), 3855–3864.

Baker, D. N., Anderson, R. C., Zwickl, R. D. and Slavin, J. A. (1987a). Average plasma and magnetic field variations in the distant magnetotail associated with near-earth substorm effects. *J. Geophys. Res.* **92**(A1), 71–81.

Baker, D. N., Bame, S. J., McComas, D. J., Zwickl, R. D., Slavin, J. A. and Smith, E. J. (1987b). Plasma and magnetic field variations in the distant magnetotail associated with near-earth substorm effects. In *Magnetotail Physics* (ed. A. T. Y. Lui), pp. 137–142. The Johns Hopkins University Press, Baltimore.

Baker, D. N., Klimas, A. J., McPherron, R. L. and Buchner, J. (1990). The evolution from weak to strong geomagnetic activity: An interpretation in terms of deterministic chaos. *Geophys. Res. Lett.* **17**(1), 41–44.

Bame, S. J., Asbridge, J. R., Felthauser, H. E., Hones, E. W. and Stong, I. B. (1967). Characteristics of the plasma sheet in the earth's magnetotail. *J. Geophys. Res.* **72**, 113.

Banks, P. M., Doupnik, J. R. and Akasofu, S.-I. (1973). Electric field observations by incoherent scatter radar in the auroral zone. *J. Geophys. Res.* **78**(28), 6607–6622.

Barfield, J. N., Lin, C. S. and McPherron, R. L. (1985). Observations of magnetic field perturbations at GOES 2 and GOES 3 during the March 22, 1979, substorms: CDAW 6 analysis. *J. Geophys. Res.* **90**(A2), 1289–1295.

Bargatze, L. F., Baker, D. N., McPherron, R. L. and Hones, E. W. (1985). Magnetospheric impulse response for many levels of geomagnetic activity. *J. Geophys. Res.* **90**(A7), 6387–6394.

Baumjohann, W. (1983). Ionsopheric and field-aligned current systems in the auroral zone: A concise review. *Adv. Space Res.* **2**(10), 52–62.

Baumjohann, W. (1986a). *Merits and Limitations of the Use of Geomagnetic Indices in Solar Wind–Magnetosphere Coupling Studies*, pp. 3–15. Terra Scientific Publishing Co., Tokyo and D. Reidel, Dordrecht.

(3) How much reconnection occurs across the distant neutral line and how is this related to substorms?
(4) During northward IMF does reconnection occur beyond the distant neutral line where antiparallel open field lines are in contact? If so, why doesn't the polar cap completely close?
(5) Do closed field lines in the viscous boundary layer get so elongated that they reconnect?

5.5 The plasma sheet

(1) What are the sources and sinks for particles in the plasma sheet?
(2) Does the plasma sheet thin during substorm growth phase?
(3) How does the plasma sheet create the intense earthward extension of the tail current during substorm growth phase?
(4) Where do the three main regions of the plasma sheet—PSBL, CPS and inner edge—map onto the ionosphere?
(5) What is the magnetospheric projection of the Harang discontinuity?

5.6 Field-aligned currents

(1) Is the statistical pattern of field-aligned currents representative of the instantaneous state at all times in a substorm?
(2) How is the unbalanced current at noon and midnight closed in the magnetosphere?
(3) Does current from the outer edge of the boundary layers close through the polar cusps?
(4) What is the relation of the substorm current wedge to the nightside Region 1 current system?
(5) What processes divert tail current into the ionosphere during the expansion phase?
(6) What regions of the plasma sheet provide this current?

5.7 Substorm onset

(1) Why does the ionsopheric expansion onset begin near midnight in the Harang discontinuity?

(2) What is the role of the inward extension of the tail current in substorm onset?
(3) Where does the expansion onset map to in the magnetotail?
(4) Why does a northward turning of the IMF so frequently trigger a substorm onset?
(5) What causes the westward progression of substorm intensifications?
(6) Why do many substorms develop in discrete steps or intensifications?
(7) How important is the auroral acceleration region and ionospheric feedback in expansion onset?

5.8 The NENL

(1) Where is the NENL typically located and what controls its point of formation?
(2) Are there different varieties of reconnection possible in the tail as it appears there is on the magnetopause?
(3) What is the ionospheric manifestation of the onset of reconnection in the CPS? When does this occur in relation to the expansion onset?
(4) Do successive intensifications generate multiple plasmoids?
(5) What causes the NENL to move tailward terminating the expansion phase?
(6) What is the source of the plasma that expands the plasma sheet behind a retreating neutral line?
(7) How much evolution of plasmoids occurs during their departure from the tail?
(8) Do flux ropes form around plasmoids when there is a substantial B_y component across the tail?
(9) How can such flux ropes be completely severed from the Earth, connecting to different meridians as they are expected to do?

5.9 Particle injection during substorms

(1) How important is the collapse of the tail field and associated inductive effects in energizing and injecting particles in the inner magnetosphere?
(2) What processes accelerate bursts of electrons and ions to hundreds of keV?
(3) How are relativistic electrons generated during magnetic activity?

Slavin, J. A., Baker, D. N., Craven, J. D., Elphic, R. C., Fairfield, D. H., Frank, L. A., Galvin, A. B., Hughes, W. J., Manka, R. H., Mitchell, D. G., Richardson, I. G., Sanderson, T. R., Sibeck, D. J., Smith, E. J. and Zwickl, R. D. (1989). CDAW 8 observations of plasmoid signatures in the geomagnetic tail: An assessment. *J. Geophys. Res.* **94**(A11), 15 153–15 175.

Smith, P. H., Bewtra, N. K. and Hoffman, R. A. (1981). Inference of the ring current ion composition by means of charge exchange decay. *J. Geophys. Res.* **86**(A5), 3470–3480.

Smith, R. A., Goertz, C. K. and Grossman, W. (1986). Thermal catastrophe in the plasma sheet boundary layer. *J. Geophys. Res.* **13**(13), 1380–1383.

Snyder, C. W., Neugeauer, M. and Rao, U. R. (1963). The solar wind velocity and its correlation with cosmic-ray variations and with solar and geomagnetic activity. *J. Geophys. Res.* **68**(24), 6361–6370.

Sonnerup, B. U. O. (1980). Theory of the low-altitude boundary layer. *J. Geophys. Res.* **85**(A5), 2017–2026.

Sonnerup, B. U. O. (1984). Magnetic field reconnection at the magnetopause: An overview. In *Magnetic Reconnection in Space and Laboratory Plasma* (ed. E. W. Hones, Jr), pp. 92–103. Geophysical Monograph 30, American Geophysical Union, Washington, D.C.

Sonnerup, B. U. O., Paschmann, G., Papamastorakis, I., Sckopke, N., Haerendel, G., Bame, S. J., Asbridge, J. R., Gosling, J. T. and Russell, C. T. (1981). Evidence for magnetic field reconnection at the Earth's magnetopause. *J. Geophys. Res.* **86**(A12), 10 049–10 067.

Southwood, D. J. (1987). The ionospheric signature of flux transfer events. *J. Geophys. Res.* **92**(A4), 3207–3213.

Southwood, D. J. and Wolf, R. A. (1978). An assessment of the role of precipitation in the magnetospheric convection. *J. Geophys. Res.* **83**(A11), 5227–5232.

Speiser, T. W. (1965). Particle trajectories in model current sheets: 1. Analytical solutions. *J. Geophys. Res.* **70**(17), 4219–4226.

Speiser, T. W. (1967). Particle trajectories in model current sheets 2. Applications to auroras using a geomagnetic tail model. *J. Geophys. Res.* **72**, 3219.

Spiro, R. W., Reiff, P. H. and Maher, L. J. Jr (1982). Precipitating electron energy flux and auroral zone conductances—an empirical model. *J. Geophys. Res.* **87**(A10), 8215–8227.

Sugiura, M. (1964). Hourly values of equatorial Dst for the IGY. *Ann. Int. Geophys. Year*, **35**, 9.

Takahashi, K. and Hones, E. W. Jr (1988). ISEE 1 and 2 observations of ion distribution at the plasma sheet–tail lobe boundary. *J. Geophys. Res.* **93**(A8), 8558–8582.

Takahashi, K., Zanetti, L. J., Lopez, R. E., McEntire, R. W., Potemra, T. A. and Yumoto, K. (1987). Disruption of the magnetotail current sheet observed by AMPTE/CCE. *Geophys. Res. Lett.* **14**(10), 1019–1022.

Tighe, W. G. and Rostoker, G. (1981). Characteristics of westward travelling surges during magnetospheric substorms. *J. Geophys.* **50**, 51–67.

Todd, H., Bromage, B. J. I., Cowley, S. W. H., Lockwood, M., van Eyken, A. P. and Wilis, D. M. (1986). EISCAT observations of bursts of rapid flow in the high latitude dayside ionosphere. *Geophys. Res. Lett.* **13**, 909–912.

Tsyganenko, N. A. (1989). On the redistribution of the magnetic field and plasma

in the near nightside magnetosphere during a substorm growth phase. *Planet. Space Sci.* **37**(2), 183–192.

Vasyliunas, V. M. (1968). A survey of low-energy electrons in the evening sector of the magnetosphere with OGO-1 and OGO-3. *J. Geophys. Res.* **73**(9), 2839–2884.

Vasyliunas, V. M. (1975). Theoretical models of magnetic field line merging. 1. *Rev. Geophys. Space Phys.* **13**(1), 303–336.

Vasyliunas, V. M. (1984). Steady state aspects of magnetic field line merging. In *Magnetic Reconnection in Space and Laboratory Plasmas*, pp. 25–31. Geophysical Monographs 30, American Geophysical Union, Washington, D.C.

Walker, R. J., Erickson, K. N., Swanson, R. L. and Winckler, J. R. (1976). Substorm-associated particle boundary motion at synchronous orbit. *J. Geophys. Res.* **81**(31), 5541–5550.

Weins, R. G. and Rostoker, G. (1975). Characteristics of the development of the westward electrojet during the expansive phase of magnetospheric substorms. *J. Geophys. Res.* **80**(16), 2109–2128.

Westcott, E. M., Stolarik, J. D. and Heppner, J. P. (1969). Electric field in the vicinity of auroral forms from motions of barium vapor releases. *J. Geophys. Res.* **74**(14), 3469–3487.

Wilcox, J. M., Schatten, K. H. and Ness, N. F. (1967). Influence of interplanetary magnetic field and plasma on geomagnetic activity during quiet-sun conditions. *J. Geophys. Res.* **72**(1), 19–26.

Williams, D. J. (1990). Why we need global observation.

Winningham, J. D., Yasuhara, F., Akasofu, S.-I. and Heikkila, W. J. (1975). The latitudinal morphology of 10-eV to 10-keV electron fluxes during magnetically quiet and disturbed times in the 2100–0300 MLT sector. *J. Geophys. Res.* **80**(22), 3148–3171.

Wygant, J. R., Torbert, R. B. and Mozer, F. S. (1983). Comparison of S3-3 polar cap potential drops with the interplanetary magnetic field and models of magnetpause reconnection. *J. Geophys. Res.* **88**(A7), 5727–5735.

Zwickl, R. D., Baker, D. N., Bame, S. J., Feldman, W. C., Gosling, J. T., Hones, E. W. Jr, McComas, D. J., Tsurutani, B. T. and Slavin, J. A. (1984). Evolution of the earth's distant magnetotail: ISEE 3 electron plasma results. *J. Geophys. Res.* **89**(A12), 11 007–11 012.